Crystal Chemistry of Low-Valence Nickelates $La_2Ni_2O_5$ and $Ln_3Ni_3O_7$ (*Ln*=Pr and Nd)

Toshihiro MORIGA

Department of Chemical Science and Technology
Faculty of Engineering
The University of Tokushima

Applied to : Department of Chemistry
Faculty of Science
Osaka University

March, 1996

Contents

Chapter 1.

General Introduction

Lanthanum-Nickelates in an Analogy of Superconductive Lanthanum Cuprates

Increasing interest is being devoted to lanthanum-nickelates. At least two major reasons exist. First, an obvious question relates to the existence of superconductivity in nickelates. Some years ago, there were claims of superconductivity in reduced forms of $La_{2-x}Sr_xNiO_4$ compounds, obtained under particular conditions of annealing and thermal cycling.[1,2] Only anomalous diamagnetism results supported these conclusions, giving rise to significant controversies about such reports. However, the same authors recently published another set of results from which they concluded that the existence of "granular superconductivity" was proven by adapted surface resistance (high-frequency) measurements.[3] Second, in connection with the above question, note the important structural similarities between semiconducting nickelates and superconducting cuprates.

For example, stoichiometric La_2CuO_4 exhibits semiconducting behavior, while it becomes superconductive ($T_c \simeq 40K$) when efficient oxygenation is achieved (introduction of interstitial oxygen).[4] Stoichiometric La_2NiO_4, in which formal valence of Ni ions is 2, is a three-dimensional antiferromagnet with $T_N<300K$,[5,6] whose crystal structure and magnetic structure are shown in Figs. 1-1(a) and 1-1(b), respectively. These structures are refined by Jorgensen et al.[7] La_2NiO_4 have the orthorhombic cell of space group B_{mab}, and can be indexed with lattice constants of a=5.473, b=5.532, and c=12.541Å. The refinement gave an octahedral polar canting angle of 5.4° with r_{Ni-O}=1.948Å in the basal plane and 2.244Å axially. Rodriguez-Carvajal et al. reported T_N=330K,[8] in agreement with the results of Yamada et al.[9] obtained by magnetic susceptibility measurements. The magnetic correlations in La_2NiO_4 are highly sensitive to the oxygen content, and the three-dimensional antiferromagnetic ordering is progressively suppressed when the amount of interstitial oxygen increase. In this case, short-range antiferromagnetic interactions remain in the basal $[NiO_{4/2}]$ plane (two-dimensional antiferromagnet) according to several authors.[8,10,11]

The magnetic susceptibility is strongly dependent on x in La_2NiO_{4+x}.[6] A small cusp or break in the susceptibility for **H**//c near 200K was reported for the single crystal

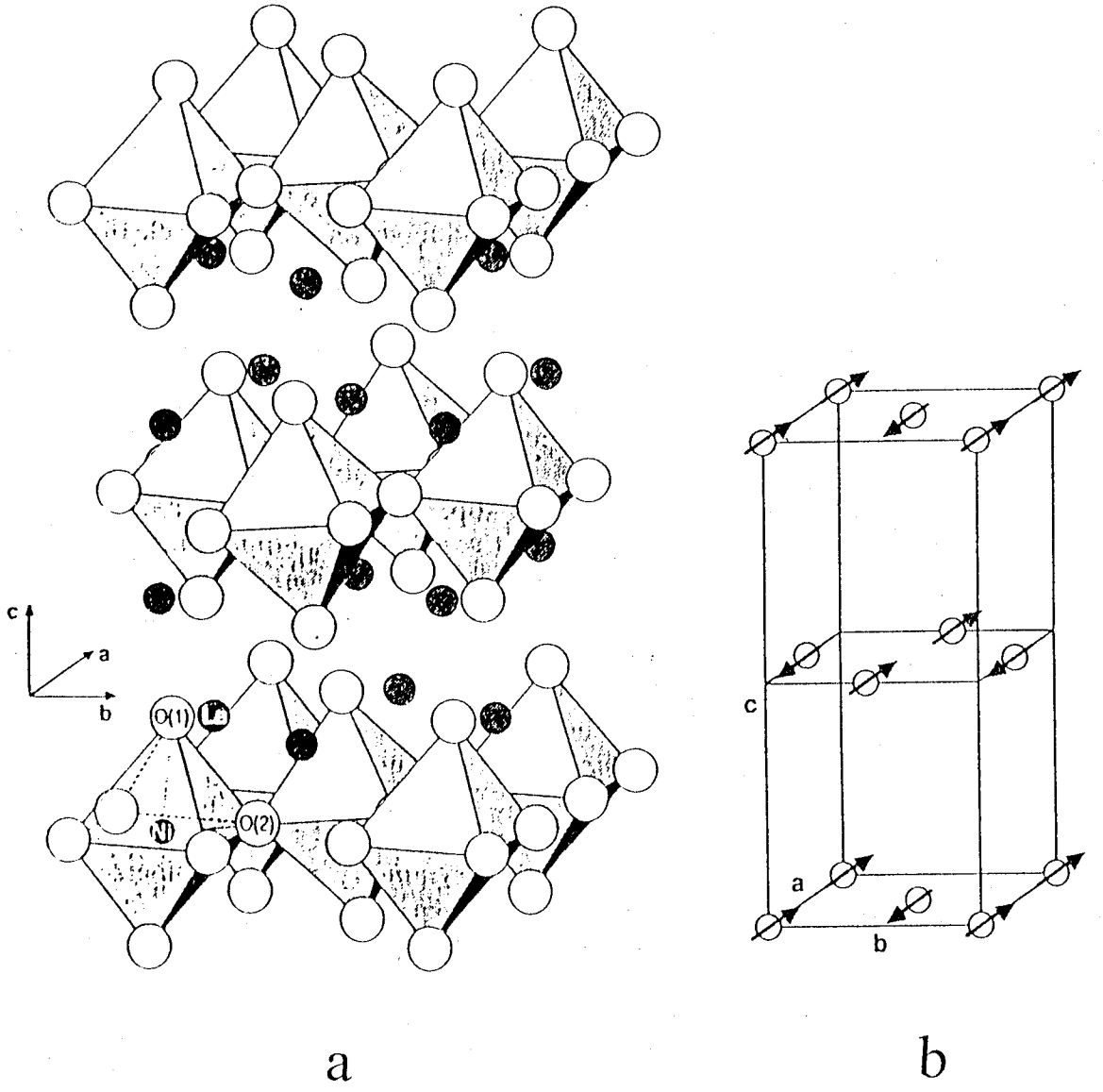

Fig. 1-1 (a): Clinographic projection of the orthorhombic *B*mab structure of La_2NiO_4. (b): The three-dimensional magnetic structure of La_2NiO_4 for $T<T_N$.

sample of x=0.02-0.077, but unobserved for $\mathbf{H} \perp c$. A smaller anomaly was observed at lower temperatures for larger x. These anomalies have been interpreted in terms of the onset of three-dimensional antiferromagnetic order with spins slightly canted out of the basal plane, producing a net magnetic moment along *c*-axis in the presence of an applied field, as has been proposed for La_2CuO_{4+x}. The each magnetic spin in neighboring NiO_6 octahedron is ordered antiparalell ([1,0,0] and [-1,0,0] in the La_2NiO_4 supercell, *i.e.*, [1,1,0] and [-1,1,0] in the fundamental perovskite-type cell) and the neighboring octahedra are slightly canted in the opposite direction. The canting of octahedron occurs around the nearly [110] axis in the supercell. The schematic views of this model from [0,0,1] and [1,-1,0] axes are represented in Fig. 1-2.

Contrary to this categories, some attempts to reduce La_2NiO_4 have been made. As for La_2CuO_4, reduction is not effective to improve its electrical properties. Lanthanide ions with intermediate size (Pr, Nd, Eu and Gd) have so-called the T'-type structure. In the T'-type Nd_2CuO_4, Cu ions have a square-planar coordination. When electron-doped by substituting Nd^{3+} ion to Ce^{4+} ion and by reducing the substitutant, *e.g.*, $Nd_{1.85}Ce_{0.15}CuO_{4-y}$, superconductivity appears with T_c=24K.[4] Crespin et al. reported that strontium-substituted phases $La_{2-x}Sr_xNiO_y$ (x=0.4 and 1.0) were synthesized and reduced under hydrogen atmosphere.[12,13] The reduction led to the composition $LaSrNiO_{3.1}$ containing formally more than 80% of Ni^+ ions. The monovalent Ni^+ ion with $3d^9$ electron configuration is isoelectronic to Cu^{2+} ion essential to high-T_c cuprate superconductors.

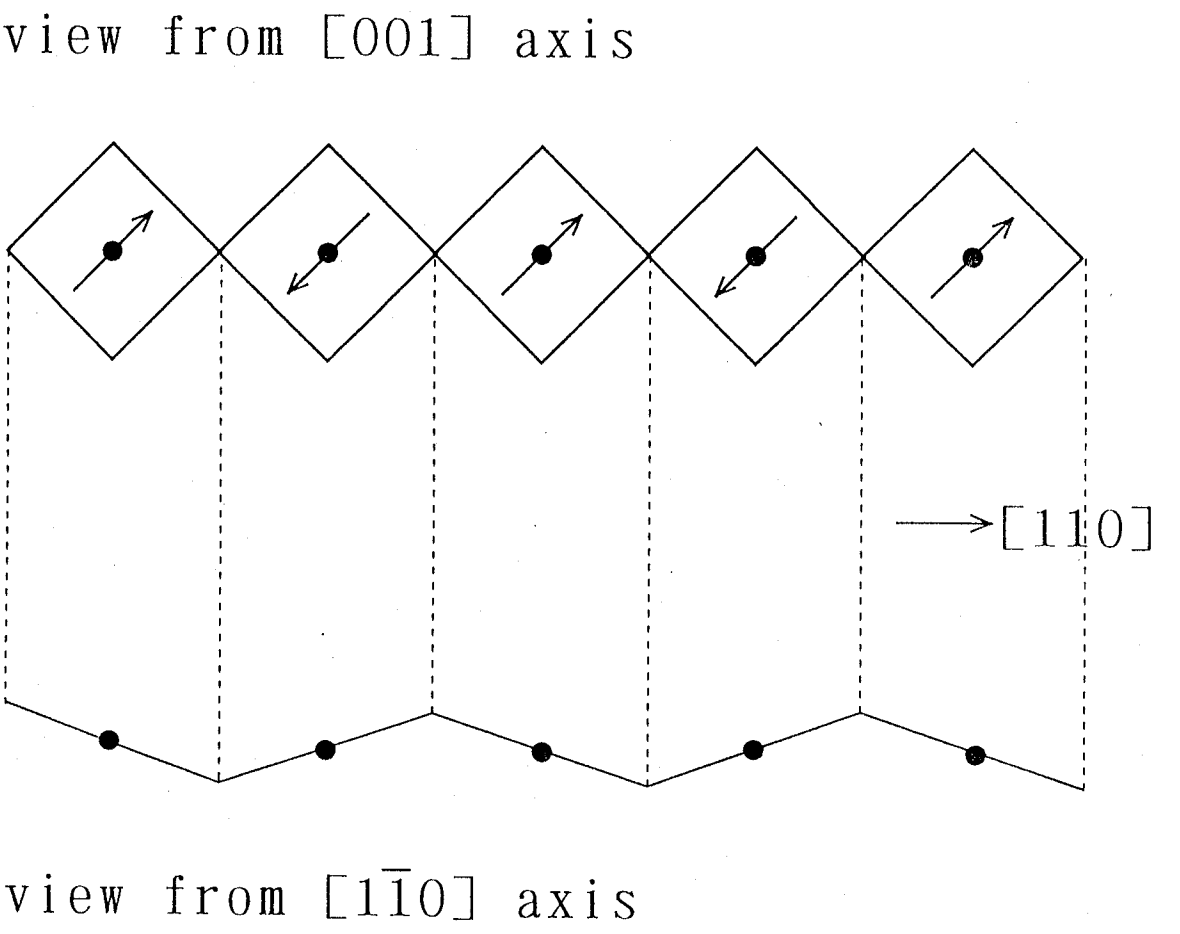

Fig. 1-2 Schematic views of canting of octahedron seen in La_2NiO_4.

Ruddlesden-Popper-type Structure

Many lanthanide cuprates and nickelates adopts the Ruddlesden-Popper-type structures.[14,15] They can be described by the stacking of finite n layers of perovskite $LnAO_3$ between rock-salt LnO layers along the crystallographic c-direction, as shown in Fig.1-3. Their formula is expressed as $(LnO)(LnAO_3)_n=Ln_{n+1}A_nO_{3n+1}$. The first member of the Ruddlesden-Popper family, n=1, is Ln_2CuO_4 for cuprates and Ln_2NiO_4 for nickelates mentioned above. For nickelates, as the number of n increases, it is reported that the electrical conductivily is enhanced significantly.[16,17] For example, La_2NiO_4 is a insulator, but the perovskite-type $LaNiO_3$ which is the member of $n=\infty$ has a metallic conductivity and temperature-independent Pauli-paramagnetism.

The creation of oxygen vacancies in the Ruddlesden-Popper family occurs in the perovskite layer. The ordered vacancies leads to interesting structures and physical properties. On the study of the n=2 member, $La_3Ni_2O_{7-x}$ (x=0, 0.08 and 0.65), by Z.Zhang *et al.*[16], these specimens showed the orthorhombic symmetry with the space group Fmmm for each and their cell constants of a and b increased monotonously with the oxygen content, whereas c parameter decreased significantly. The decrease of the c parameter is due to the loss of apical oxygens connecting the nickel ions of a double-perovskite layer. In $La_3Ni_2O_7$, a metallic behavior was observed. $La_3Ni_2O_{6.35}$ showed a semiconducting one.

Laccore has proposed the structural models for $La_4Ni_3O_{10}$ and the reduced form $La_4Ni_3O_8$ as shown in Fig.1-4.[14] During the reduction process, only apical oxygens suffer changes, two of them (denoted as O2) per formula unit being removed, the two others (O4) being shifted. The origin of the shift of apical oxygen O4 could be related to the preference of both Ni^{2+} and Ni^{+} for square-planar coordination rather than for pyramidal coordination. Oxygens forms a cubic arrangement, like anions in the fluorite-type structure. All nickel ions are in the ***square-planar coordinations***, which can be hardly seen even in the cuprates.

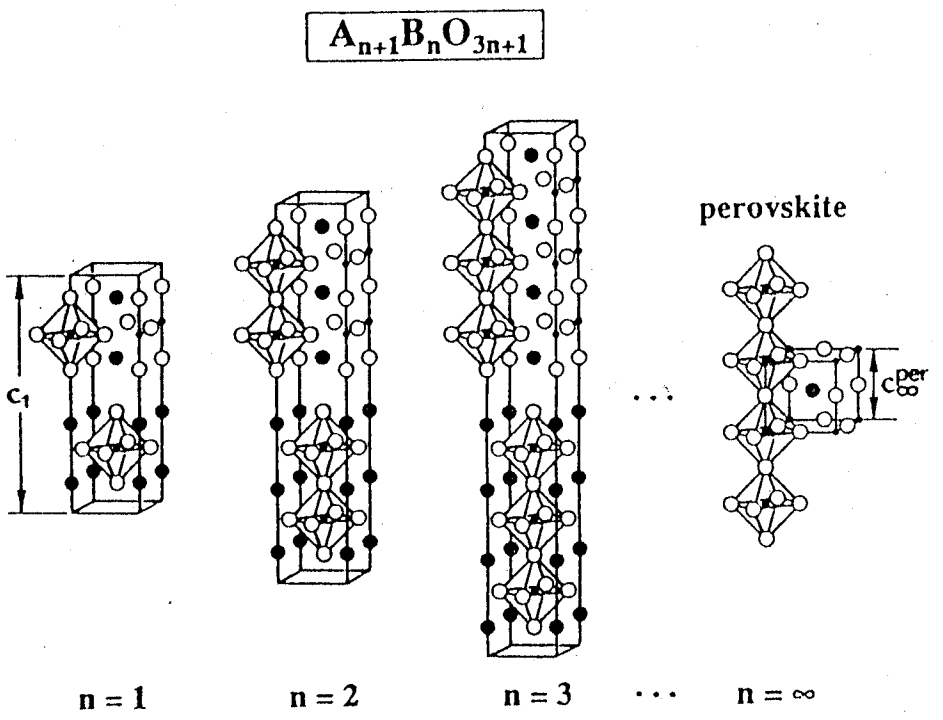

Fig. 1-3 The Ruddlesden-Popper structural type series. Solid circles represent cations (large=A, small=B), and open circles represent oxygen.

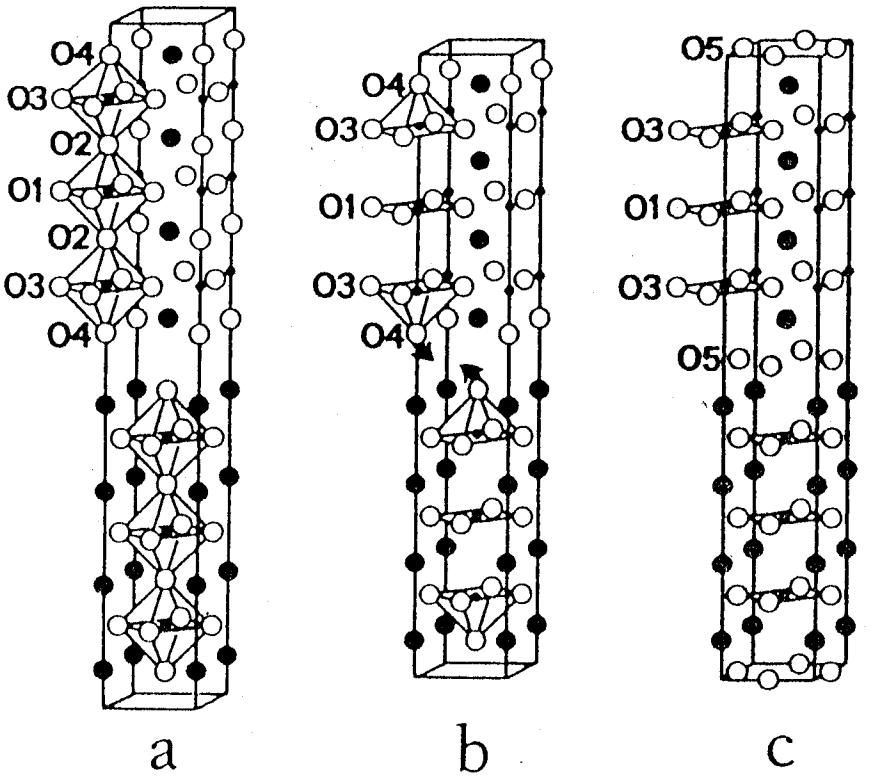

Fig. 1-4 The structure of $La_4Ni_3O_{10}$ (a), of the reduced forms $La_4Ni_3O_8$ as expected (b) and effectively observed (c). The thick arrow means the shift of oxygen O4 toward oxygen position O5. The symbols are the same as Fig. 1-4.

Review of Oxygen-deficient Perovskites

The structures of Ruddlesden-Popper family derive from the perovskite-type structure, whose formulas is expressed as ABO_3. It can be described as a $BO_{6/2}$ framework of corner-shared octahedra that contains A cations within 12-coordinated sites, as shown in Fig. 1-5(a).[18] An oxygen-deficient perovskite structure can be described as a $BO_{6/2-x/2}$ framework, wherein some of the A and B cations are less than 12- and 6-coordinate, respectively. This particular description emphasizes the dimensionality, local A and B cation coordination, and overall symmetry of the compounds. Alternatively, the perovskite-type structure can be described as a cubic-packed arrangement of AO_3 layers between which one-fourth of the octahedral interstices are filled by B cations, as shown in Fig. 1-5(b). A similar description of oxygen-deficient perovskites can be described as close-packed ABO_{3-x} layers. This description emphasizes the ionic bonding and three-dimensional structural similarity of the compounds.

Two general formulas will be used to categorize oxygen-deficient perovskites, $A_mB_mO_{3m-x}$ and $A_nB_nO_{3n-1}$. The former will be used to emphasize structural similarity, and the latter to facilitate comparison of the degree of oxygen deficiency among compounds. Note that the percentage of vacant sites in the latter notation is simply 100(1/3n). The $A_mB_mO_{3m-x}$ notation provides a convenient way to describe perovskites that have ordered vacancies. In this notation, x is an integer and therefore m is an integral multiple of the number of perovskites blocks in the unit cell. The notation will be used extensively to group compounds into those derived from double perovskites (m=2, $A_2B_2O_{6-x}$), triple perovskite (m=3, $A_3B_3O_{9-x}$), an so on. The equivalent $A_nB_nO_{3n-1}$ notation will be provided by each example to emphasize the degree of reduction. As n decrease, the number of vacancies increases.

In general, ordered oxygen-deficient perovskites $A_nB_nO_{3n-1}$ exist for n=1 to ∞, that is, ABO_2 to ABO_3. Oxygen ions are generally removed from [100]c or [110]c rows or (001)c planes (shown in Fig. 1-6), and in the case of very deficient structures the vacancies are removed from a row and a plane.[19] Removal of oxide ions from [100]c rows results in the formation of MO_4 square-planes through MO_5 square-pyramids,

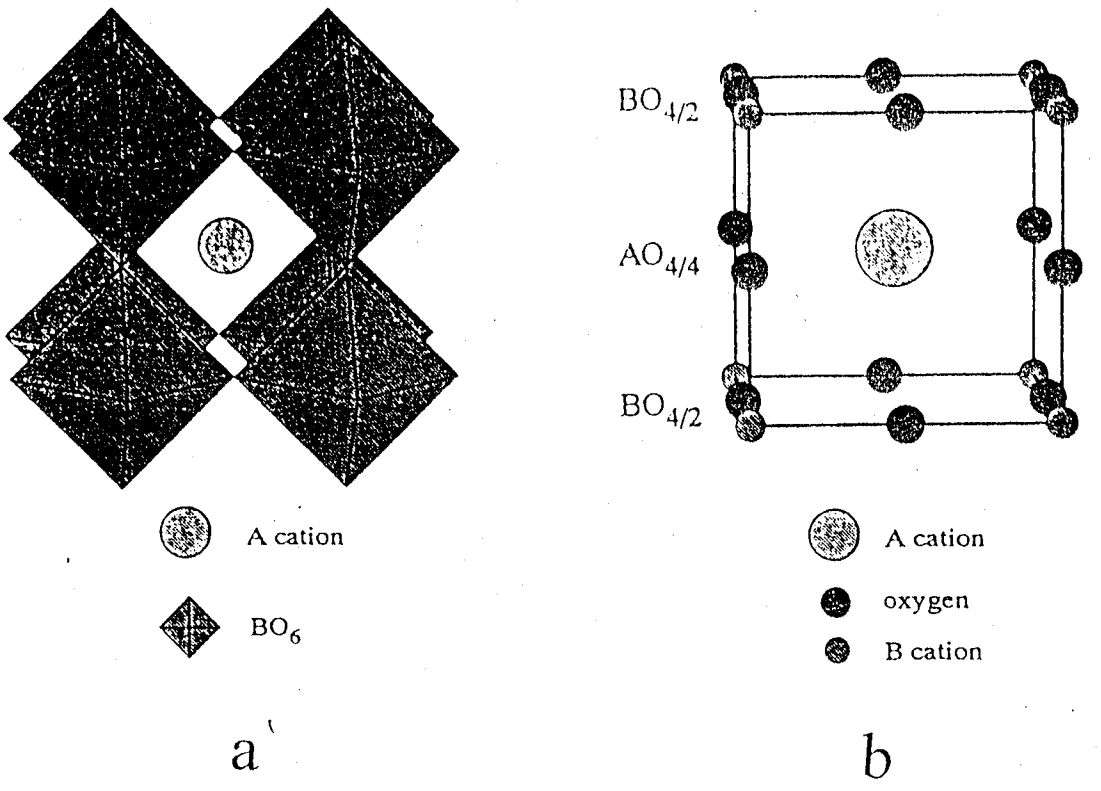

Fig. 1-5 Two depictions of the perovskite-type structure.

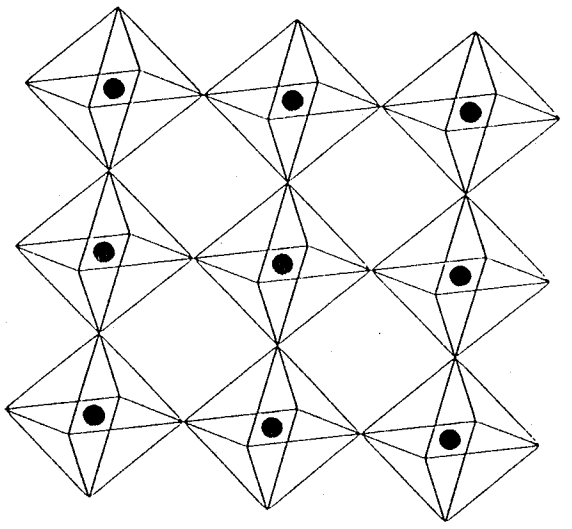

perovskite

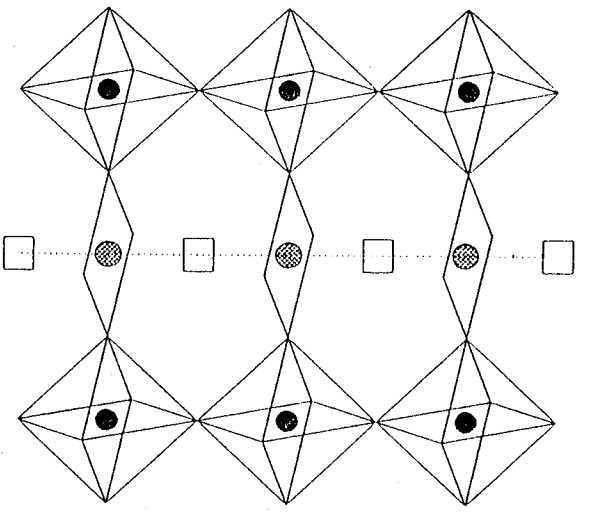

[100]c

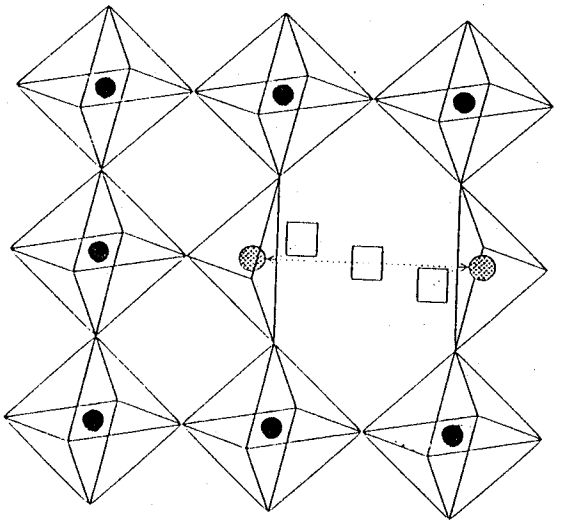

[110]c

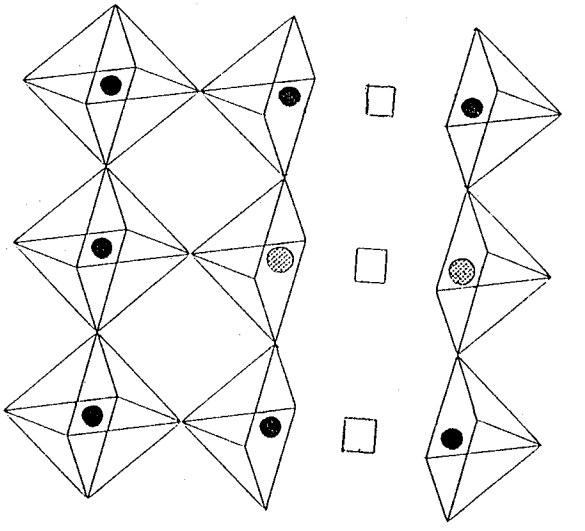

[100]c+[010]c or (001)c

Fig. 1-6 Three common oxygen defect patterns found in oxygen-deficient perovskites. Solid circles and squares represent B cation and oxygen vacancy, respectively.

removal from [110]c rows results in the formation of MO_4 tetrahedra, and removal from (100)c planes results in MO_5 square-pyramids.[19] The compounds in Table 1-1 demonstrate the diversity of vacancy patterns and coordination polyhedra found in oxygen-deficient perovskites.[20,21,22,23,24,25,26,18,27]

The descriptions $A_mB_mO_{3m-x}$ emphasize the relationship to the aristotype, that is, the manner in which the oxide ions have been removed from stoichiometric perovskite. Some of the unit cells have a $\sqrt{2}a_p$ or larger expansion of two axes. The expansion of the cells results from displacement of oxide ions, order of oxygen vacancies, or both. Large supercells can result if both mechanisms are operational. The notation a_p refers to the unit cell edge of cubic perovskite, which is typically 3.8-4.1Å.

Although the cohesive energy of a metal oxide is dominated by spatially isotropic electrostatic interactions, the arrangement of the vacancies within a slice and from slice to slice is largely controlled by spatially anisotropic (directional) covalent interactions of the B cations and oxide ions.[28] The sizes, electronic configurations and coordination preferences of the B cations control the arrangement of vacancies around each B cation and, along with A cation size and coordination preferences. The physical and chemical differences in A and B cations from compound to compound account for the variety of known vacancy patterns.

The structural difference between $Ca_2Mn_2O_5$[20] and $LaSrCuGaO_5$[21] is the prototype demonstrating the influence that electronic configurations and coordination preferences of the B cations have on the manner of the slice of AO_{3-x} which form a pseudocubic closest-packed arrangement, that is, the arrangement of oxygen vacancies. In $Ca_2Mn_2O_5$ (Fig. 7(a)), the manganese cations are all d^4-Mn^{3+} and prefer five-fold square-pyramidal sites rather than six-coordinated and four-coordinated sites as $LaSrCuGaO_5$ (Fig. 7(b)). The slices of AO_{3-x} stack such that the manganese cations take the square-pyramidal coordination. In $LaSrCuGaO_5$, the copper cations are d^9-Cu^{2+}, which are known as Jahn-Teller ions. The gallium cations are d^{10}-Ga^{3+}, which prefer small, spherical pseudotetrahedral sites. There are many examples of Cu^{2+} ions in square-pyramidal or square-planar coordination, but in this case the coordination preference of the smaller gallium ions cause the defects, and the copper ions remain

Table 1-1. Oxygen-deficient Perovskites

$A_mB_mO_{3m-x}$	CN(B cation)	CN(A carion)	B-O polyhedra	EC(B cation)	ref.
m=2					
$Ca_2Mn_2O_5$	5,5	10,10	SSSS	d^4, d^4	21
$LaSrCuGaO_5$	6,4	8,8	OTOT'	d^9, d^{10}	22
$LaSrCuAlO_5$	5,4	8,9	STST'	d^9, d^0	23
$Ca_2Co_2O_5$	5,5	8,12	SSSS	d^6, d^6	24
m=3					
$YBa_2Cu_3O_6$	5,5,2	8,8,8	SLSSLS	d^9, d^{10}, d^9	25
$YBa_2Cu_3O_7$	5,5,4	8,10,10	SPSSPS	d^9, d^8, d^9	26
$LaSr_2Fe_3O_8$	6,6,4	12,8,8	OTOOT'O	d^5, d^5, d^5	27
m=4					
$Ba_2La_2Cu_2Sn_2O_{11}$	5,5,6,6	12,12,12,8	SOOSSOOS	d^9, d^{10}, d^{10}, d^9	19
$Ca_4Ti_2Fe_2O_{11}$	6,6,6,4	10,12,12,10	OTOOOT'OO	d^0, d^5, d^0, d^5	28

CN: coordination number, EC: electron configuration,

O: octahedral, S: square-pyramidal, P: square-planar, T: tetrahedral, L: linear

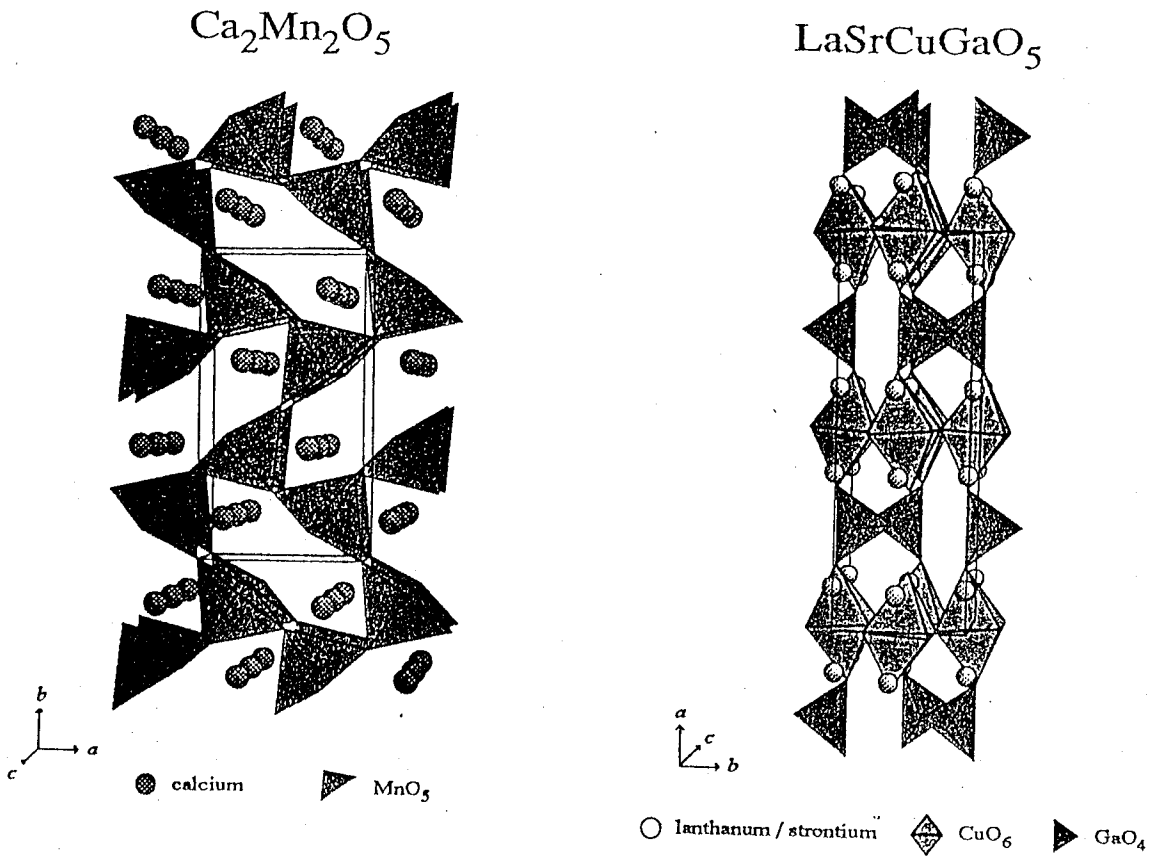

Fig. 1-7 (left): Structure of $Ca_2Mn_2O_5$. (right): Structure of $LaSrCuGaO_5$ named the brownmillerite-type structure.

elongated six-coordinate. The slices of AO_{3-x} such that the copper ions take the elongated octahedral coordination and gallium cations are the tetrahedral coordination. This structure is called the brownmillerite-type one.

The size of the A cation also influences the coordination of B cation by oxide ions. For example, the layered perovskites $La_{2-y}Ln_yCuO_4$ (*Ln*= lanthanide) take three kinds of typical structure depending on the size of *Ln* and the value of y.[4] In case of *Ln*=La, that is La_2CuO_4, the T-type structure with octahedral $CuO_{6/2}$ coordination is stabilized. However, replacement of the La^{3+} ion by a smaller Ln^{3+} ion leads to the T'-type structure with square-planar $CuO_{4/2}$ coordination. If a larger La^{3+} ion is partially replaced by a significantly smaller Ln^{3+}, the pure T- or T'-type structure cannot be stabilized. Instead a new hybrid structure, designated T* with pyramidal $CuO_{5/2}$ coordination, is stabilized.

Purpose of This Study

Although many investigations in connection with defect chemistry in the Ruddlesden-Popper-type nickelates (La_2NiO_4, $La_3Ni_2O_7$ and $La_4Ni_3O_{10}$ *etc.*) have been carried out so far, as described above, there is only two papers reported by Crespin *et al.*[29,30] concerning with the significantly-oxygen-deficient perovskite $LaNiO_{3-x}$ ($0 \leq x \leq 1$). They have reported the existence of $La_2Ni_2O_5$ ($LaNiO_{2.5}$) and $LaNiO_2$ with the infinite-layer structure in reduction of the perovskite-type $LaNiO_3$ to decomposition products of La_2O_3 and nickel metal. Assuming oxidation states +3 and -2 for lanthanum and oxygen, respectively, the average formal valence of nickel in $La_2Ni_2O_5$ and $LaNiO_2$ are +2 and +1, respectively. However, they showed only the TGA data in reduction of $LaNiO_3$ and X-ray diffraction and XAFS data of these reductants. They concluded the brownmillerite-type structure as a model of $La_2Ni_2O_5$, in which the coordination styles of nickel ions are octahedral and ***tetrahedral*** coordinations. After their work, Rao et al. had claimed that the nickel ions in $La_2Ni_2O_5$ are octahedral and ***square-planar*** coordinations,[31,32] from the concept that the $3d^8$-Ni^{2+} ion is stable in the high-spin state when they are coordinated octahedrally or stable in the low-spin state when coordinated square-planarly. Concerning $LaNiO_2$, it is thought that all the nickel ions have monovalent state isoelectric to Cu^{2+} ion which is the base of high-T_c cuprate superconductors. However, Rao et al. never showed the physical properties at all.[31,32]

An electron diffraction study of the oxygen-deficient $LaNiO_{3-x}$ by Gonzalez-Carbet *et al.* shows that compositional variations lead to the formation of new superstructures corresponding to a homologous series of the general formula $La_nNi_nO_{3n-1}$ when x=0.5, 0.33, 0.25 and 0.2, *i.e.*, for n=2 ($La_2Ni_2O_5$), 3 ($La_3Ni_3O_8$) and 4 ($La_4Ni_4O_{11}$), respectively.[33,34] These members can be described as being formed by ordered intergrowths of n-1 octahedral layers alternating with one layer in which Ni^{2+} adopts square-planar coordination. $La_2Ni_2O_5$ and $La_4Ni_4O_{11}$ could have been isolated until now. These oxygen-vacancy-ordered phases are confirmed only by electron diffraction method, not by X-ray diffraction method.

In this study, topotactic reductions of the perovskite-type $LnNiO_3$ were

investigated to elucidate the way of oxygen defect ordering and to characterize the low-valence nickel ion Ni^{+}. Synthesizing and characterizing the compounds with the Ni^{+} ions isoelectronic to Cu^{2+} is required to understand the high-T_c cuprate superconductivity. Regrettably, since the formal valence of nickel ions is divalent or sometimes trivalent, one must prepare the compounds with monovalent nickel ions by topotactic reduction of the parent compounds. The topotactic reduction would induce some kinds of ordering of oxygen vacancies. The array of oxygen vacancies reflects the preference of reduced nickel ions. It is important to examine the local structure around the reduced nickel ions.

In Chapters 2 and 3, the reduction process of the perovskite-type $LaNiO_3$ and was elucidated, and structure and physical properties (especially magnetic property) of the resultant reductants are analyzed. In Chapter 4, substitution effect of La^{3+} to Pr^{3+} or Nd^{3+} on reactivity toward reduction of the perovskite-type $LnNiO_3$ was studied. The smaller ion prefers the smaller coordination number. The produced square-planarly coordinated nickel ions in $LnNiO_{3-x}$ (Ln=Pr and Nd) would be more stabilized, as seen in T- and T'-types Ln_2CuO_4. The relationship between the electronic states of nickel ions and the local structures or coordination states around the nickel ions were also investigated through these chapters. Finally, in Chapter 5, the general discussion is given based on the information of Chapters 2, 3, and 4.

References

[1] Z.Kakol, J.Spalek, and J.M.Honig, *J. Solid State Chem.*, **79**, 288 (1989).

[2] J.Spalek, Z.Kakol, and J.M.Honig, *Solid State Commun.*, **71**, 511 (1989).

[3] H.A.Blackstead, D.B.Pulling, J.Spalek, and J.M.Honig, *Solid State Commun.*, **80**, 405 (1991).

[4] T.P.Sheahen, " Introduction to High-Temperature Superconductivity", Plenum Press, New York (1994).

[5] D.J.Buttrey, J.M.Honig, and C.N.R.Rao, *J. Solid State Chem.*, **64**, 287 (1986).

[6] P.Gopalan, M.W.McElfresh, Z.Kakol, J.Spalek, and J.M.Honig, *Phys. Rev. B*, **45**, 249 (1992).

[7] J.D.Jorgensen, B.Dabrowski, P.Shiyou, D.R.Richards, and D.G.Hinks, *Phys. Rev. B*, **40**, 2187 (1989).

[8] J.Rodrigues-Carvajal, M.T.Fernandez-Diaz, and J.L.Martinez, *J. Phys.: Condens. Matter*, **3**, 3215 (1991).

[9] K.Yamada, T.Omata, K.Nakajima, S.Hosoya, T.Sumida, and Y.Endoh, *Physica C*, **191**, 15 (1992).

[10] R.R.Schartman and J.M.Honig, *Mater. Res. Bull.*, **24**, 671 (1989).

[11] T.Freltoft, D.J.Buttrey, G.Aeppli, D.Vaknin, and G.Shirane, *Phys. Rev. B*, **44**, 5046 (1991).

[12] M.Crespin, J.M.Bassat, P.Odier, P.Mouron, and J.Choisnet, *J. Solid State Chem.*, **84**, 165 (1990).

[13] M.Crespin, C.Landron, P.Odier, J.M.Bassat, P.Mouron, and J.Choisnet, *J. Solid State Chem.*, **100**, 281 (1992).

[14] P.H.Lacorre, *J. Solid State Chem.*, **97**, 495 (1992).

[15] C.N.R.Rao and B.Raveau, "Transition Metal Oxides", VCH Publishers, New York (1995).

[16] Z.Zhang, M.Greenblatt, and J.B.Goodenough, *J. Solid State Chem.*, **108**, 402 (1994).

[17] K.Sreedhar, M.McElfresh, D.Perry, D.Kim, P.Metcalf, and J.M.Honig, *J. Solid State Chem.*, **110**, 208 (1994).

[18] M.T.Anderson, J.T.Vaughey, and K.R.Poeppelmeier, *Chem. Mater.*, **5**, 151 (1993).

[19] J.A.M.van Roosmalen and E.H.P.Cordfunke, *J. Solid State Chem.*, **93**, 212 (1991).

[20] K.R.Poeppelmeier, M.E.Leonowicz, and J.M.Longo, *J. Solid State Chem.*, **44**, 89

(1982).

[21] J.T.Vaughey, J.B.Wiley, and K.R.Poeppelmeier, *Z. Anorg. Allg. Chem.*, **598/599**, 327 (1991).

[22] J.B.Wiley, M.Sabat, S.J.Hwu, K.R.Poeppelmeier, A.Reller, and T.Williams, *J. Solid State Chem.*, **87**, 250 (1990).

[23] K.Vidyasagar, J.Gopalakrishnan, and C.N.R.Rao, *Inorg. Chem.*, **23**, 1206 (1984).

[24] P.Bordet, C.Chaillout, J.J.Capponi, J.Chenavas, and M.Narezio, *Nature*, **327**, 687 (1987).

[25] M.A.Beno, D.W.Soderholm, D.W.Capone, J.D.Jorgensen, K.I.Schuller, C.U.Serge, K.Zhang, and D.J.Grace, *Appl. Phys. Lett.*, **51**, 57 (1987).

[26] P.D.Battle, T.C.Gibb, and P.Lightfoot, *J. Solid State Chem.*, **84**, 237 (1990).

[27] J.M.Gonzalez-Carbet and M.Vallet-Regi, *J. Solid State Chem.*, **68**, 266 (1987).

[28] C.N.R.Rao and J.Gopalakrishnan, " New directions in Solid State Chemistry", Canbridge University Press, New York (1989).

[29] M.Crespin, P.Levitz, and L.Gatineau, *J. Chem. Soc., Faraday Trans. 2*, **79**, 1181 (1983).

[30] P.Levitz, M.Crespin, and L.Gatineau, *J. Chem. Soc., Faraday Trans. 2*, **79**, 1195 (1983).

[31] K.Vidyasagar, A.Reller, J.Gopalakrishnan, and C.N.R.Rao, *J. Chem. Soc., Chem. Commun.*, **1985**, 7 (1985).

[32] C.N.R.Rao, J.Gopalakrishnan, K.Vidyasagar, A.K.Ganguli, A.Ramanan, and L.Ganapathi, *J. Mater. Res.*, **1**, 280 (1986).

[33] J.M.Gonzalez-Carbet, M.J.Sayagues, and M.Vallet-Regi, *Solid State Ionics*, **32/33**, 721 (1989).

[34] M.J.Sayagues, M.Vallet-regi, A.Caneiro, and J.M.Gonzalez-Carbet, *J. Solid State Chem.*, **110**, 295 (1994).

Chapter 2.

Synthesis of Oxygen-Deficient Lanthanum Nickelates $LaNiO_{3-x}$ ($0 \leq x \leq 0.5$) and Their Magnetic Properties

Introduction

Copper oxides of the perovskite-type and related structures, such as La_2NiO_{4+x}, have been extensively studied with regards to superconductivity in the latest decade.[1,2,3,4] A non-copper oxide superconductor has not yet been found among transition metal oxides, except for $Li_{1+x}Ti_{2-x}O_4$.[5] Nickel double oxides with a perovskite-related structure are antiferromagnetic, similar to copper oxides.

Metallic conductivity with Pauli-paramagnetism has been observed in trivalent nickelate $LaNiO_3$.[6] $LaNiO_3$ has a rhombohedrally-distorted perovskite-type structure isostructural with $LaCuO_3$. In the perovskite-type structure, oxygen content directly affects the magnetic and electrical properties. Control of the valence state of nickel ions without changing the basic structure would enable one to produce novel and interesting magnetic and electrical properties. Crespin et al. have reported that a low-temperature reduction of $LaNiO_3$ under H_2 gas has led to a new compound, $La_2Ni_2O_5$, which could be indexed in the monoclinic system with the following parameters: a=11.068, b=11.168, c=7.824Å, and β= 92.21°.[7,8] They proposed the structural model of $La_2Ni_2O_5$ with Ni^{2+} ions located in both distorted octahedra and tetrahedra, *i.e.*, a brownmillerite-type structure, determined by powder X-ray diffraction data. They also reported the presence of $LaNiO_2$ with monovalent Ni^+ ions. $LaNiO_2$ is considered to be isostructural with an infinite-layer superconductor (Ca, Sr)CuO_2[9] or (Sr, La)CuO_2[10]. Rao et al. indexed the $La_2Ni_2O_5$ with a tetragonal cell of a=7.816 and c=7.468Å and deduced that it had a new type of ordering with octahedra and square-planar coordinations of Ni^{2+} ions[11,12]. An electron diffraction study of the $LaNiO_{3-x}$ ($0 \leq x \leq 0.5$) system by Gonzalez-Calbet et al., showed the existence of a family of phases with the general formula $La_nNi_nO_{3n-1}$[13]. Although their structural model for $La_2Ni_2O_5$ basically agreed with Rao's one, their diffraction pattern could be indexed by Crespin's monoclinic unit cell rather than Rao's. Detail crystal structural information is required. These authors gave little information about the magnetic and electrical properties of $La_2Ni_2O_5$ and its related phase with a chemical composition of around $LaNiO_{2.5}$.

In this chapter, oxygen-deficient $LaNiO_{3-x}$ phases were synthesized by a

topotactic reduction of $LaNiO_3$ in H_2 flow at low temperatures. A Rietveld structural refinement of $La_2Ni_2O_5$ was carried out on powder X-ray diffraction data. The magnetic properties were measured and discussed in relation to the reduction process of $LaNiO_3$ to $La_2Ni_2O_5$.

Experimental

A polycrystalline sample of $LaNiO_3$ was prepared by a coprecipitation method. A solid-state reaction between La_2O_3 and NiO gave significant amounts of La_2NiO_4 and NiO as impurities. Then the coprecipitation method was applied using aqueous solutions of $La(NO_3)_3 \cdot 6H_2O$ and $Ni(NO_3)2 \cdot 6H_2O$ as starting materials. An aqueous solution of tetramethylammonium hydroxide ($2.8 mol \cdot dm^{-1}$) was added to form a sol of 1:1 metallic hydroxide. After washing with ethanol to remove organic materials, the coprecipitant was dried at 200°C in air and fired at 850°C in and O_2 flow for 30h to obtain the rhombohedral $LaNiO_3$.

$LaNiO_3$ was reduced in H_2 and N_2 gas mixtures with appropriate molar-rations at various temperatures from 275 to 400°C. The specimen used for the Rietveld analysis was obtained by annealing the reduced one in diluted H_2 gas (H_2:N_2=1:99, abbreviated 1%-H_2/N_2 gas hereafter) at 350° for 16h to improve its crystallinity. The gas flow rate was about $15 cm^3 min^{-1}$. Powder X-ray diffraction data were collected using a Rigaku RAD-RB diffractmeter with monochromatized CuKα radiation (50kV-150mA). A step scan technique was applied in the measurements within the 2θ range from 20 to 100° for Rietveld analysis. The stepping angle was 0.02° and the measurement time was 10s at each point. A simulation of the X-ray diffraction patterns and the Rietveld analysis were carried out using the program "RIETAN" provided by F.Izumi[14]. The oxygen contents of the samples were analyzed using a Horiba EMGA-2800 device. The samples were reduced in a carbon crucible to convert their oxygen to carbon monoxide in He as a carrier gas. The amount of carbon monoxide was determined by measuring the IR absorbance.

The magnetic susceptibility was measured in the temperature range between 77 and 473K by the Faraday method at a magnetic field strength of 0.9T. Corrections were made in order to compensate for the diamagnetic susceptibility of the silica-glass sample bucket and the reduced specimens (*e.g.* χ_{dia}=$-6.1 \times 10^{-5} emu \cdot mol^{-1}$ in $LaNiO_{2.5}$).

XAFS (X-ray absorption fine structure) spectra near Ni K-edge were measured at BL-7C branch line with Si(111) double monochromator in the Photon Factory, KEK.

The samples were dispersed in hexagonal boron nitride and pressed into pellets. data were collected in a transmittance mode with upstream slits set at 0.3mm x 5mm and nitrogen-filled ionization chambers were used as detectors. Analyses of the XAFS data were performed with the Program Library provided by H.Sakane. In this work, XANES (X-ray absorption near edge structure) region of XAFS spectra was analyzed, from which information on coordination geometry or symmetry can be obtained.

XPS (X-ray photoelectron spectroscopy) measurements were conducted for powdered samples pressed into a disk form immediately before the analysis. The instrument used was a Shimadzu ESCA-1000 device with MgKα radiation (10kV-30mA). The resolution of the concentric hemispherical analyzer was higher than 0.1eV. The binding energy measured (E_b) was calibrated with reference to the C1s level (284.8eV). A 20-seconds' Ar-etching was performed on the surface of the sample before measurement to remove contaminations on the surface. The Ar-etching for the sample was carried out at a source power of 2kV-20mA to remove contaminations on the surface.

Results and Discussion

Variation of powder X-ray diffraction patterns, XANES spectra, and magnetic susceptibilities from $LaNiO_3$ to $La_2Ni_2O_5$

Powder X-ray diffraction patterns of rhombohedrally-distorted perovskite-type $LaNiO_3$ and its reduced samples at 275°C in H_2 flow for 4 and 8h are shown in Fig.2-1, respectively. The oxygen content z in $LaNiO_{2.5+z}$ of the reduced specimens were 0.04 and 0.01. All of the diffraction peaks of the product reduced for 8h were consistent with those of $La_2Ni_2O_5$ reported by Crespin et al.[7] However, there were small peaks which could be ascribed to neither $LaNiO_3$ nor $La_2Ni_2O_5$ in the 4h-reduced specimen. They were denoted as the asterisks in the figure.

Figure 2-2 shows the Ni K-edge XANES spectra of $LaNiO_{3-x}$. The spectrum for $LaNiO_3$ showed absorption peak in the pre-edge region observed at *ca.* 8333eV, which can be assigned to the 1s→3d transition. This peak decreased in intensity and faded away in the specimens reduced for more than 2h. A new peak assigned to the 1s→4p one appeared clearly in the spectra reduced for more than 1h at *ca.* 8338eV. The 1s→3d transition would be expected to appear as a relatively small peak associated with octahedral and square-planar geometries and a fairly intense absorption for tetrahedral and pyramidal complexes.[15] The 1s→4p transition appears rather strongly in the planar Ni ion, but is not observed in the octahedral one.[15] The variation in these XANES spectra, therefore, indicates that the planar coordination is mainly formed even in the specimen reduced for 1h, and not the pyramidal or the tetrahedral one.

The magnetic properties were quite different between two kinds of the reduced specimens, as shown in Fig. 2-3. Although both specimens showed antiferromagnetic behavior below 140K, an abrupt change in the susceptibility was found at about 230K in the 4h-reduced specimen. The phase giving the small diffraction peaks is thought to be responsible for this magnetism. Small amount of excess oxygen would lead to the ferromagnetic phase. The ferromagnetic phase appeared in an early step of the reduction was also obtained by the reduction in a diluted H_2 flow, as described later.

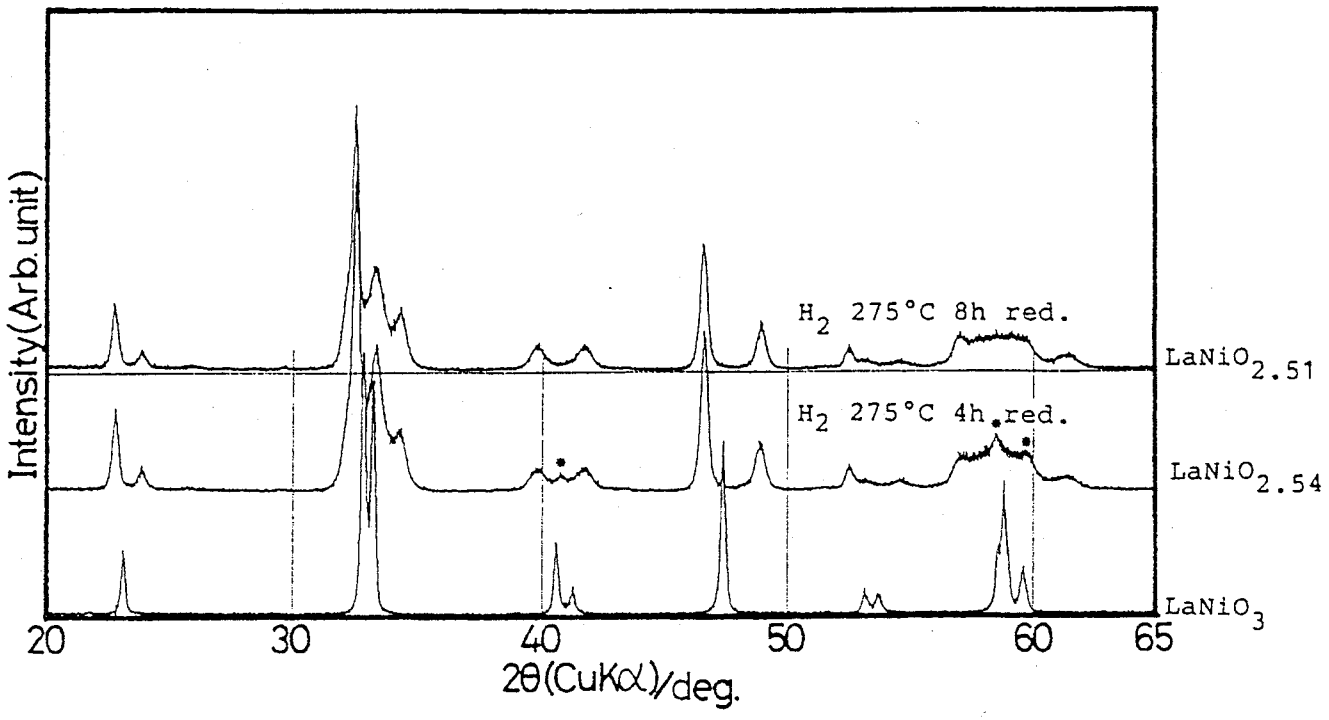

Fig. 2-1 Powder X-ray diffraction patterns of $LaNiO_{3-x}$ reduced under H_2 gas flow at 275°C. The asterisks represent the peaks which could not be ascribed to either $LaNiO_3$ nor $LaNiO_{2.5}$ reported by Crespin et al.

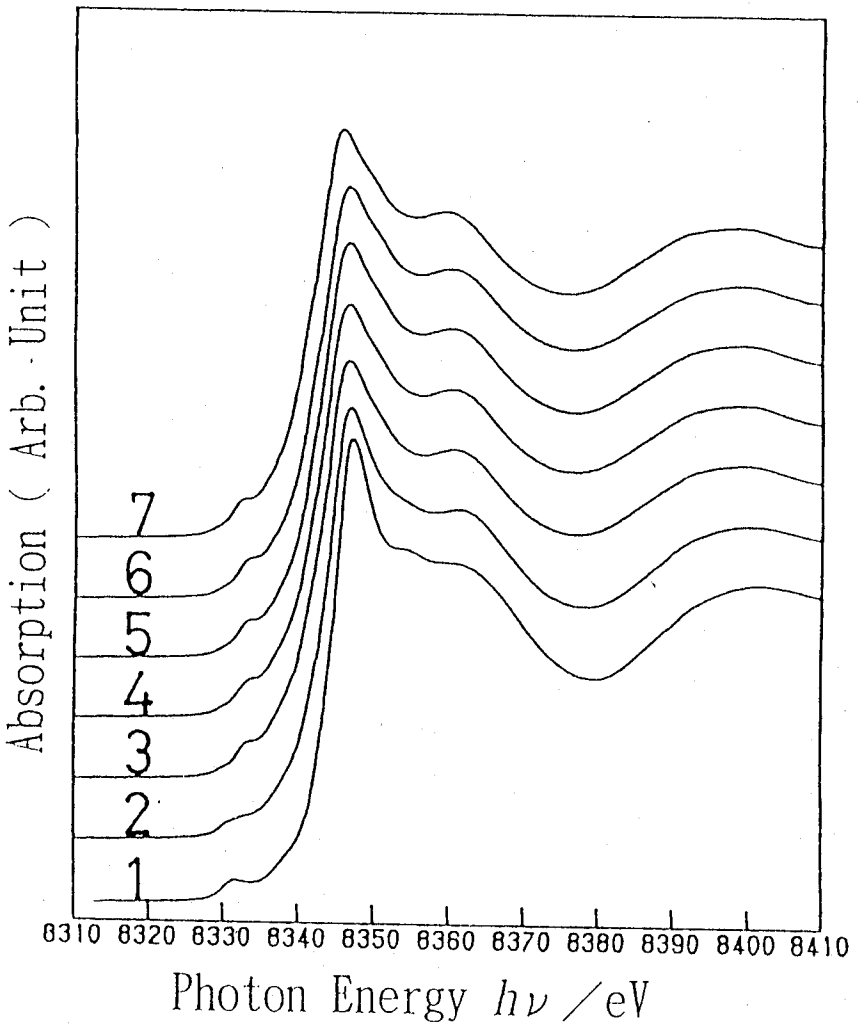

Fig. 2-2 The Ni K-edge XANES spectra of $LaNiO_{3-x}$. 1: $LaNiO_3$, 2: $LaNiO_{2.69}$, 3: $LaNiO_{2.59}$, 4: $LaNiO_{2.57}$, 5: $LaNiO_{2.54}$, 6: $LaNiO_{2.51}$, and 7: $LaNiO_{2.48}$.

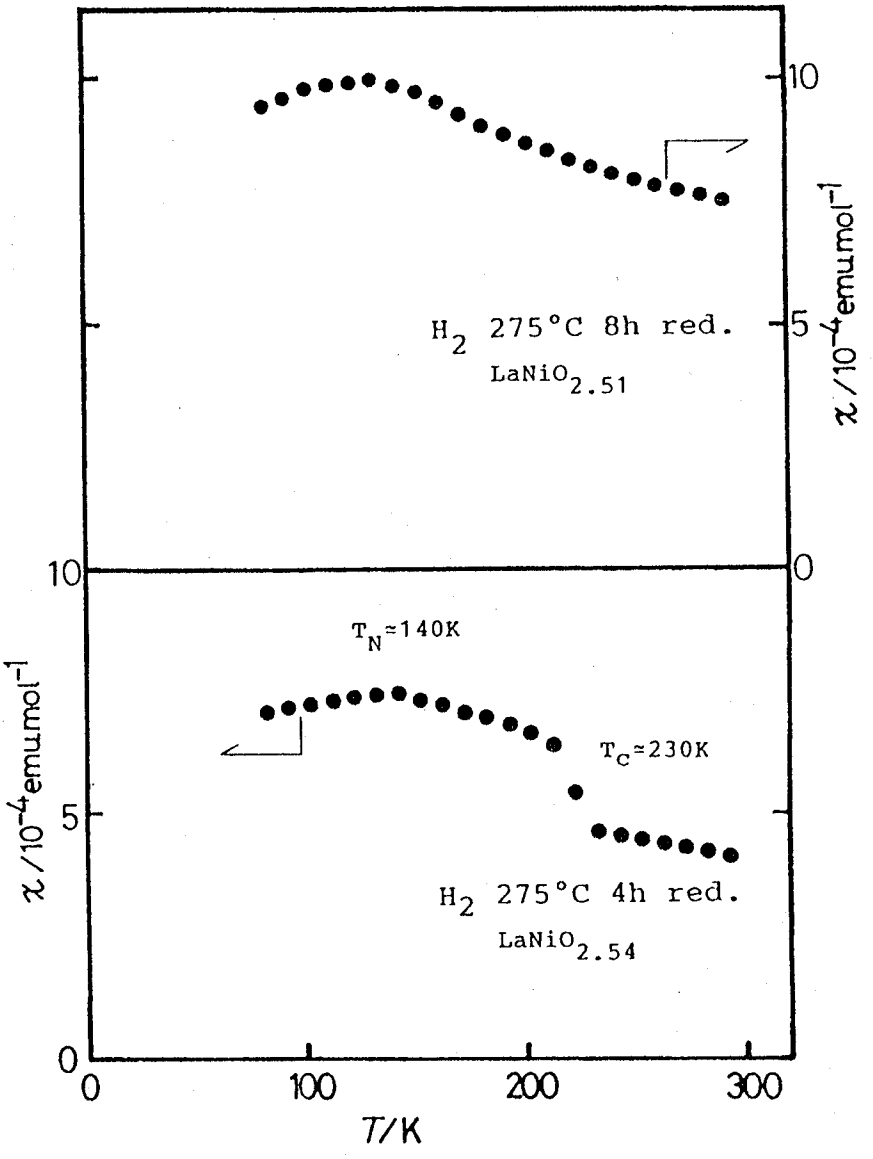

Fig. 2-3 Variations of the magnetic susceptibility in $LaNiO_{3-x}$ as a function of temperature.

A further reduction led to La_2O_3 and an amorphous-like phase of nickel metal. Crespin et al. reported the presence of $LaNiO_2$ having monovalent nickel ions which is isoelectronic to Cu^{2+}.[8] It was not obtained in the present experiment. Recently, Rakshit and Gopalakrishnan have pointed out that $LaNiO_3$ containing sodium impurity and the sodium-free $LaNiO_3$ differ in the manner in which they are reduced by H_2 gas.[16] The former is converted to $La_2Ni_2O_5$ and then to $LaNiO_2$, whereas the latter gives $La_2Ni_2O_5$ and then a mixture of La_2O_3 and Ni metal. That is, the formation of pure $LaNiO_2$ containing only Ni^+ ions is doubtful.

Crystal Structure and Magnetic Property of $LaNiO_{2.5}$

Since the as-reduced specimen under H_2 gas flow at 275°C for 16h had poor crystallinity, it was annealed under 1%-H_2/N_2 gas at 350°C for 30h. The oxygen content of the product was $LaNiO_{2.48}$. This product could be indexed with a monoclinic cell of $a\simeq7.83$, $b\simeq7.80$, $c\simeq7.47$Å, and $\beta\simeq93.7°$, related to the primitive cubic perovskite by an expression of $2a_p$ x $2a_p$ x $2a_p$, though Rao et al. indexed the $La_2Ni_2O_5$ with a tetragonal cell having almost the same lattice lengths.[11] A refinement of this structure proceeded by assuming a space group of $C_{2/c}$[17] (unique axis *b*, cell choice 1) and the ideal composition of $LaNiO_{2.50}$. Initial coordinates were taken as follows: La, 8(f), (x,y,z), $x\simeq y\simeq z\simeq0.25$; Ni(1), 4(a), (0,0,0); Ni(2), 4(b), (0,1/2,0); O(1), 8(f), (x,y,z), $x\simeq0.25$, $y\simeq z\simeq0$; O(2), 8(f), (x,y,z), $x\simeq z\simeq0$, $y\simeq0.25$; O(3), 4(e), (0,y,1/4), $y\simeq0$. The refinement was carried out in stage by stage; the atomic coordinates were fixed in initial calculations, but were subsequently allowed to vary after the scale, background, half-width and unit cell parameters so as to be close to their optimum values; finally, the thermal parameters were varied. When the isotropic thermal parameters were refined, those for the O(1), O(2), and O(3) sites had to be constrained to the same value. The preferred-orientations of the sample were not taken into account. The observed, calculated and difference plots of the result in the Rietveld analysis of $LaNiO_{2.48}$ are shown in Fig. 2-4. The final parameters for the refinement are summarized in Tables 2-1 and 2-2. The reliability factors exhibit rather high values, which may be due to the poor crystallinity for the Rietveld analysis. The integrated diffraction

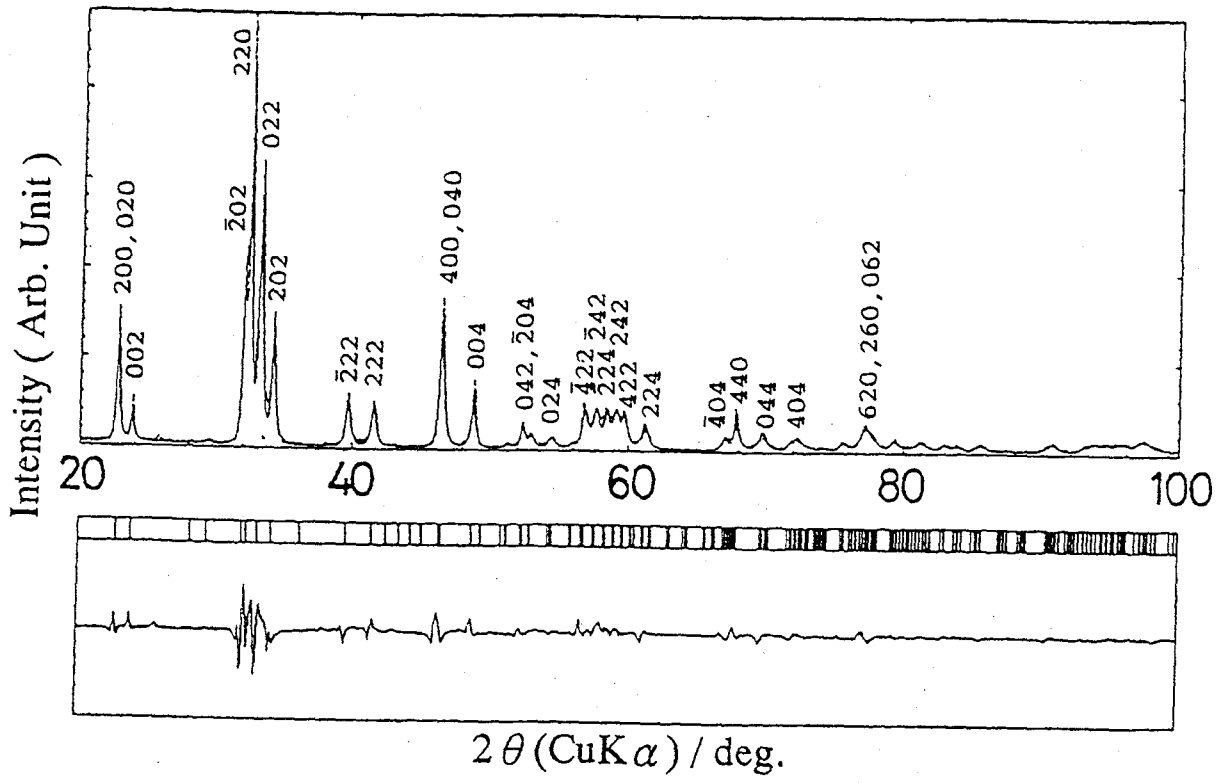

Fig. 2-4 Observed and calculated diffraction patterns, and their difference plot as a result of Rietveld analysis of $La_2Ni_2O_5$.

Table 1. Some Crystallographic Data Obtained by the Rietveld Refinement of $LaNiO_{2.48}$

Ideal composition	$LaNiO_{2.5}$		
Space group	$C2/c$		
Scale factor	0.00152(2)	Lattice constant a/Å	7.8329(8)
FWHM parameter U	1.8(3)	b/Å	7.7971(9)
V	−0.16(2)	c/Å	7.4739(7)
W	0.13(3)	β/°	93.693(6)
Asymmetry parameter	−0.13(1)	R_F/%[a]	2.65
Gaussian fraction	0.19(2)	R_p/%[b]	12.04
FWHM(Gauss)/		R_{wp}/%[c]	13.60
FWHM(Lorentz)	2.10(9)	R_e/%[d]	5.05
		R_I/%[e]	5.74

a) $R_F = \Sigma_k|[I_k(\mathrm{obs})]^{1/2} - [I_k(\mathrm{cal})]^{1/2}|/\Sigma_k[I_k(\mathrm{obs})]^{1/2}$, where $I_k(\mathrm{obs})$ and $I_k(\mathrm{cal})$ are the integrated observed and calculated intensities, respectively. b) $R_p = \Sigma_i|y_i(\mathrm{obs}) - y_i(\mathrm{cal})|/\Sigma_i y_i(\mathrm{obs})$, where $y_i(\mathrm{obs})$ and $y_i(\mathrm{cal})$ are the observed intensity and the calculated one, respectively. c) $R_{wp} = \{\Sigma_i w_i[y_i(\mathrm{obs}) - y_i(\mathrm{cal})]^2/\Sigma_i w_i y_i(\mathrm{obs})^2]\}^{1/2}$. d) R_e is the expected R_{wp}. e) $R_I = \Sigma_k|I_k(\mathrm{obs}) - I_k(\mathrm{cal})|/\Sigma_k I_k(\mathrm{obs})$.

Table 2. Positional and Isotropic Thermal Parameters of $LaNiO_{2.48}$

Atom	Position[a]	x	y	z	B/Å^2
La	8(f)	0.248(2)	0.241(2)	0.247(3)	0.43(17)
Ni(1)	4(a)	0	0	0	1.2(4)
Ni(2)	4(b)	0	1/2	0	1.0(2)
O(1)	8(f)	0.23(2)	0.06(1)	0.01(1)	2.3(14)[b]
O(2)	8(f)	−0.03(1)	0.27(1)	−0.01(1)	2.3[b]
O(3)	4(e)	0	0.01(2)	1/4	2.3[b]

a) Multiplicity and Wyckoff notation. b) Thermal parameters for oxygens were constrained to be equal each other.

intensities agreed well between the observed and calculated values.

Figure 2-5 shows a schematic representation of the structure of $La_2Ni_2O_5$. this compound comprises one-dimensionally linked NiO_6 octahedra along the *c*-axis and NiO_4 square-planes connecting the octahedra chains. The structure is basically the same as that of Rao's model.[11] However, it was found that the neighboring NiO_6 octahedra are slightly tilted and rotated in opposite directions. As mentioned above, its Ni K-edge XANES spectrum supports the presence of 4-fold square-planar Ni ions, not 4-fold tetrahedral ones. From another point of view, infinite $[NiO_{4/2}]$ layers can be considered to form the *ab*-planes, where /2 means that the neighboring polyhedra are corner-shared with each other.

Valence States of Ni ions in $LaNiO_{2.5}$

The interatomic Ni(1)-O distances obtained by the Rietveld analysis were 1.85Å (to O(1) in the $[NiO_{4/2}]$ plane), 2.12Å (O(2) in the plane) and 1.87Å (to O(3) perpendicular to the $[NiO_{4/2}]$ plane), respectively. The Ni(2)-O distances were 1.86Å (to O(2)) and 2.13Å (to O(1)). The distortions of the $[NiO_{6/2}]$ octahedra and the $[NiO_{4/2}]$ square-planes are appreciably large. A schematic drawing of the Ni-O coordination is shown in Fig. 2-6. An alternate arrangement of the longer and shorter Ni-O bond lengths in the $[NiO_{4/2}]$ plane was found. This manner is characteristics of a two-dimensional cooperative Jahn-Teller ordering, as seen in the perovskite-type $LaMnO_3$ with the d^4-Mn^{3+} ion.[18]

Two types of possible valence states of Ni ions in $La_2Ni_2O_5$ can be considered. One is that Ni^{2+} ions adopt a 6-fold octahedral and a 4-fold square-planar coordinations in the same proportion. Ni^{2+} ions have $3d^8$ electrons. The Ni^{2+} ion in an octahedral site is generally stable in the high-spin state with two unpaired electrons in the e_g orbitals. That in the center of a square-plane is stable in the low-spin state without any unpaired electrons. The cooperative Jahn-Teller ordering can arise only with high-spin d^4-, d^9- and low-spin d^7-transition-metal cations, which have one e_g electron.[18,19] In both coordination styles of the Ni^{2+} ions mentioned above, the cooperative Jahn-Teller ordering would

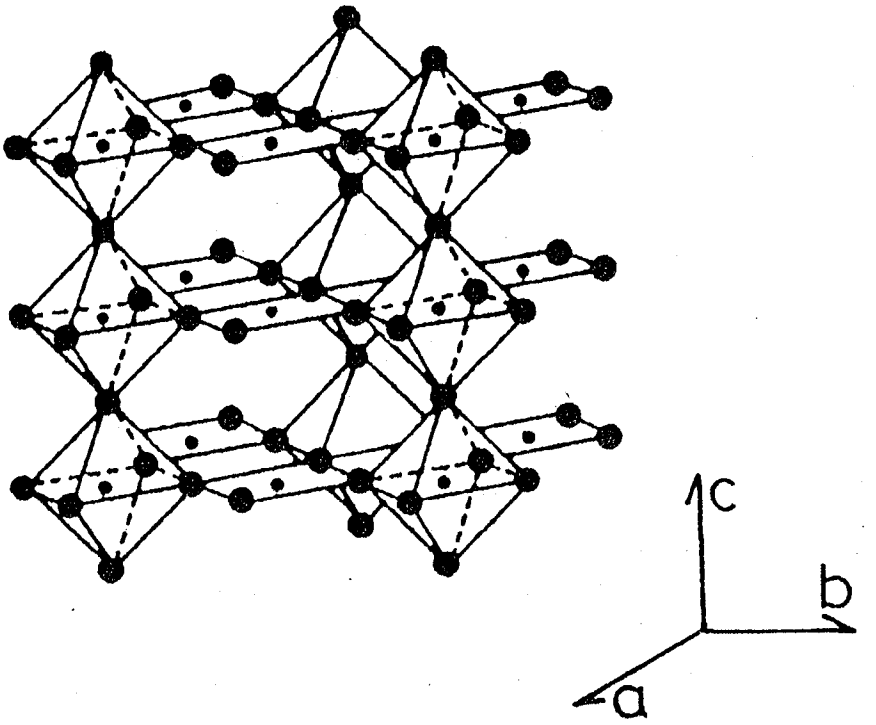

Fig. 2-5 Schematic representation of the structure of $LaNiO_{2.5}$. The large and small solid circles indicate oxide ions and Ni ions, respectively. Lanthanum ions are not shown for simplicity.

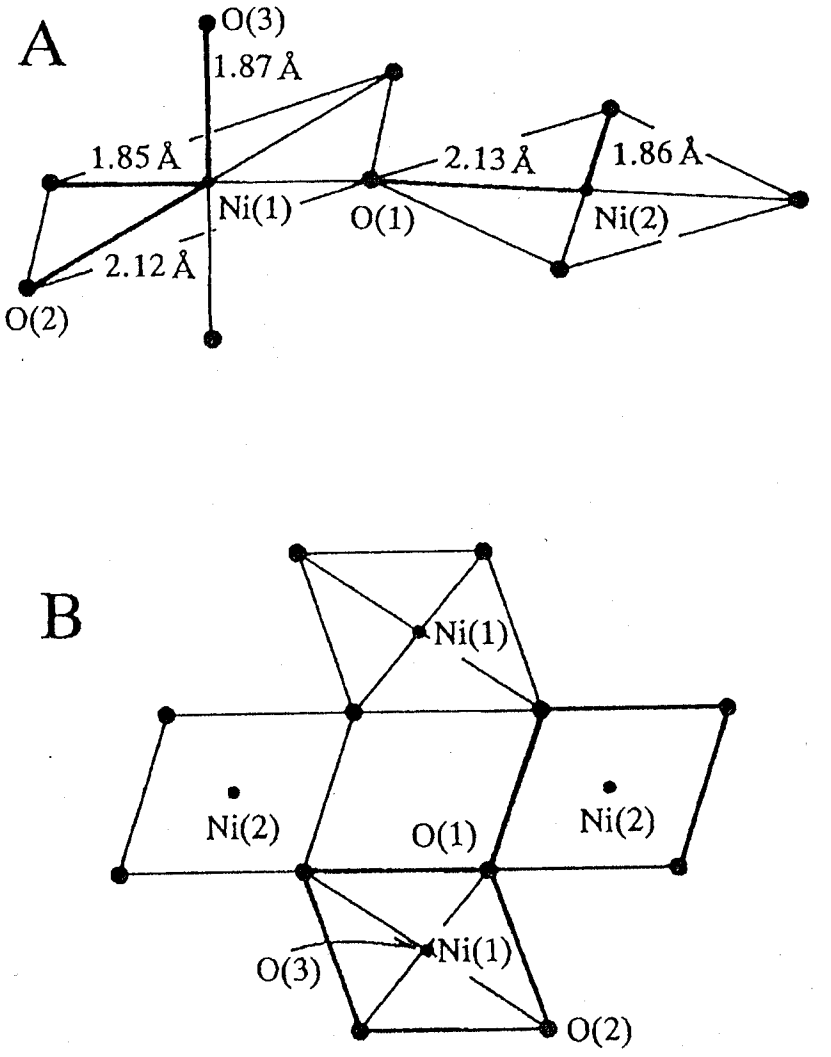

Fig. 2-6 A) Coordination polyhedra, $Ni(1)O_6$ and $Ni(2)O_4$, and Ni-O distances in $La_2Ni_2O_5$. B) Schematic view of the polyhedra from the *c*-axis.

hardly occur. The other is that the Ni^{3+} ion with $3d^7$ electrons adopts a 6-fold octahedral coordination and Ni^{+} ion with $3d^9$ electrons adopts a 4-fold square-plane in analogy with Cu^{2+} ion. The low-spin d^7-Ni^{3+} and d^9-Ni^{+} ions are of the Jahn-Teller types. It might be better to consider that the Ni(1) ions adopt a trivalent state in the octahedral coordination and that the Ni(2) ions adopt a monovalent state in the square-planar coordination.

The observed average interatomic Ni^{3+}(1)-O distance in this octahedron is 1.946Å. This value agrees well with that of 1.91Å, which is the effective ionic radius sum between the 6-fold Ni^{3+} ion with a low-spin state and the 2-fold O^{2-} ion.[20] The observed Ni^{+}(2)-O distance in this square-plane is 1.995Å. on the average. A gain of one electron increases the Ni-O distance by ca. 0.1Å.[8] The Ni^{+}-O distance can, therefore, be expected to be 1.94Å, as follows:

0.49Å (square-planar Ni^{2+}) + 0.1Å (increment) + 1.35A (2-fold O^{2-}) = 1.94A.

The distance between Ni^{+}-O ions in $LaNiO_2$ determined by XAFS was reported to be 1.985Å.[8] The observed value agrees well with both the expected and reported values. The Ni^{2+}-O distance in an octahedron with a high-spin state is estimated to be 2.04Å, while that in a square-plane is estimated to be 1.84Å. These values cannot explain the observed bond distances obtained in the present investigation. Compounds containing Ni^{+} ions have been known only in $LaNiO_2$ (presence of this compound is thought to be doubtful!),[8] $(La_{1.6}Sr_{0.4})NiO_{3.5}$,[21] and $LaSrNiO_{3.1}$.[22] Crespin et al., who had first synthesized $La_2Ni_2O_5$,[7] paid little attention to the valence states of the Ni ions. A comparison of the interatomic distance clarifies the presence of two kinds of Ni ions in $La_2Ni_2O_5$. It is very interesting that two kinds of the Ni ions coexist, having a difference of 2 in valence electrons. Such a disproportionation was reported in the perovskite-type $CaFeO_3$ by Mössbauer spectroscopy, in which Fe^{4+} ions disproportionate into Fe^{3+} and Fe^{5+} ions below 290K.[23]

Figure 2-7 represents the XPS spectra of $LaNiO_{3-x}$ in a binding energy region of 848 to 866eV. The $Ni2p_{3/2}$ photoline of the spectrum of $LaNiO_3$ appeared at 855.5eV (in Fig. 2-7a), which is in a good agreement with that in a previous report.[24] The photoline at 851.0eV was assigned to $La3d_{3/2}$. The binding energy of $Ni2p_{3/2}$ in Ni_2O_3 has been reported to be 855.9eV[25]. The Ni ions in $LaNiO_3$ take only the trivalent state. Therefore,

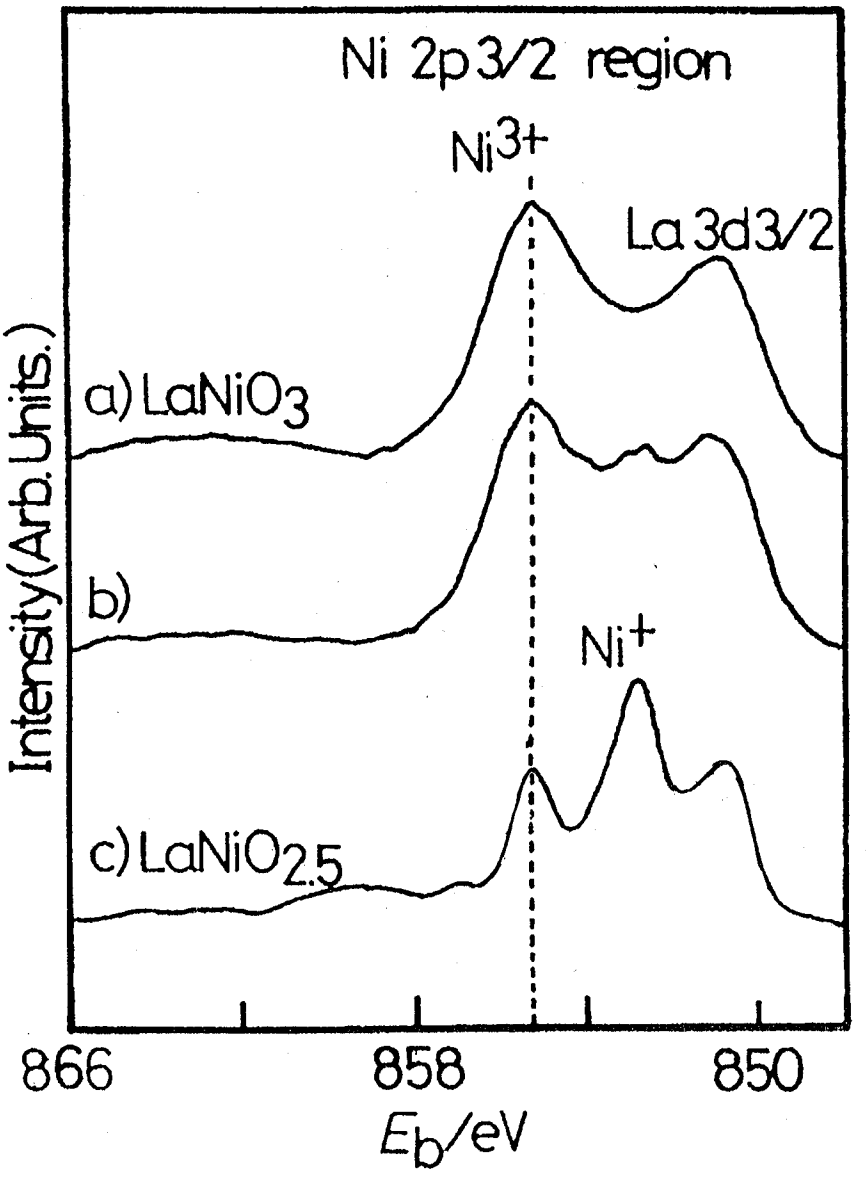

Fig. 2-7 Narrow scan XPS spectra in Ni2p3/2 region of a) $LaNiO_3$, b) Ar-etched $LaNiO_3$ for 3 min, and c) $La_2Ni_2O_5$.

the observed line at 855.5eV is attributable to the Ni_{3+} ion in $LaNiO_3$. After 3 min of Ar-etching, a novel and slight line at 852.5eV appeared (Fig. 2-7b). It may be due to a reduction of Ni ions. The doublet photolines in the $Ni2p_{3/2}$ region of $La_2Ni_2O_5$ were observed at binding energies of 855.6 and 852.5eV (Fig. 2-7c). The line assigned to $La3d_{3/2}$ was not clearly observed. The former line has the same energy as the Ni^{3+} ion. The energy of the latter is lower than that of divalent Ni^{2+} (853.5-854.0eV in NiO),[25] and almost equal to that of Ni metal (852.5eV).[25] However, neither diffraction peaks nor ferromagnetism at room temperature due to Ni metal were detected in this specimen. It is reasonable to consider that the latter photoline is attributable to the Ni^{+} ion. At least two kinds of valence states of Ni ions coexisted in $La_2Ni_2O_5$. One is Ni^{3+} and the other is lower than Ni^{2+}, which may be Ni^{+}.

Magnetic Property of $La_2Ni_2O_5$

Figure 2-8 represents the temperature dependence of the magnetic susceptibility of $LaNiO_{2.48}$. Its susceptibility almost obeyed a Curie-Weiss behavior above 140K, and the effective magnetic moment was $1.8\mu_B$ per Ni ion. Since the Ni^{3+} ion in the low-spin state has one unpaired electron., the total spin angular momentum (S) is 1/2. That of the Ni^{+} ion with one unpaired electron is also 1/2. The effective magnetic moment calculated from the ideal $LaNiO_{2.5}$ with these spin configurations is $1.73\mu_B$ per Ni ion. This value is in a good agreement with the observed one.

The ordered arrangement of the d_{x2-y2} and d_{z2} orbitals in the $[NiO_{4/2}]$ plane in the structure of $LaNiO_{2.5}$ is shown in Fig. 2-9. Here, in case of discussing on the local arrangements of the orbitals of the Ni ions, the elongated axis in the NiO_6 octahedron or NiO_4 square-plane is defined as the z-axis for convenience. The cooperative Jahn-Teller effect makes the d_{z2} orbital of the Ni^{+} ion directed to the d_{x2-y2} one of the Ni^{3+} ion in the $[NiO_{4/2}]$ plane. In a similar matter, the d_{z2} orbital of the Ni^{3+} ion directs to the d_{x2-y2} of the Ni^{+} ion. As the Ni-O distance along the d_{z2} orbital is elongated compared to that along the d_{x2-y2} one, the potential energy of d_{z2} is lower than that of d_{x2-y2}. It is naturally that the d_{z2} orbital of Ni^{3+} ion has one electron and the d_{x2-y2} has no electrons. Similarly, d_{z2} orbital of Ni+ ion is fully occupied and the d_{x2-y2} has one electron. That is, in Fig. 2-9, Ni ions with

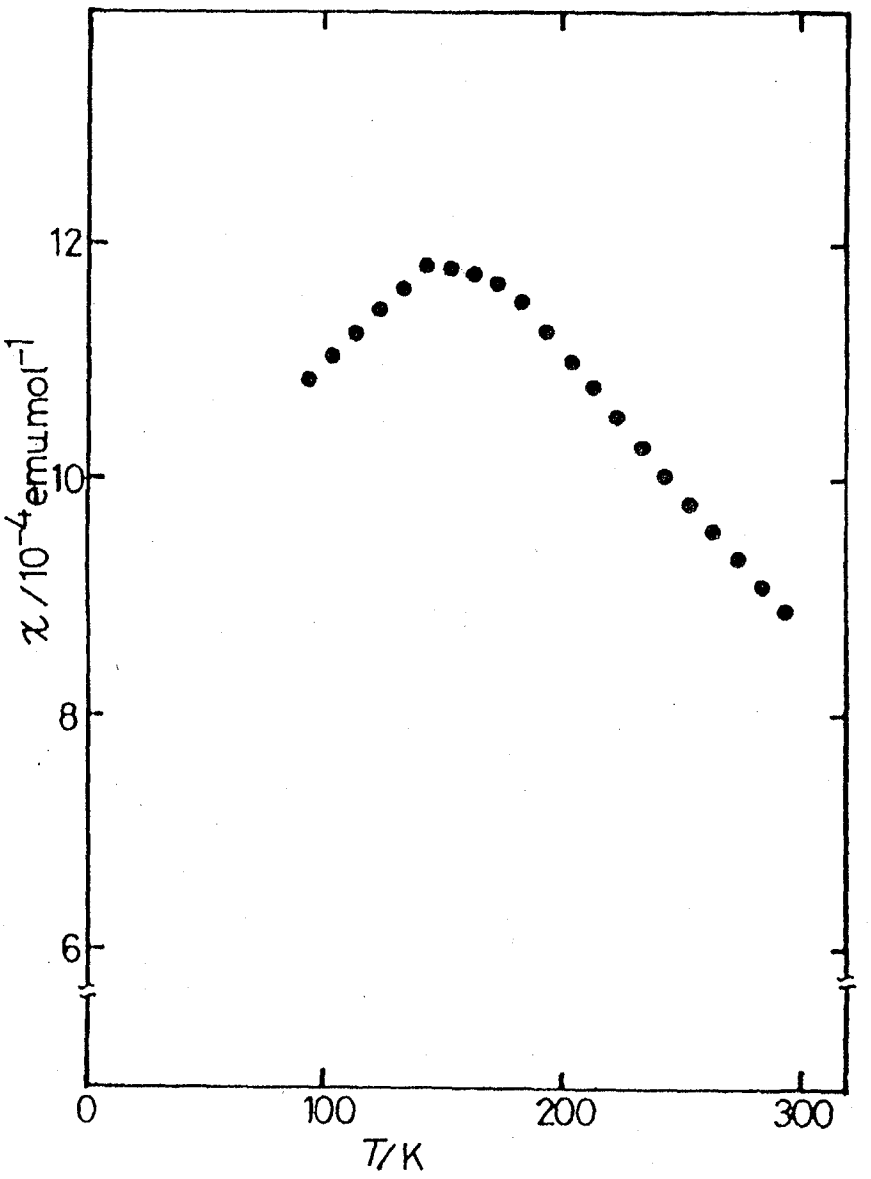

Fig. 2-8 Temperature dependence of magnetic susceptibility of $LaNiO_{2.48}$.

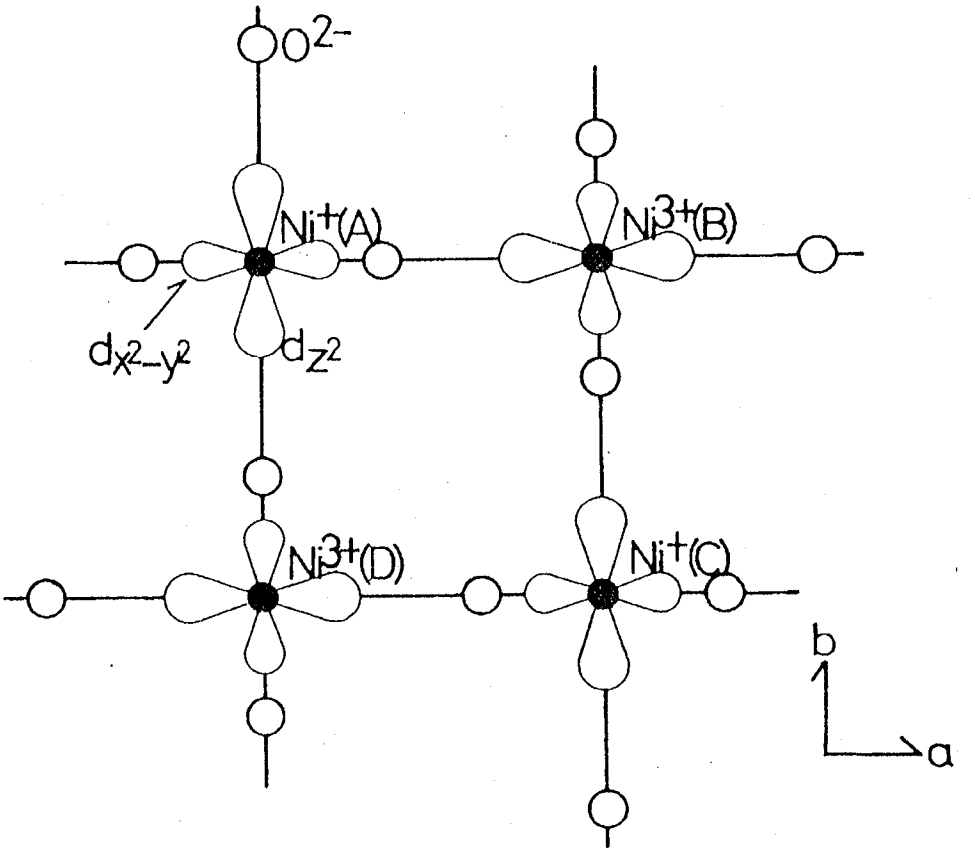

Fig. 2-9 Ordered arrangement of the dx^2-y^2 and dz^2 orbitals in the $[NiO_{4/2}]$ plane in the structure of $La_2Ni_2O_5$. The elongated axis or orbital in the polyhedra is chosen as the *z*-axis or dz^2 orbital for convenience.

their orbital half-filled are arranged along the *a*-axis. Superexchange interaction between metals with their orbital half-filled via oxide ion is reported to be antiferromagnetic.[18] Along the *b*-axis, alternate arrangement of Ni ions with their orbitals vacant and fully occupied can be seen. Superexchange interaction in such an arrangement is very weak or negligible.[18] As for the direction to the *c*-axis, it is also very weak or negligible since $d_{x^2-y^2}$ orbital of $Ni^{3+}O_6$ octahedron has no electrons. The antiferromagnetism observed in $La_2Ni_2O_5$ should result from the interactions mentioned above.

Intermediate Nonstoichiometric Phase $LaNiO_{2.5+z}$

The ferromagnetic phase appeared in an early step of the H_2 reduction could be prepared by mildly reducing $LaNiO_3$ under 1%-H_2/N_2 gas at 350°C for 30h. The crystallinity of this reductant was better than that obtained by the 4h-reduction in H_2 at 275°C. Figure 2-10 shows the diffraction pattern of this specimen. Its oxygen amount (z) was 0.03 in $LaNiO_{2.5+z}$. The ratio of this ferromagnetic phase to the antiferromagnetic $LaNiO_{2.5}$ seemed to increase, but the specimen was not monophasic. The temperature dependence of the magnetization of $LaNiO_{2.53}$ is shown in Fig. 2-11, which also has a sharp drop at about 230K.

A simulation of the diffraction pattern of the ferromagnetic phase is represented in the lower part of Fig. 2-10. The structural model used in this simulation was almost the same as the antiferromagnetic $La_2Ni_2O_5$, except for using the space group of orthorhombic I_{bam} instead of monoclinic $C_{2/c}$. Detail atomic coordinates will be shown in the next chapter. Excess oxygen was assumed to occupy statistically the apical site between the two sheets of $[NiO_{4/2}]$ square-planes. The lattice constants were assumed to be a=7.824, b=7.808, and c=7.468Å. This structural model can satisfactorily explain the diffraction pattern of $LaNiO_{2.53}$, especially the peaks denoted by a solid circle. The observed intensity of the peak appearing at about 41° is weaker than that appearing at about 47° in $LaNiO_{2.53}$. This is in conflict with the result of the simulation. It is due to the fact that this specimen is made up of ferromagnetic $LaNiO_{2.5+z}$ and antiferromagnetic $La_2Ni_2O_5$, and that the former peak is split into three peaks appearing around there, *i.e.*,

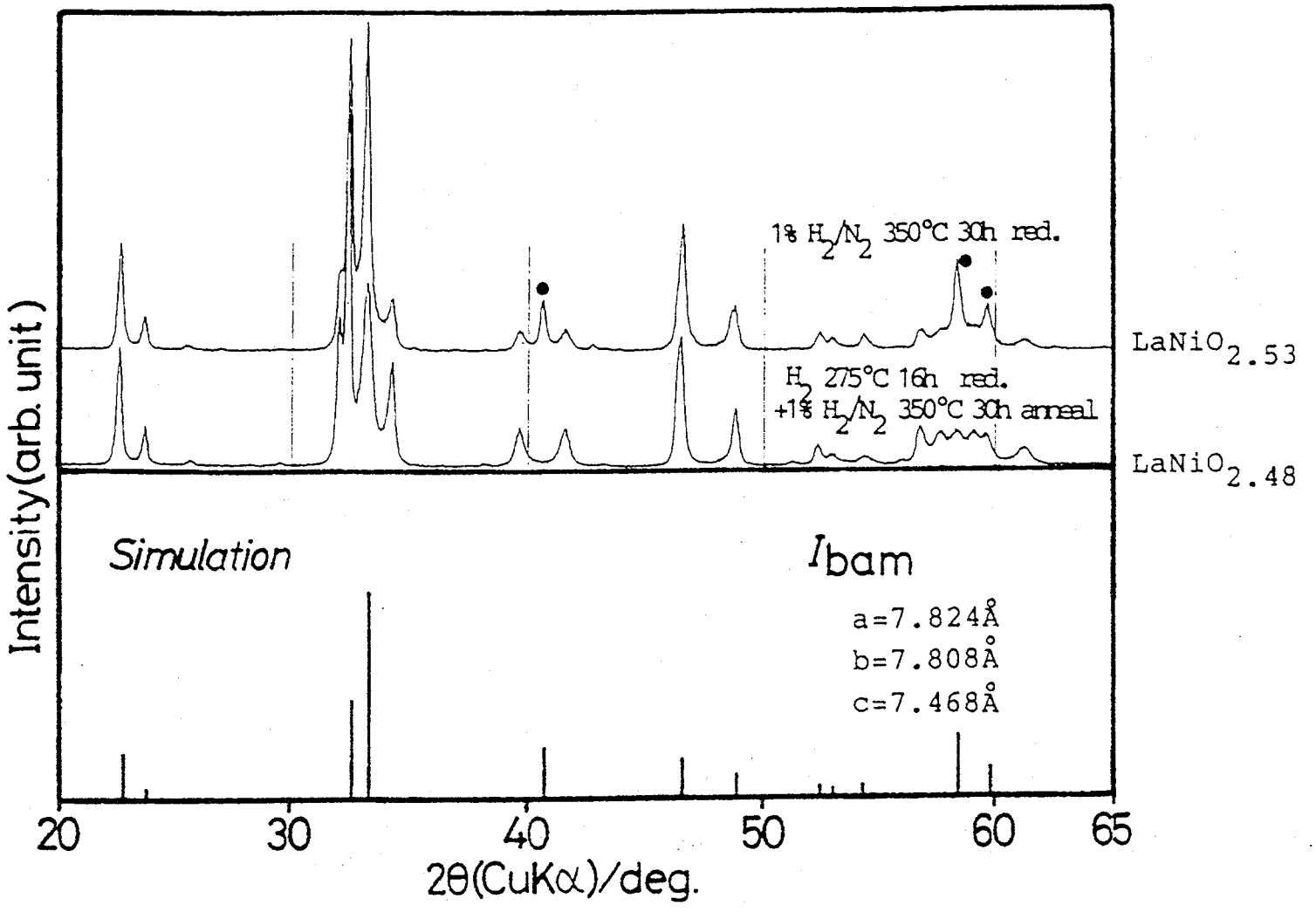

Fig. 2-10 (Upper part): diffraction patterns of $LaNiO_{2.53}$ containing a ferromagnetic phase, and antiferromagnetic $LaNiO_{2.48}$. (lower part): simulation of the diffraction pattern of the ferromagnetic phase. The peaks denoted by a solid circle are characteristic of the orthorhombic ferromagnetic phase.

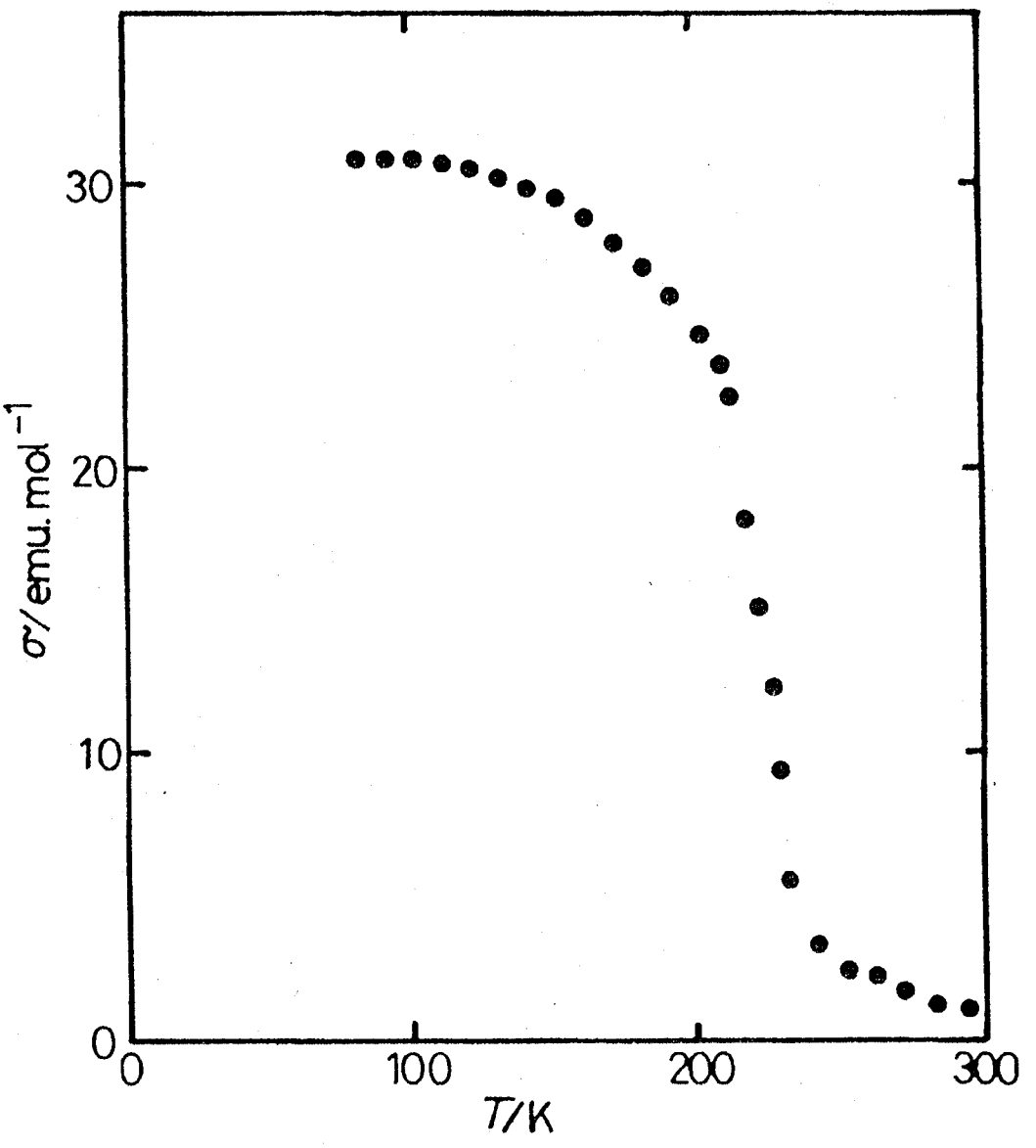

Fig. 2-11 Temperature dependence of magnetization of $LaNiO_{2.53}$.

both sides of the peak are assigned to $La_2Ni_2O_5$. It is likely that the compound which had been reported by Rao et al. to be orthorhombic $La_2Ni_2O_5$[11] comprises of this ferromagnetic $LaNiO_{2.5+z}$.

Magnetic susceptibility measurements of La_2NiO_{4+y} have been reported in several papers.[3,4] A small cusp or break in the susceptibility near to 200K was observed for nonstoichiometric $La_2NiO_{4.02}$. This anomaly has been interpreted in terms of the onset of antiferromagnetic order with spins slightly canted out of the *ab*-plane. This phenomenon induced a net magnetic moment along the *c*-axis in the presence of an applied field. In $LaNiO_{2.5+z}$ with a slight oxygen nonstoichiometry, if its magnetic spin is supposed to lie in the same *ab*-plane as $La_2NiO_{4.02}$, this consideration would be applicable. In the infinite $[NiO_{4/2}]$ layers formed in the ab-plane, neighboring NiO_6 octahedra and NiO_4 square-planes were alternatively canted and rotated in opposite directions. This ferromagnetism appearing in $LaNiO_{2.5+z}$ may result from this spin canting out of the *ab*-plane.

References

[1] J.D.Schirber, B.Morosin, R.M.Merrill, P.F.Hlava, E.L.Venturini, J.F.Kwap, P.J.Nigrey, R.J.Baughman, and D.S.Ginley, *Physica C (Amsterdam)*, **152**, 121 (1988).

[2] D.Jorgensen, B.Dabrowski, S.Pei, D.G.Hinks, L.Solerholm, B.Morosin, J.E.Shirber, E.L.Venturini, and D.S.Ginley, *Phys. Rev. B*, **38**, 11337 (1988).

[3] T.Freltoft, D.J.Buttrey, G.Aeppeli, D.Vaknin, and G.Shirane, *Phys. Rev. B*, **44**, 5046 (1991).

[4] P.Gopalan, M.W.McElfresh, Z.Kakol, J.Spalek, and J.M.Honig, *Phys. Rev. B*, **45**, 249 (1992).

[5] D.C.Johnston, H.Prakash, W.Zachariasen, and R.Viswanathan, *Mater. Res. Bull.*, **8**, 777 (1973).

[6] J.B.Goodenough and P.M.Raccah, *J. Appl. Phys.*, **36**, 1031 (1965).

[7] M.Crespin, P.Levitz, and L.Gatineau, *J. Chem. Soc., Faraday Trans. 2*, **79**, 1181 (1983).

[8] P.Levitz, M.Crespin, and L.Gatineau, *J. Chem. Soc., Faraday Trans. 2*, **79**, 1195 (1983).

[9] T.Siegrist, S.M.Zahurak, D.W.Murphy, and R.S.Roth, *Nature*, **334**, 231 (1988).

[10] G.Er, Y.Miyamoto, F.Kanamaru, and S.Kikkawa, *Physica C, (Amsterdam)*, **181**, 206 (1991).

[11] K.Vidyasagar, A.Reller, J.Gopalakrishnan, and C.N.R.Rao, *J. Chem. Soc., Chem. Commun.*, **1985**, 7 (1985).

[12] C.N.R.Rao, J.Gopalakrishnan, K.Vidyasagar, A.K.Ganguli, A.Ramanan, and L.Ganapathi, *J. Mater. Res.*, **1**, 280 (1986).

[13] J.M.Gonzalez-Carbet, M.J.Sayagues, and M.Vallet-Regi, *Solid State Ionics*, **32/33**, 721 (1989).

[14] F.Izumi, *J. Miner. Soc. Jpn.*, **17**, 37 (1985).

[15] G.J.Colpas, M.J.Maroney, C.Bagyinka, M.Kumar, W.S.Willis, S.L.Suib, N.Baidya, and P.K.Mascharak, *Inorg. Chem.*, **30**, 920 (1991).

[16] S.Rakshit and P.S.Gopalakrishnan, *J.Solid State Chem.*, **110**, 28 (1994).

[17] "International Tables for X-ray Crystallography", Kynoch Press, Birmingham (1974), Vol. IV.

[18] J.B.Goodenough, "Magnetism and Chemical Bond", Interscience, New York (1963).

[19] J.B.Lee, "A New Concise Inorganic Chemistry", 3rd ed., Van Nostrand Reinhold Co., Ltd, Berkshire (1977).

[20] R.D.Shannon, *Acta Crystallog., Sect. A*, **32**, 751 (1976).

[21] M.Crespin, J.M.Bassat, P.Odier, P.Mouron, and J.Choisnet, *J. Solid State Chem.*, **84**, 165 (1990).

[22] M.Crespin, C.Landron, P.Odier, J.M.Bassat, P.Mouron, and J.Choisnet, *J. Solid State Chem.*, **100**, 281 (1992).

[23] Y.Takeda, R.Kanno, T.Takada, O.Yamamoto, M.Takano, N.Nakayama, and Y.Bando, J. Solid State Chem., 63, 237 (1986).

[24] J.L.G.Fierro and L.G.Tejuca, *Appl. Surf. Sci.*, **27**, 453 (1987).

[25] D.Briggs and M.P.Seah, " Practical Surface Analysis by Auger and X-ray Photoelectron Spectroscopy", John Wiley & Sons, Sussec (1983).

Chapter 3.

Characterization of the nonstoichiometric ferromagnetic phase appearing in reduction of $LaNiO_3$ to $La_2Ni_2O_5$

Introduction

It is well-known that the perovskite-type double oxide containing 3d-transition metals and rare-earth metals vary their electronic and/or magnetic properties with change in the valence of the 3d-transition metal. Topotactic intercalation or deintercalation of oxide ions can be useful in controlling the oxygen content and the valence state of the 3d-transition metal. In the Chapter 2, it has been reported that low-temperature reduction of the perovskite-type $LaNiO_3$ under H_2 gas led to an antiferromagnetic compound $La_2Ni_2O_5$ ($LaNiO_{2.5}$) with T_N=140K, and that small amount of excess oxygen led to a new phase $LaNiO_{2.5+z}$.[1] A structural refinement has revealed that $LaNiO_{2.5}$ comprised one-dimensionally linked $Ni^{3+}O_6$ octahedra along the *c*-axis and $Ni^{+}O_4$ square-planes connecting the octahedral chains. The new phase seemed to be indexed to the orthorhombic system and to be ferromagnetic with T_c=230K. However, the precise oxygen content, valence states of Ni^+ ions, and physical properties of the new intermediate phase could not be clarified since a considerable amount of $LaNiO_{2.5}$ coexisted as an impurities. It seemed that reduction of $LaNiO_3$ to $LaNiO_{2.5}$ predominantly proceeded in the vicinity of the surface under such a nonequilibrium H_2 flow.

An electron diffraction study of the $LaNiO_{3-x}$ perovskite-related system by Gonzalez-Carbet *et al.* shows that compositional variations lead to the formation of new superstructures corresponding to a homologous series of the general formula $La_nNi_nO_{3n-1}$ when x=0.5, 0.33, 0.25 and 0.2, *i.e.*, for n=2 ($La_2Ni_2O_5$), 3 ($La_3Ni_3O_8$) and 4 ($La_4Ni_4O_{11}$), respectively.[2,3] These members can be described as being formed by ordered intergrowths of n-1 octahedral layers alternating with one layer in which Ni^{2+} adopts square-planar coordination, shown in Fig. 3-1. Even members, $La_2Ni_2O_5$ and $La_4Ni_4O_{11}$, could have been isolated until now.

In this chapter, a monophasic $LaNiO_{2.5+z}$ was synthesized by a topotactic vacuum reduction of $LaNiO_3$ and its electrical and magnetic properties were clarified. The reduction process from $LaNiO_3$ to $La_2Ni_2O_5$ was discussed based on the results obtained.

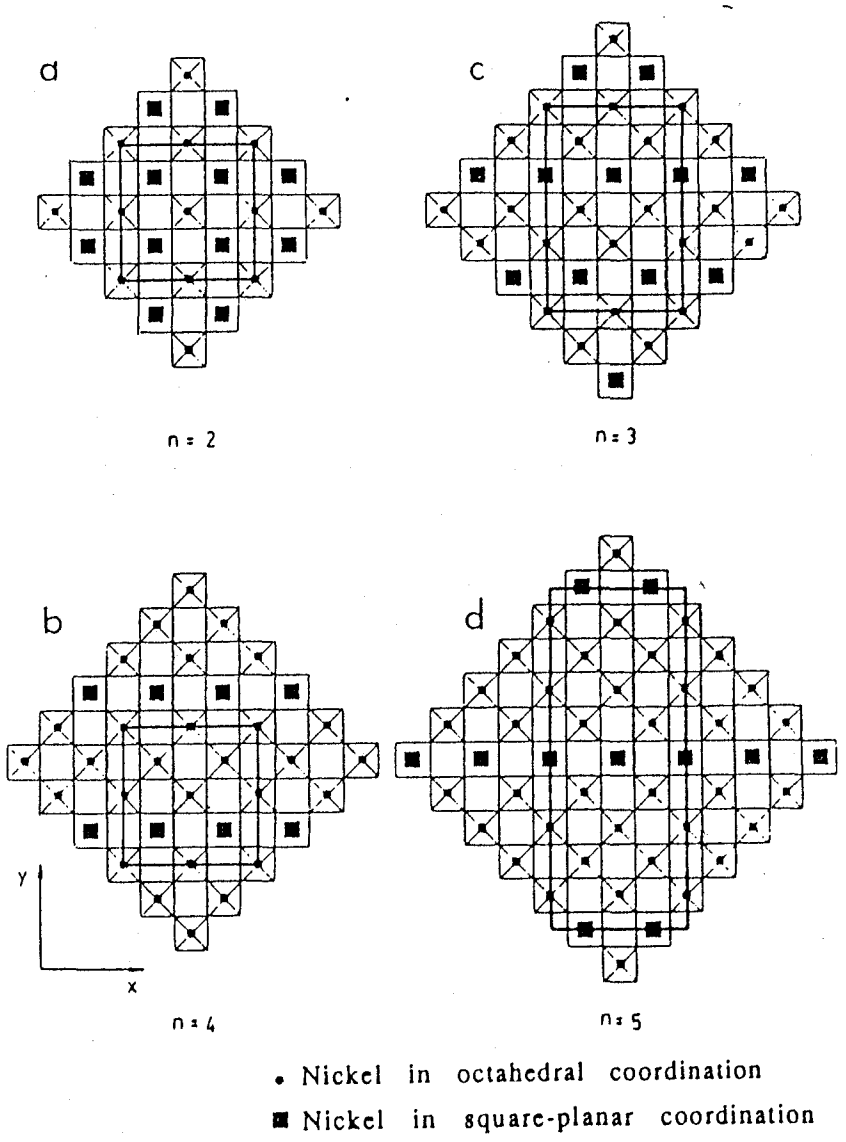

Fig. 3-1 Structural model of a) $La_2Ni_2O_5$ (n=2) and b) $La_4Ni_4O_{11}$ (n=4) along the [001] projection; hypothetical model corresponding to c) $La_3Ni_3O_8$ (n=3) and d) $La_5Ni_5O_{14}$ (n=5) along the same projection.

Experimental

A polycrystalline sample of $LaNiO_3$ was prepared by the coprecipitation method mentioned in the Chapter 2. The resultant $LaNiO_3$ was reduced mildly in a quartz tube (length : 60cm, volume : $150cm^3$), evacuated with a rotary pump to avoid being contaminated by $LaNiO_{2.5}$. Aluminum metal powder was used as a reducing agent (an oxygen getter). The period for reduction was 16h. The oxygen content was controlled by changing the amount of reducing agent or the temperature near the specimen and/or the reducing agent, and was confirmed by an iodometric titration.

Iodometric titration was performed as follows.[4,5] An appropriate amount of the sample was dissolved into a HCl solution, subsequently added the buffer-solution (CH_3COONH_4 : CH_3COOH = 1:1, pH~3) to clarify the end-point of the titration. All of nickel ions in the oxide were reacted and converted to NiI_2 under excess KI. Then, liberating I_2 was titrated with a 0.02N solution of sodium thiosulfate. The titration process was carried out in an atmosphere of Ar to suppress an oxidation of Ni ions by air. The reaction schemes are described as follows.

$$Ni^{2+p} + (2+p)I^- \longrightarrow NiI_2 + (p/2)I_2$$
$$I_2 + 2Na_2S_2O_3 \longrightarrow 2NaI + Na_2S_4O_6$$

Powder X-ray diffraction patterns of reduced specimens were taken by use of a Rigaku 7121 diffractometer with monochromatized CuKα radiation to identify their crystalline phases. Temperature dependence of the electrical resistivity in a range of 5K to room temperature was measured by a dc four probe method using a Toyo Sanso K.K. TC-300ER system. Indium was used as an electrode. Magnetic susceptibility was measured in a temperature range between 73K to room temperature by the Faraday method at a magnetic field strength of 0.9T. Magnetization of the ferromagnetic phase was also measured on a vibrating sample magnetometer (VSM) at the temperature of 200K.

XPS measurement was conducted for powdered samples. X-ray absorption

near-edge structure spectra around Ni K-edge of $LaNiO_{3-x}$ were measured. The conditions in both the measurements were described in the Chapter 2.

Results and Discussion

Structural Model for the ferromagnetic $LaNiO_{2.60}$

In the case of aluminum metal as a reducing agent, the reduction can proceed with the following reaction;

$$LaNiO3 + \frac{1-2x}{3} Al \longrightarrow LaNiO2.5+x + \frac{1-2x}{6} Al2O3.$$

To prepared the new intermediate phase with x=0.1, the molar $LaNiO_3$/Al ratio would be 1/0.267. However, the reduction did not proceed unless the ratio was about 1/1, which may be due to residual oxygen in the ampoule or due to that the oxidation of Al metal did not proceed to inside. Table 3-1 shows the conditions of the reductions and the oxygen content of the resultant reductant, and Fig. 3-2 shows the variation in X-ray diffraction patterns of the reductants shown in Table 3-1. If the amount of the reducing agent was the same, the reduction proceeded and the oxygen content of the reductant decreased by higher temperature treatment. The as-prepared $LaNiO_{2.92}$ and $LaNiO_{2.75}$ could be identical to the rhombohedral perovskite-type structure. In contrast, the diffraction patterns of the reductant with $0.04 \leq x \leq 0.15$ in $LaNiO_{2.5+x}$ were mainly ferromagnetic phase which had been described in the Chapter 2. As for $LaNiO_{2.54}$, those assigned to the antiferromagnetic phase $La_2Ni_2O_5$ appeared only slightly. Notably, the peak positions and their intensities of $LaNiO_{2.60}$ agreed well with those of the pattern which was simulated, based on the structure of $La_2Ni_2O_5$, by using the program RIETAN.[6] The space group of orthorhombic I_{bam}, which is the minimal non-isomorphic supergroup of that of $C_{2/c}$ ($I_{2/b}$) was chosen. This choice is on the assumption that $LaNiO_{2.60}$ is produced by topotactic oxygen elemination from $La_2Ni_2O_5$. The lattice constants were a=7.824, b=7.808 and c=7.468Å, respectively. This unit cell can be expressed by an expression of $2a_p$ x $2a_p$ x $2a_p$, where a_p represents a lattice length of the fundamental perovskite unit cell. Coordinates were taken as follows; La, 8(e), (1/4, 1/4, 1/4); Ni(1), 4(c), (0, 0, 0); Ni(2), 4(d), (1/2, 0, 0); O(1), 16(k), (x, y, z), $x \simeq y \simeq z \simeq 0.25$; O(2), 4(a), (0, 0, 1/4); O(3), 4(b), (1/2, 0, 1/4). The

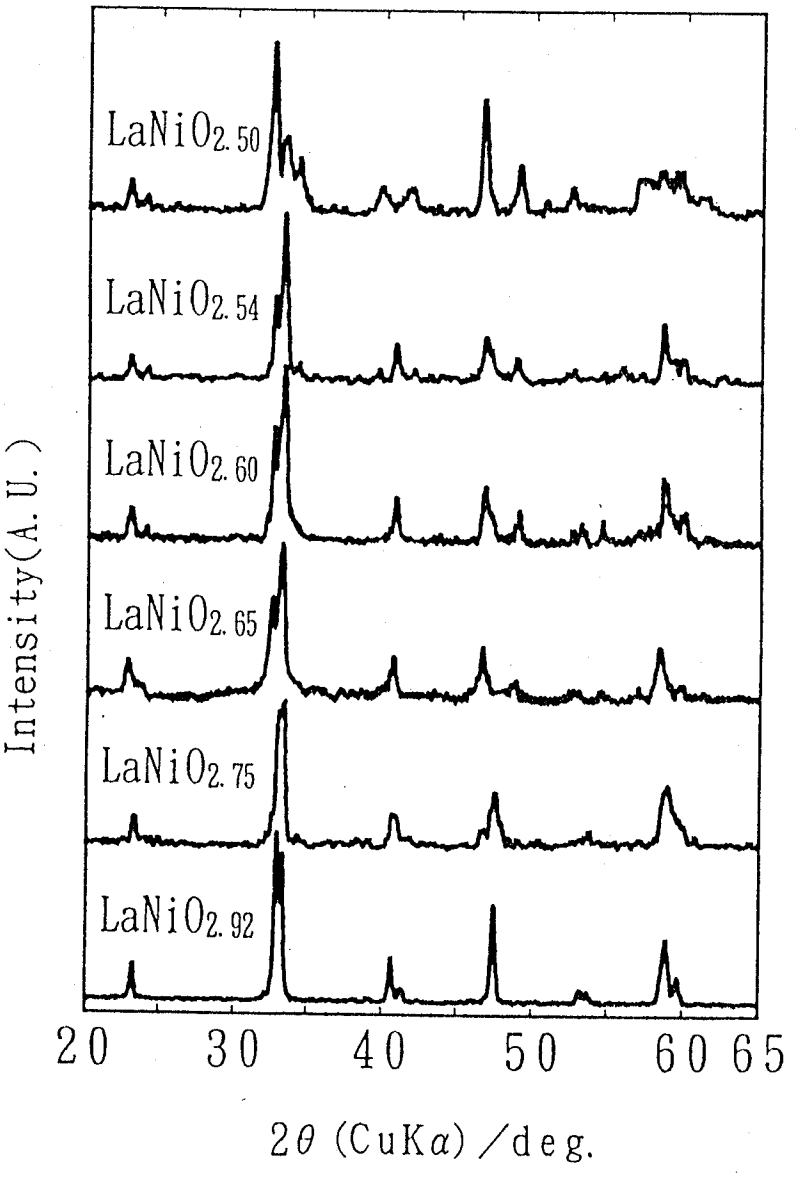

Fig. 3-2 Variation in X-ray diffraction patterns of $LaNiO_{3-x}$ prepared by the vacuum reduction.

Table 3-1
Reducing conditions and oxygen content of the resultant products

Product	$LaNiO_3$: Al	Temp. [a] (°C)	Temp. [b] (°C)
$LaNiO_{2.92}$	–	–	–
$LaNiO_{2.75}$	1 : 0.4	350	950
$LaNiO_{2.65}$	1 : 1	310	850
$LaNiO_{2.60}$	1 : 1	335	850
$LaNiO_{2.54}$	1 : 1	350	850
$LaNiO_{2.50}$	1 : 1.5	400	850

[a] Near $LaNiO_3$; [b] near Al.

occupation probability of the O(3) site was fixed to be 0.20. The observed and calculated patterns are represented in Fig. 3-3. The structural refinement of this specimen could not be done because of its poor crystallinity.

The recent papers mentioned in the introduction reported that three phases $La_2Ni_2O_5$, $La_3Ni_3O_8$, and $La_4Ni_4O_{11}$ exist in a reduction process of $LaNiO_3$ observed by the electron diffraction microscopy.[3] This study by X-ray diffraction clarified that the orthorhombic phase in the composition of $LaNiO_{2.60}$ exists between $LaNiO_3$ and $La_2Ni_2O_5$. Since the diffraction pattern of this phase can almost be identical to that in the composition of $LaNiO_{2.65}$, the stoichiometric composition of the phase may be $La_3Ni_3O_8$ (= $LaNiO_{2.67}$). Unfortunately, $La_3Ni_3O_8$ cannot be explained by this orthorhombic unit cell. As the indices are all even, the lattice length can be cut in half, *i.e.*, a=3.912, b=3.904 and c=3.734Å. The superstructure peaks assigned to ordered $La_3Ni_3O_8$ cannot be detected until now. This reduced lattice would correspond to the fundamental lattice of $La_3Ni_3O_8$.

Temperature dependence of electrical resistivity of $LaNiO_{3-z}$ is shown in Fig. 3-4. The observed resistivity at room temperature increased with an increase of z. The specimens with the perovskite-type structure ($LaNiO_{2.92}$ and $LaNiO_{2.75}$) show metallic conductivity in the temperature range of 5K to room temperature, whereas those with the new orthorhombic structure show semiconductive one. It seemed that a change in the elevation of the resistivity of these orthorhombic specimens occurred at 200-230K.

Temperature dependence of magnetic susceptibility of $LaNiO_{2.60}$ is represented in Fig. 3-5. The ferromagnetic transition at T_c=230K was observed, which corresponds to the temperature where a change in the elevation of the resistivity observed. Its susceptibility obeyed a Curie-Weiss type behavior above 230K, and the effective magnetic moment was 1.7μ_B per Ni ion. Since a Ni^{3+} in the low-spin state and a Ni^{+} ion have one unpaired electron, their spin angular momentum is 1/2. That of a Ni^{2+} ion in the high-spin state is 1, and that of a Ni^{2+} ion in the low-spin state is 0. If it is assumed that $LaNiO_{2.60}$ is composed of Ni^{3+} and Ni^{2+} ions, the observed magnetic moment cannot be explained. As Ni^{+} ion, with the $3d^9$ electron configuration, is stable, it forms a square-planar coordination. The effective magnetic moment, calculated by assuming that

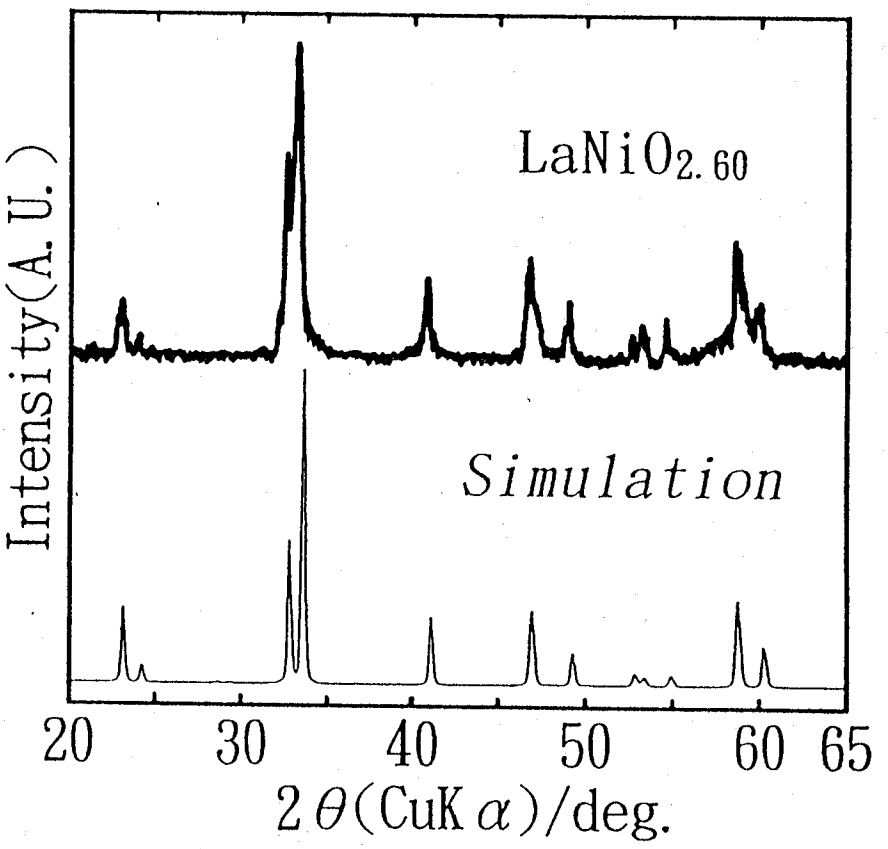

Fig. 3-3 The observed and simulated diffraction patterns of $LaNiO_{2.60}$.

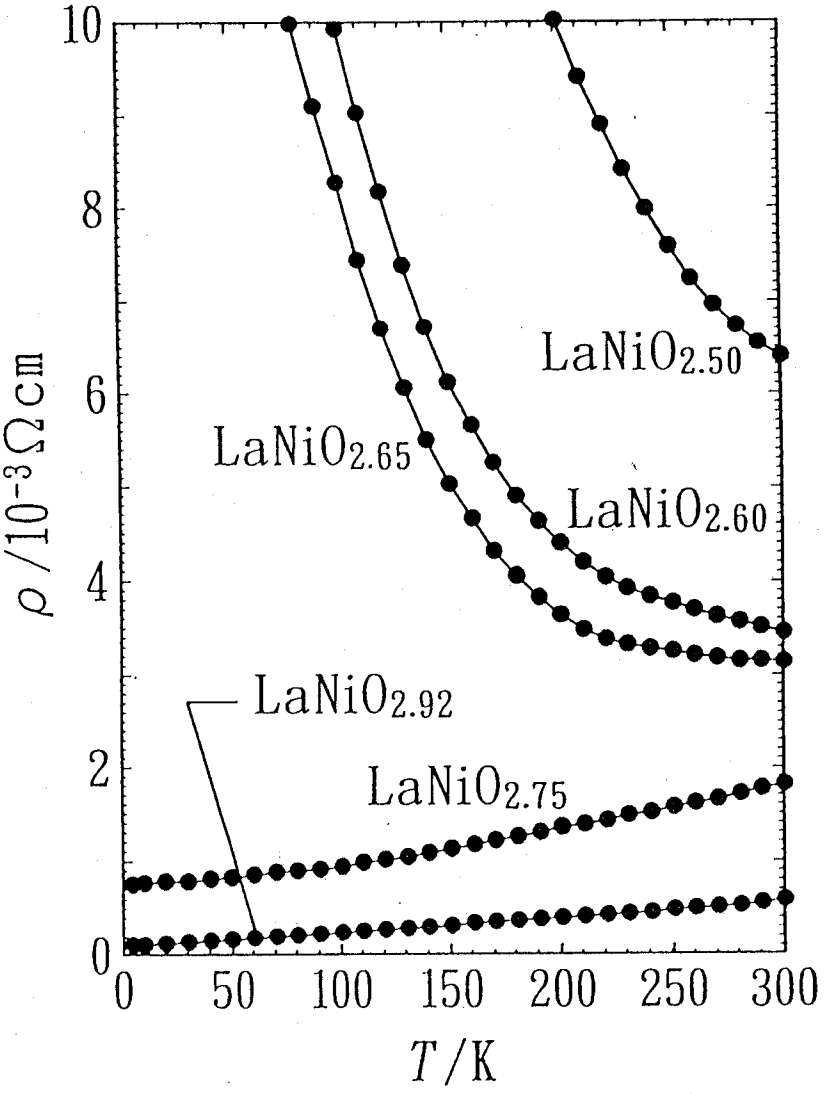

Fig. 3-4 Temperature dependence of electrical resistivity of $LaNiO_{3-x}$.

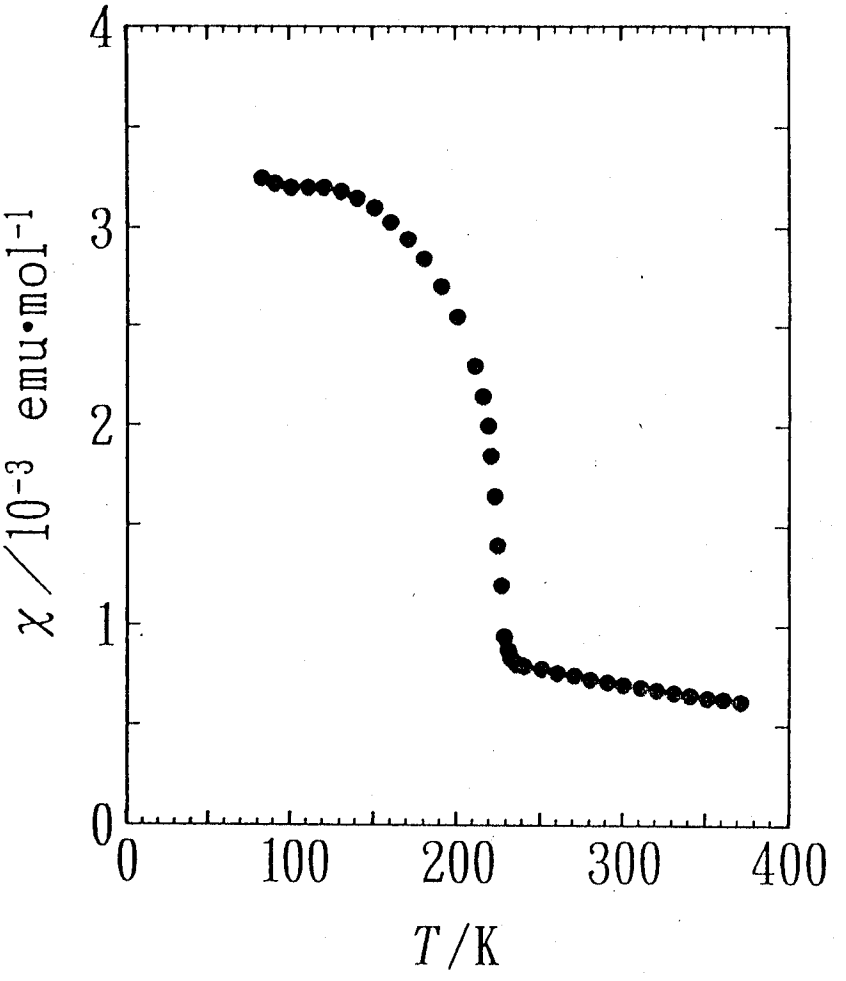

Fig. 3-5 Temperature dependence of magnetic susceptibility of $LaNiO_{2.60}$.

$LaNiO_{2.60}$ have $Ni^{3+}O_6$ octahedra and $Ni^{+}O_4$ square-planar as seen in $La_2Ni_2O_5$, is $1.73\mu_B$. This value is in a good agreement with this model.

Figure 3-6 shows magnetization of $LaNiO_{2.60}$ as a function of magnetic field at 200K. The behavior up to about 5.3kOe was similar to that of ferromagnetic materials, whereas linear relationship was observed in the magnetic field of more than 5.3kOe. This phenomenon is indicative of weak ferromagnetism.[7] $La_2Ni_2O_5$ is an antifferomagnet. If the array of the ordered spins are the same as $La_2Ni_2O_5$,[+] this magnetic behavior would arise from the slight canting of the antiferromagnetically ordered spins, which have been observed in the layered perovskite La_2NiO_{4+y}.[8,9] A small cusp or break in the susceptibility near to 200K was observed for slightly-nonstoichiometric La_2NiO_{4+y}. This anomaly has been interpreted in terms of the onset of antiferromagnetic order with spins slightly canted out of the *ab*-plane. This phenomenon induced a net magnetic moment along the *c*-axis in the presence of an applied field. The ferromagnetism appearing in $LaNiO_{2.60}$ ($\simeq La_3Ni_3O_8$) would result from this spin canting out of the *ab*-plane.

Topotactic Reduction of $LaNiO_3$ under the Equilibrium Conditions

Fig. 3-7 represents the variation of the Ni K-edge XANES spectra of $LaNiO_{3-x}$. In the same manner as mentioned in the Chapter 2, as the oxygen content (3-x) decreases, the peak intensity for $1s \rightarrow 3d$ transition decreases and that for $1s \rightarrow 4d$ transition increased.[10,11] XPS spectrum in the $Ni2p_{3/2}$ region for $LaNiO_{2.60}$ in Fig. 3-8 shows the existence of Ni^{3+} and Ni^{+}.[1] These phenomena are indicative of that the square-planar Ni^{+} ion is mainly formed in the reductants. It can be concluded that $LaNiO_{2.60}$ as well as $La_2Ni_2O_5$ is comprised of $Ni^{3+}O_6$ octahedra and $Ni^{+}O_4$ square-planes and the ratio of $Ni^{3+}O_6$ and $Ni^{+}O_4$ in $LaNiO_{2.60}$ is 6/4. The reduction of $LaNiO_3$ to $La_2Ni_2O_5$ is thought to proceed by the mechanism where $Ni^{3+}O_6$ turns into $Ni^{+}O_4$ in the topotactic elimination of oxide ions.

[+] In the next section, $LaNiO_{2.60}$ was considered to be composed of the same Ni ions with unpaired electron as $La_2Ni_2O_5$.

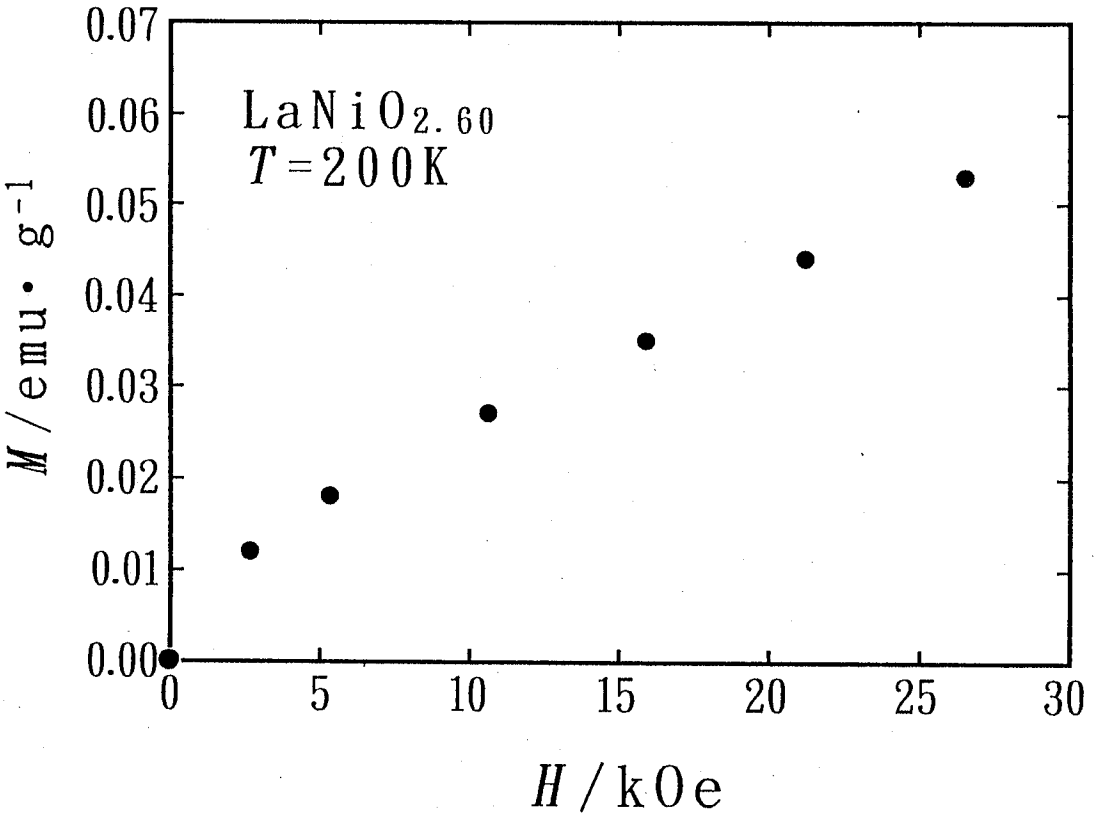

Fig. 3-6 Applied field dependence of magnetization of $LaNiO_{2.60}$.

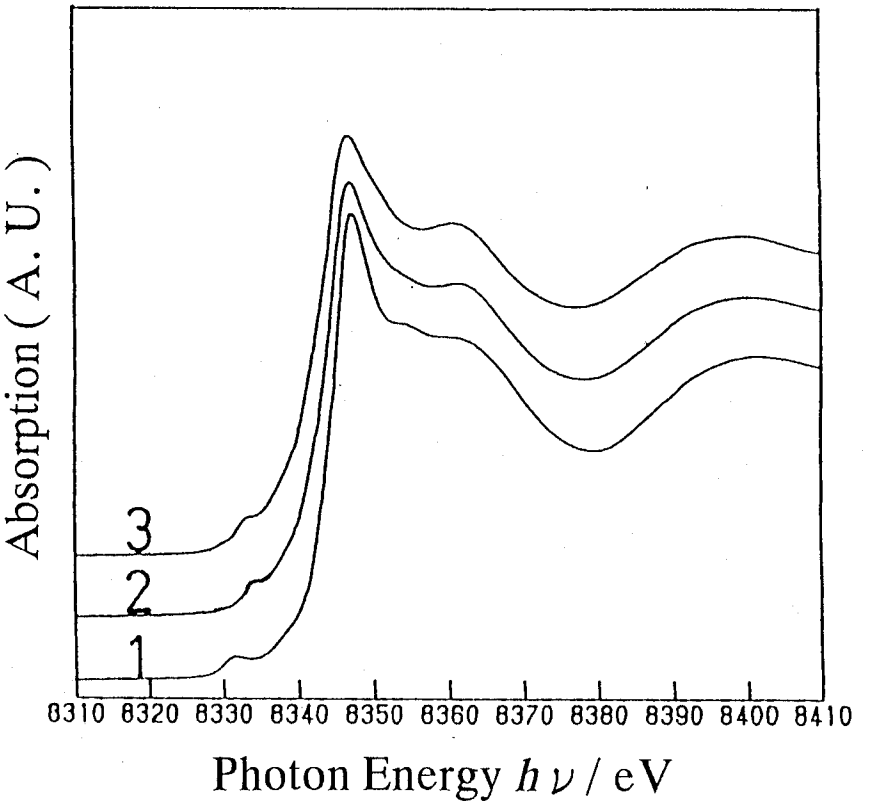

Fig. 3-7 The Ni K-edge XANES spectra of 1) $LaNiO_3$, 2) $LaNiO_{2.60}$, and 3) $La_2Ni_2O_5$.

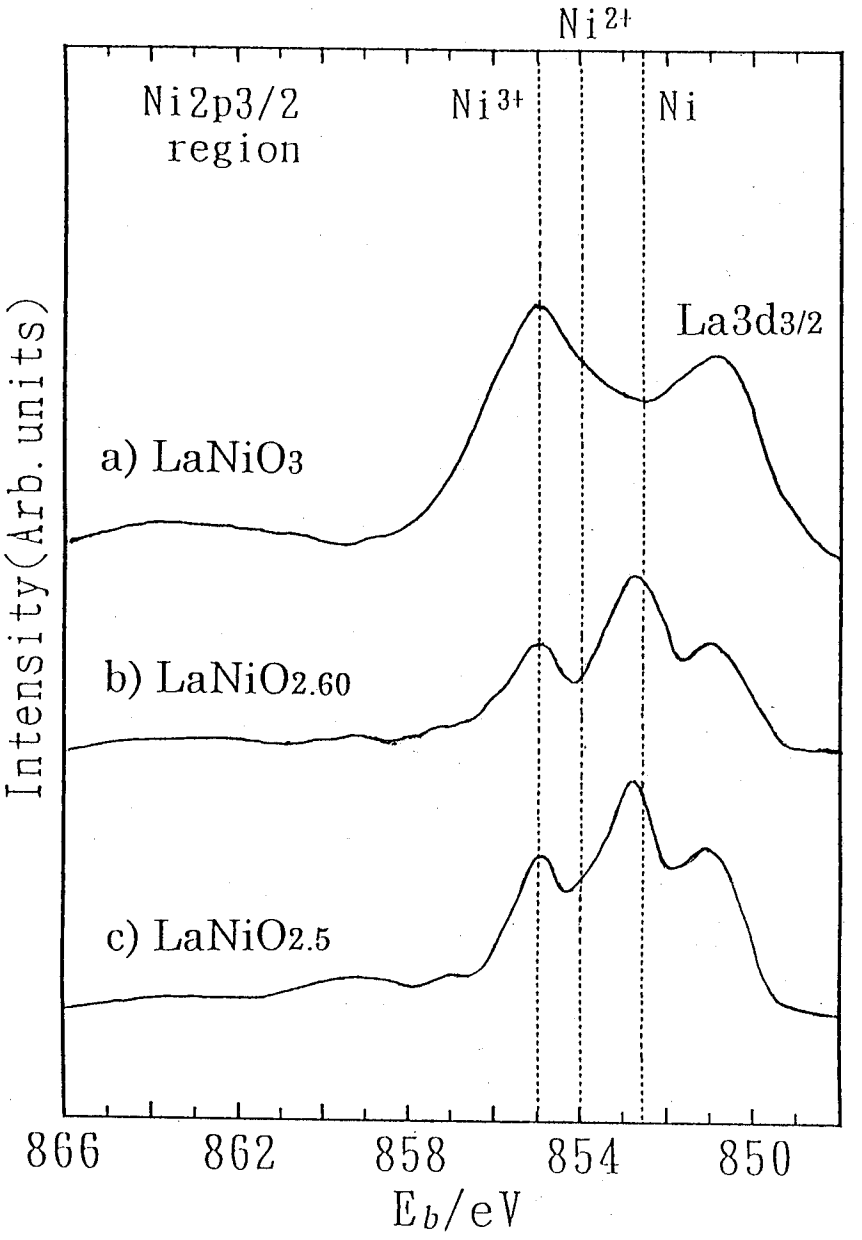

Fig. 3-8 Narrow scan XPS spectra in Ni2p3/2 region of a) $LaNiO_3$, b) $LaNiO_{2.60}$, and c) $La_2Ni_2O_5$.

References

[1] T.Moriga, O.Usaka, T.Imamura, I.nakabayashi, I.Matsubara, T.kinouchi, S.Kikkawa, and F.Kanamaru, *Bull. Chem. Soc. Jpn.*, **67**, 687 (1994).

[2] J.M.Gonzalez-Carbet, M.J.Sayagues, and M.Vallet-Regi, *Solid State Ionics*, **32/33**, 721 (1989).

[3] M.J.Sayagues, M.Vallet-Regi, A.Caneiro, and J.M.Gonzalez-Carbet, *J. Solid State Chem.*, **110**, 295 (1994).

[4] Y.Maeno, H.Teraoka, and K.Matsukuma, *Kotai-Butsuri (Solid State Physics)*, **26**, 235 (1991).

[5] T.Moriga, S.Takemoto, H.Tsukaguchi, I.Nakabayashi, and K.Koto, *J. Ceram. Soc. Jpn.*, **101**, 962 (1993).

[6] F.Izumi, *J. Miner. Soc. Jpn.*, **17**, 37 (1985).

[7] S.Chikazumi, " Physics of Ferromagnetism, Vol.1 - Magnetic Properties of Matter -", Shokabo, Tokyo (1978) [in Japanese].

[8] T.Freltoft, D.J.Buttrey, G.Aeppli, D.Vakinin, and G.Shirane, *Phys. Rev. B*, **44**, 5046 (1991).

[9] P.Gopalan, M.W.McElfresh, Z.Kakol, J.Spalek, and J.M.Honig, *Phys. Rev. B*, **45**, 249 (1992).

[10] G.J.Colpas, M.J.Maroney, C.Bagyinka, M.Kumar, W.S.Willis, S.L.Suib, N.Baidya, and P.K.Mascharak, *Inorg. Chem.*, **30**, 920 (1991).

[11] T.Moriga, S.Kikkawa, M.Takahashi, F.Kanamaru, and I.Nakabayashi, *Jpn. J. Appl. Phys.*, **32** Suppl. 32-2, 764 (1993).

Chapter 4.

Substitution effects of lanthanide ions (Ln^{3+}) on reduction of the perovskite-type $LnNiO_3$

Introduction

Double oxide containing trivalent nickel ions and lanthanum ions with the perovskite-type structure have been studied extensively. $LaNiO_3$ has been known to show the metallic conductivity and Pauli-paramagnetism.[1] This compound has a rhombohedrally-distorted perovskite-type structure, and can be synthesized under an ambient pressure. The perovskite-type $LnNiO_3$ with a trivalent lanthanide ion having a smaller radius than La^{3+} has been prepared under high oxygen pressures above 15MPa.[2,3] These compounds crystallize into an orthorhombic crystal system. The $PrNiO_3$ and $NdNiO_3$ showed metallic conductivities in higher temperature region, and they had metal-insulator transition with minor structural changes at 130K and 200K for Ln=Pr and Nd, respectively.[3,4,5] Recently, some low temperature synthetic procedures with the coprecipitation method were applied to prepare the rhombohedral $NdNiO_3$.[6,7] It makes possible to avoid the use of high oxygen pressures. However, resultant $NdNiO_3$ had a poor crystallinity and a small amount of impurity phases.

In the Chapter 2, two kinds of oxygen-deficient phase around $LaNiO_{2.5}$ have been found by a low-temperature hydrogen reduction of the perovskite-type $LaNiO_3$.[8,9] An antiferromagnetic $LaNiO_{2.5}$ with T_N=140K, in which the average formal oxidation state of nickel is +2, seemed to be stoichiometric and a small amount of excess oxygen led to a new ferromagnetic phase $LaNiO_{2.60}$ with T_c=230K. Its structural refinement revealed that the former, with space group $C_{2/c}$, comprised one-dimensionally-linked NiO_6 octahedra along the c-axis connected with NiO_4 square-planes. A cooperative Jahn-Teller distortion was observed in both the coordination polyhedra, where the octahedrally coordinated Ni ions were trivalent state with the low-spin state and the square-planar Ni ones were monovalent.

The Ni^+ ion is isoelectronic to Cu^{2+} ion in high T_c cuprate superconductors. However, divalent nickel is more common and reductive conditions are necessary to introduce the monovalent state. The monovalent nickel ions have been reported to be able to stabilize in the reductants of Ruddlesden-Popper-type series $Ln_{n+1}Ni_nO_{3n+1}$ by Lacorre[10] and Zhang et al.[11] Especially, Lacorre has succeeded in the synthesis of $Ln_4Ni_3O_8$ (Ln=La,

Pr and Nd), in which the average formal oxidation state of nickel is +1.33, and clarified the structural passage from $Ln_4Ni_3O_{10}$ to $Ln_4Ni_3O_8$.

Though Crespin et al. had reported the existence of $LaNi^{+}O_2$ with an infinite-layer structure as seen in superconductive (Ca, Sr)CuO_2 and (Sr, La)CuO_2,[12,13] the reduction did not proceed to the composition of $LaNiO_2$ in the previous work mentioned in the Chapter 2. The smaller Ln^{3+} ions prefer the smaller coordination number and the smaller oxygen content. Substitution of La^{3+} to Pr^{3+} or Nd^{3+} may lead all of the trivalent nickels in $LnNiO_3$ to be reduced to monovalent ones in the infinite-layer-type $LnNiO_2$ structure.

In this Chapter, the perovskite-type $LnNiO_3$ (Ln=Pr, Nd) were synthesized by use of a conventional HIP (hot isostatic press) device. Oxygen deficient phase of $LnNiO_{3-x}$ were prepared by a reduction of $LnNiO_3$ in a diluted hydrogen gas flow at low temperature. XAFS and XPS data were collected to investigate the local structure and electronic states of nickel ions. Rietveld structural analyses of the reductants were carried out based on the possible structural models.

Experimental

A polycrystalline precursor of LnNiO$_3$ (Ln=Pr and Nd) was prepared by a coprecipitation method. Ln(NO$_3$)$_3$·6H$_2$O and Ni(NO$_3$)$_2$·6H$_2$O were used as starting materials. A 6N solution of diethylamine was added into the metal nitrate solution to form the sol of these metal hydroxide. After washing with ethanol, the coprecipitant was dried at 200°C in air and fired at 850°C in an O_2 flow for 30h. HIP technique was applied to the product in order to make it crystallize into the perovskite-type LnNiO$_3$. The product was pressed into pellet of 10mm in diameter and 2-3mm in thickness, and covered with gold sheet. A mixed gas (Ar:O_2=80:20 in molar ratio) was used as a pressure medium. A pressure of 20MPa was applied for 144h on the sample with Ln=Pr. The sample with Ln=Nd was treated under a pressure of 50MPa for 20h. The oxidizing temperature was in the range of 850-950°C. The resulted LnNiO$_3$ was reduced in a H_2 and N_2 gas mixture (H_2:N_2=10:90) at 350°C for several hours. The gas flow rate was 15cm^3/min.

Powder X-ray diffraction data were collected using a Rigaku 7121 diffractometer with monochromatized CuKα radiation (35kV-20mA) for phase identification and using a Mac-Science MXP^{18} diffractometer for an in-situ measurement in reduction (50kV-150mA). The scanning rates were 1°/min for phase identification and 4°/min for the in-situ measurement, respectively. The flow rate of the mixed-gas was 30cm^3/min in the in-situ diffractometry. A simulation of the X-ray diffraction patterns and Rietveld analysis for the reductants were carried out using the program RIETAN94 provided by F.Izumi.[14]

Neutron diffraction data of $Pr_3Ni_3O_7$ were taken on a time-of-flight (TOF) neutron powder diffraction diffractometer, HRP[15], at the KENS pulsed spallation neutron source in KEK. The specimen was contained in a cylindrical vanadium cell of dimensions, 5mm in radius, 55mm in height, and 200μm in thickness. The average scattering angle, 2θ, was fixed at 170°, and intensity data were collected at 300K.

The oxygen contents in the product were determined by an iodometric titration.[16] When the average valence of nickel ions in the specimen was thought to be less than +2, the titration was performed by mixing with an appropriate amount of LnNiO$_3$

with trivalent nickel ions whose precise oxygen content had been determined in advance. The contribution of the standard sample was subtracted and the oxygen content of the given specimen was calculated. The oxygen content in the product was also confirmed by use of Horiba EMGA-2800 device mentioned in the Chapter 2.

The reduction of $LnNiO_3$ was also conducted on a thermogravimetric balance in flowing the diluted H_2. The rate of gas flow was $30cm^3$/min. The heating rate was 10°C/min up to 350°C and the temperature was held at 350°C. Al_2O_3 (99.99%) was used as a standard sample of heat.

Magnetic susceptibility of the reductants was measured in the temperature range between 77 and 660K by the Faraday method at a magnetic field strength of 0.9T. Magnetization of the ferromagnetic phase was also measured on a vibrating sample magnetometer (VSM) at the temperature of 200K. Differential scanning calorimetry (DSC) measurement was also performed on the reductants by use of Rigaku DSC-50 device in the temperature range from 173 up to 373K to verify the magnetic transitions due to an order-arrangement of unpaired electrons. The furnace was cooled by liquid nitrogen in prior to the measurements. The inside of DSC device was filled with the dried N_2 gas. The heating rate was 5°C/min. All the samples were packed into an aluminum pan to minimize the difference of the heat radiation.

XPS measurement was conducted for powdered samples. X-ray absorption near-edge structure spectra around Ni K-edge of $LnNiO_{3-x}$ were measured. The conditions in both the measurement were described in the Chapter 2.

Results and Discussion

Reduction Process of Perovskite-type $LnNiO_3$ (Ln=Pr and Nd)

Figures 4-1(a) and 4-1(b) show variations of the in-situ X-ray diffraction patterns of $LnNiO_{3-x}$ (*Ln*=Pr in (a) and *Ln*=Nd in (b)) under the reducing atmosphere. The 112 peak around $2\theta \simeq 34°$ in the orthorhombic perovskite-type structure ($a \simeq b \simeq 5.4$Å, $c \simeq 7.6$Å)[3] faded out and the new peaks gradually appeared on both sides of the peak. The peaks assigned to PrO_x ($1.5 \leq x \leq 2$) and NiO could not be detected. These are characteristic of a topotactic reaction in an oxygen elimination. Topotactic reduction seemed to be over in about three hours. The oxygen contents z in the $LnNiO_z$ reduced for three hours by the iodometric titration were 2.34 for *Ln*=Pr and 2.30 for *Ln*=Nd, respectively. For reference, the oxygen content in the perovskite-type $LnNiO_z$ before the reduction was 2.61 for *Ln*=Pr★ and 2.70 for *Ln*=Nd, respectively. The fact that the oxygen content in $PrNiO_{2.61}$ is smaller than that in $NdNiO_{2.70}$ would be ascribed to lower oxygen pressure treatment for Pr-compound than for Nd-compound in order to suppress the oxidation of Pr^{3+} to Pr^{4+}. Both the perovskite-type compounds had significant amounts of oxygen vacancy. However, the synthesized perovskite-type phase is described as "$LnNiO_3$" for simplicity hereafter.

A common feature of the reduction curves of $LnNiO_3$ was the only one-step behavior as illustrated in Fig. 4-2. The plateau in the respective weight-loss curves is associated with an intermediate phase corresponding to the composition of $PrNiO_{2.34}$★ and $NdNiO_{2.30}$. The final products of the hydrogen reduction was amorphous-like Ni metal and the rare-earth oxide. The oxygen amount in the stable reductants calculated from the results of thermogravimetric analysis agreed well with those by iodometric titration. Considering their oxygen contents, the ideal composition appears to be

---

★ The oxygen content for Pr-compounds before and after the reduction was also determined by using Horiba EMGA-2800 device, from which total oxygen content can be obtained. The results obtained by this apparatus were z=2.63 and z=2.34 in PrNiOz, respectively. This fact shows the Pr ions in both compounds basically take trivalent state.

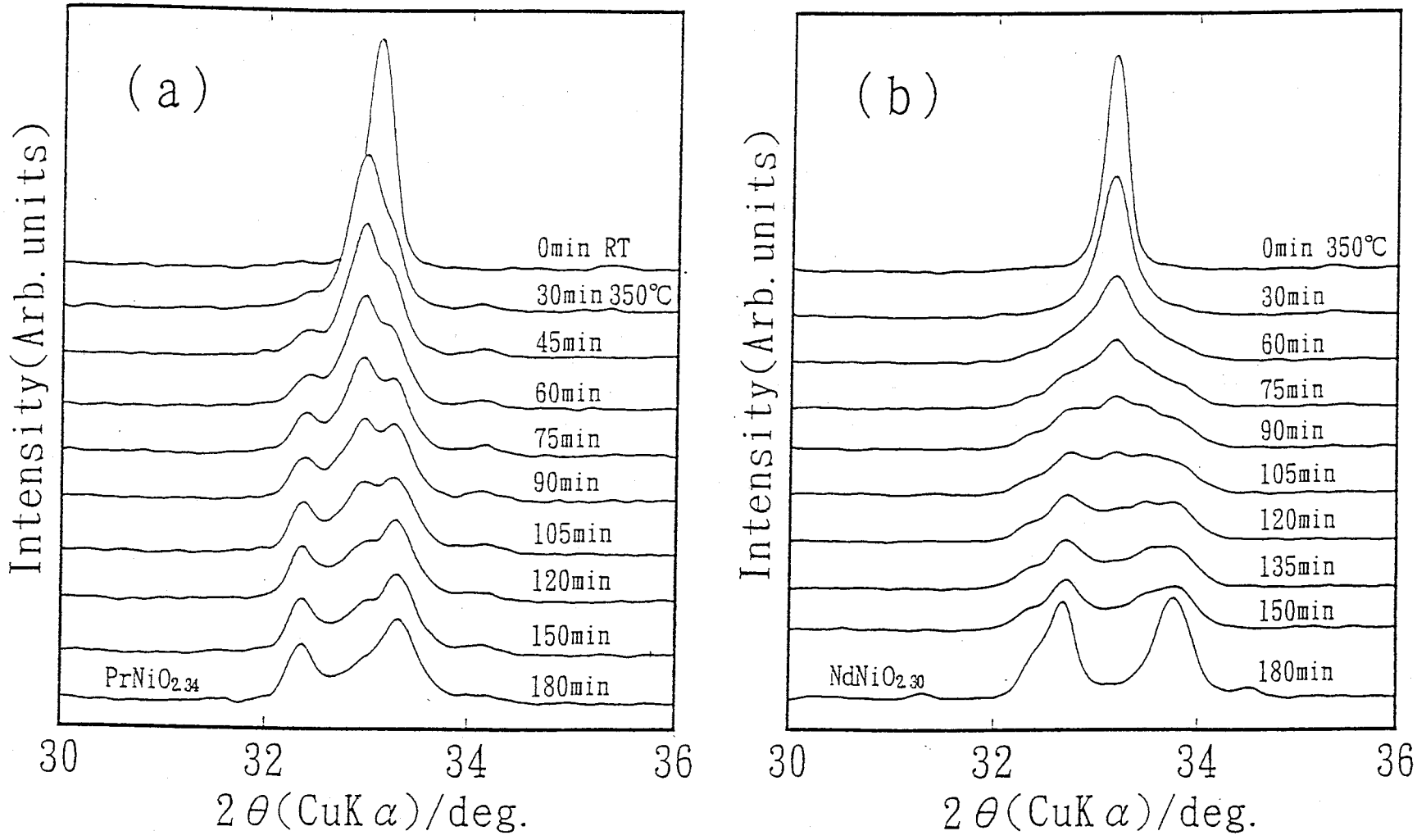

Fig. 4-1 Variations of in-situ diffraction patterns of $LnNiO_{3-x}$; a) *Ln*=Pr and b) *Ln*=Nd in the diluted H_2 atmosphere at 350°C.

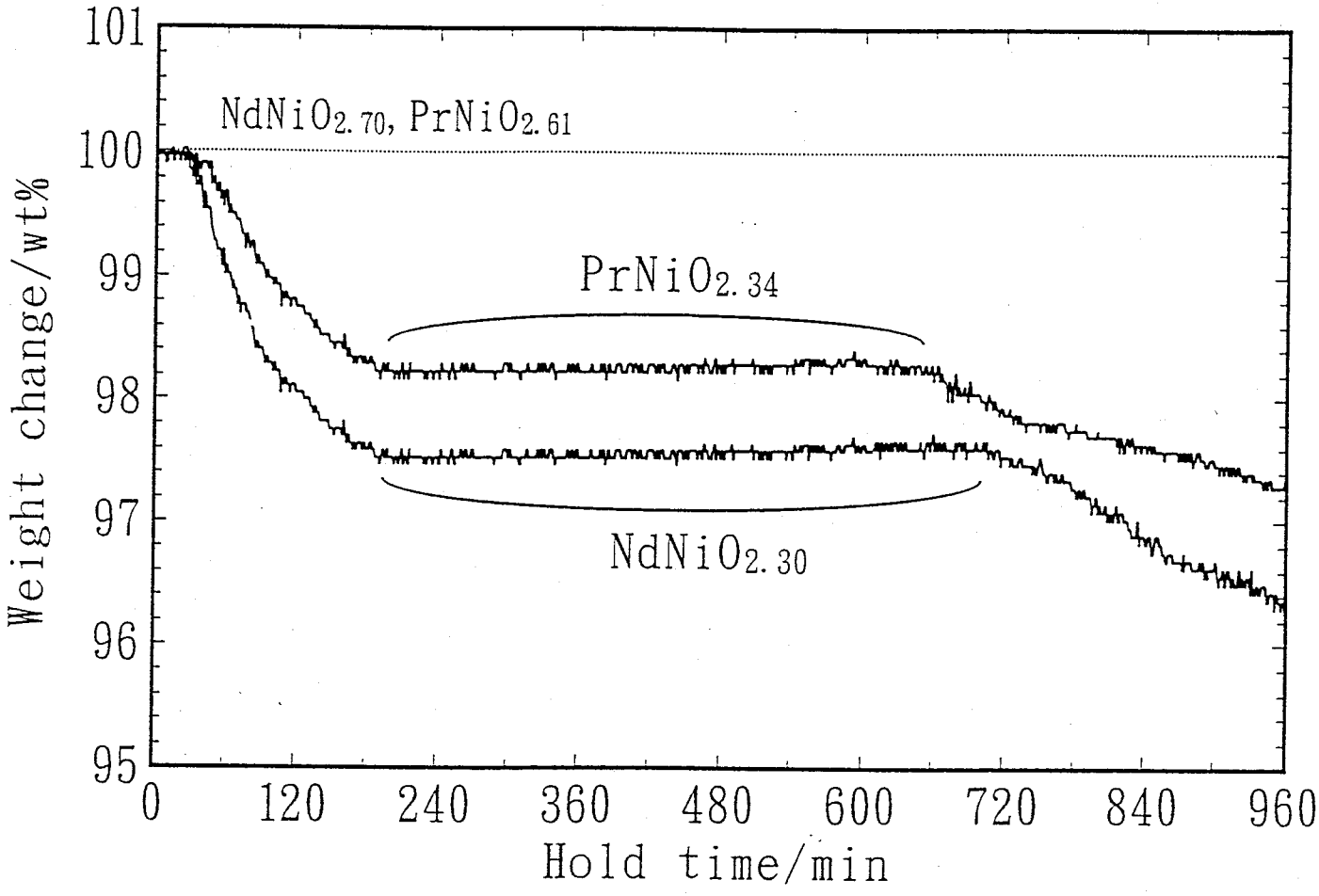

Fig. 4-2 Thermogravimetric analyses of $LnNiO_{3-x}$ (*Ln*=Pr and Nd) in the diluted H_2 atmosphere at 350°C.

$Ln_3Ni_3O_7$. The reductant phase containing Pr or Nd was found to have smaller oxygen content compared to that containing La (*i.e.* $La_2Ni_2O_5$). Unfortunately, $PrNiO_2$ and $NdNiO_2$ could not be obtained in the present experiment.

Structural model for reduced $Ln_3Ni_3O_7$

Powder X-ray diffraction patterns of $PrNiO_{2.34}$ and $NdNiO_{2.30}$ are presented in Fig. 4-3. All of the peaks which appeared in $PrNiO_{2.34}$ could be indexed with a tetragonal cell of a=3.870 and c=3.655Å. The simulation of a diffraction pattern for $Pr_3Ni_3O_7$ was also shown in Fig. 4-3. In the simulation, we assumed that the space group of $P_{4/mmm}$[17] was chosen and the atomic coordinations were taken as follows: Pr, 1(d), (1/2, 1/2, 1/2); Ni, 1(a), (0, 0, 0); O(1), 2(f), (1/2, 0, 0); O(2), 1(b), (0, 0, 1/2). The occupation probability of the O(2) site was fixed to be 1/3. The observed and calculated patterns agreed well with each other. If the ideal composition of $Pr_3Ni_3O_7$ is speculated for $PrNiO_{2.34}$, the compound cannot be explained using this unit cell. This may be due to the fact that the scattering intensity of oxide ion for X-rays is much smaller than that of Pr^{3+} or Nd^{3+} ion, so that the ordered arrangement of oxide ions cannot be analyzed. Further structural analysis such as a neutron diffraction diffractometry will be needed.

For $NdNiO_{2.30}$, it could be satisfactorily indexed in the monoclinic system with a=11.041, b=3.765, c=11.770Å and β=92.13°. The powder X-ray diffraction data are summarized in Table 4-1. This unit cell can be expressed by an expression of $3a_p$ x a_p x $3a_p$, where a_p represents a lattice length of the fundamental perovskite unit cell. The fundamental cell volume of the perovskite for $PrNiO_{2.34}$ was 54.9Å^3, whereas that for $NdNiO_{2.30}$ was 54.3Å^3. A symmetry reduction was observed by substituting Pr^{3+} to Nd^{3+}, as usually seen in the perovskite-type $LnNiO_3$ (Ln=Nd, Sm and Ho) and the T'-type $(La_{0.85}LnSr_{0.15})CuO_4$ (Ln=La, Pr and Nd).[18]

Figure 4-4 represents temperature dependence of magnetic susceptibility of the reduced $PrNiO_{2.34}$ and $NdNiO_{2.30}$. Their susceptibility obeyed the Curie-Weiss behavior above 300K for Ln=Pr and 350K for Ln=Nd, respectively. No magnetic transition points assigned to both NiO and Ni metal were observed. However, both curved have a rising

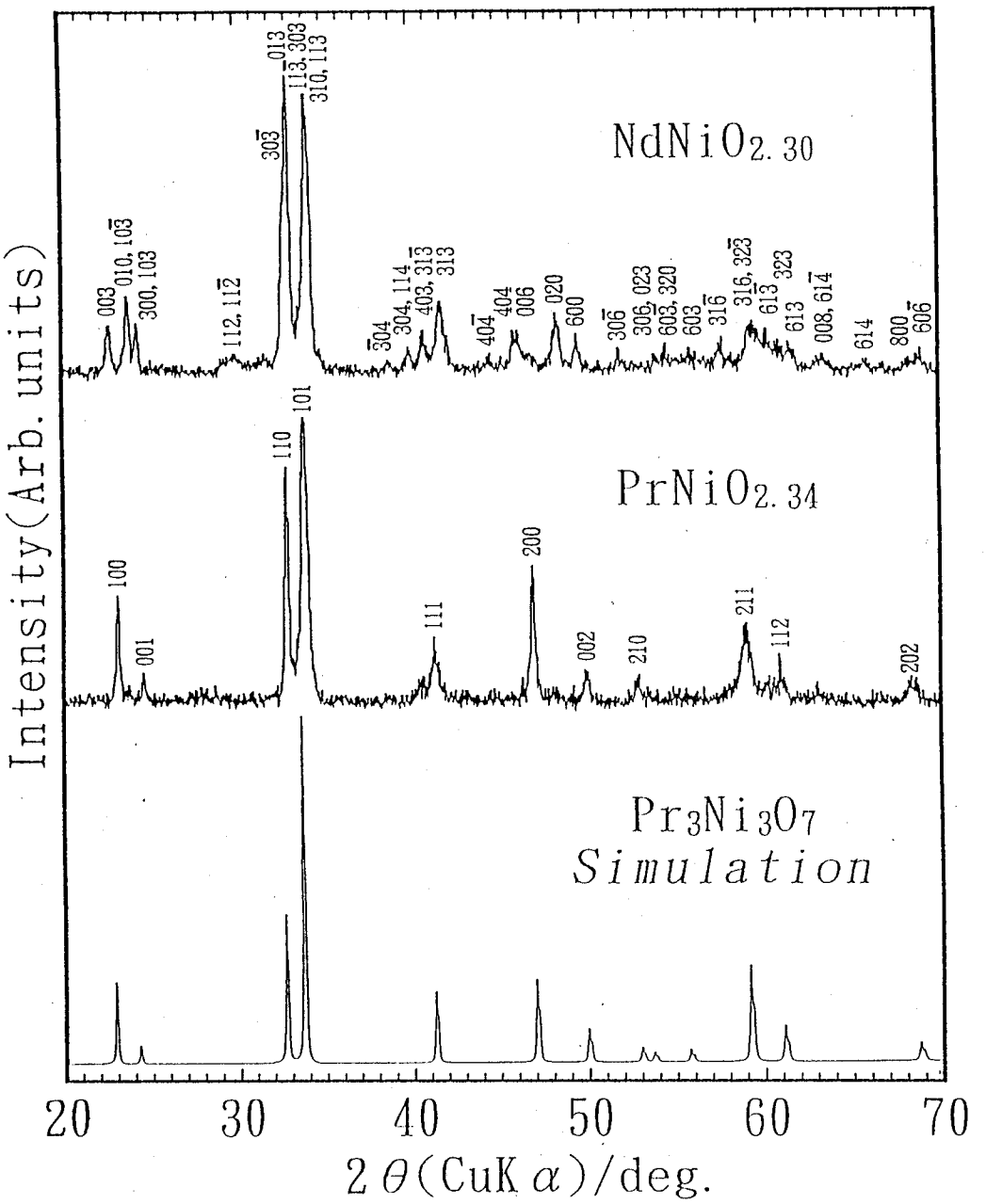

Fig. 4-3 Powder X-ray diffraction patterns of $NdNiO_{2.30}$ and $PrNiO_{2.34}$, together with the simulated pattern of $Pr_3Ni_3O_7$.

Table 4-1
Powder X-ray diffraction data of $NdNiO_{2.30}$. ($a=11.041(7)$ Å, $b=3.765(3)$ Å, $c=11.770(8)$ Å, $\beta=92.13(6)°$)

$h\,k\,l$	d_{obs} (Å)	d_{calc} (Å)	Δd (Å)
0 0 3	3.920	3.921	0.001
0 1 0	3.752	3.765	0.013
1 0 −3		3.738	−0.014
3 0 0	3.666	3.677	0.011
1 0 3		3.652	−0.014
1 1 −2	3.054	3.067	0.013
1 1 2		3.032	−0.018
3 0 −3	2.734	2.733	−0.001
0 1 3	2.711	2.716	0.005
1 1 −3	2.643	2.653	0.010
3 0 3	2.636	2.634	−0.002
3 1 0	2.626	2.631	0.005
1 1 3		2.621	−0.005
3 0 −4	2.324	2.329	0.005
3 0 4	2.256	2.256	0
1 1 4		2.255	−0.001
4 0 3	2.215	2.217	0.002
3 1 −3		2.212	−0.003
3 1 3	2.162	2.158	−0.004
4 0 −4	2.046	2.050	0.004
4 0 4	1.975	1.975	0
0 0 6	1.961	1.960	−0.001
0 2 0	1.882	1.883	0.001
6 0 0	1.840	1.839	−0.001
3 0 −6	1.760	1.757	−0.003
3 0 6	1.708	1.704	−0.004
0 2 3	1.699	1.697	−0.002
6 0 −3	1.687	1.689	0.002
3 2 0	1.675	1.657	0
3 1 −6	1.594	1.593	−0.001

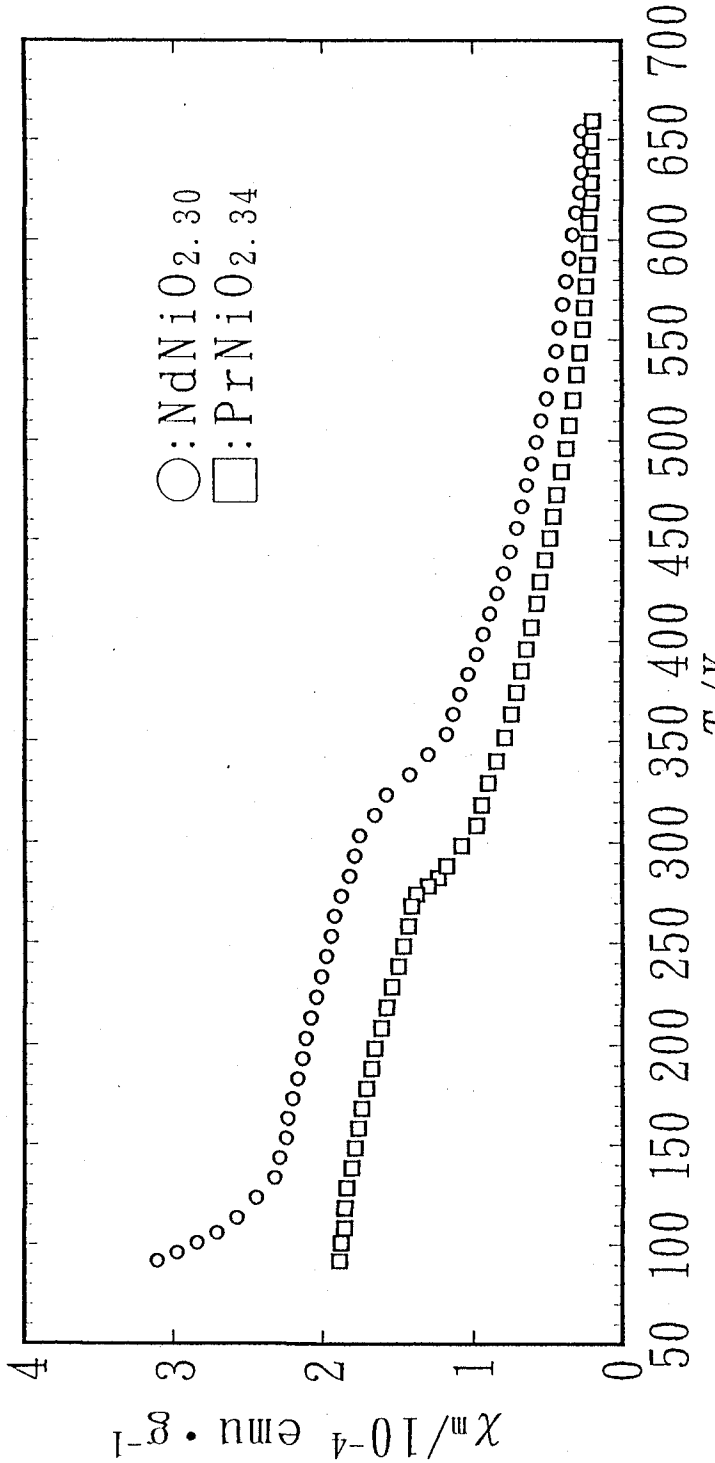

Fig. 4-4 Temperature dependence of magnetic susceptibility of $PrNiO_{2.34}$ and $NdNiO_{2.30}$.

between 270 and 300K for *Ln*=Pr and between 300 and 350K for *Ln*=Nd, respectively. These phenomena would result from a magnetic ordering between neighboring nickel ions through an oxide ion. Figure 4-5 shows magnetization of $NdNiO_{2.30}$ as a function of magnetic field at 273K. The behavior up to about 10.6kOe was similar to that of ferromagnetic materials, whereas linear relationship was observed in the magnetic field of more than 10.6kOe. It was confirmed that weak ferromagnetism appeared below the magnetic transition temperatures, similar to $LaNiO_{2.60}$ ($\simeq La_3Ni_3O_8$) mentioned in Chapter 2. The superexchange interaction among Ni-O-Ni acts more strongly if Ni-O distance becomes shorter. The fundamental cell volume of the Pr-compound was larger than that of the Nd-compound. It can be considered that the mean Ni-O distance in the Pr-compound is longer than that in the Nd-compound. Therefore, the transition temperature for Ln=Nd would be higher than that for *Ln*=Pr. For $NdNiO_{2.30}$, another magnetic transition was observed around 100K, but the origin is not clear yet.

Figure 4-6 shows DSC thermograms for $NdNiO_{2.30}$ and $PrNiO_{2.34}$. Both the thermograms have a sharp endothermic peak at T_c=282K for $PrNiO_{2.34}$ and at T_c=333K for $NdNiO_{2.30}$, respectively. Each peak is indicative of the spin-ordering of unpaired electrons since the T_c obtained by this DSC measurement agrees well with the magnetic measurement.

In view of the oxygen content, $PrNiO_{2.34}$ and $NdNiO_{2.30}$ have monovalent Ni^+ ions isoelectric to Cu^{2+}. Figure 4-7 shows XPS spectra of $LnNiO_{3-x}$ in a binding energy of the $Ni2p_{3/2}$ region. In the spectrum for $La_2Ni_2O_5$ with Ni^{3+} and Ni^+ ions, the corresponding doublet peaks at 855.6eV and 852.5eV have been observed,[9] as discussed in Chapter 2. Since nickel ions in the perovskite-type "$LnNiO_3$" (*Ln*=Pr and Nd) take divalent and trivalent states, the broad $Ni2p_{3/2}$ photoline appeared at 854.8eV, which exists between 855.9eV (Ni^{3+} in Ni_2O_3)[19] and 853.5-854.0eV (Ni^{2+} in NiO).[19] On the other hand, the photoline with a peak top at 853.0eV appeared with a tailing toward the higher binding energy side in both the reduced specimens. The results of curve-fitting analysis are drawn with thin lines in Fig. 4-7. In the $PrNiO_{2.34}$ and $NdNiO_{2.30}$, therefore, nickel ions would take more than two valence states, which may be monovalent and trivalent one.

Figure 4-8 illustrates Ni K-XANES spectra of $LnNiO_{3-x}$. The spectra for both

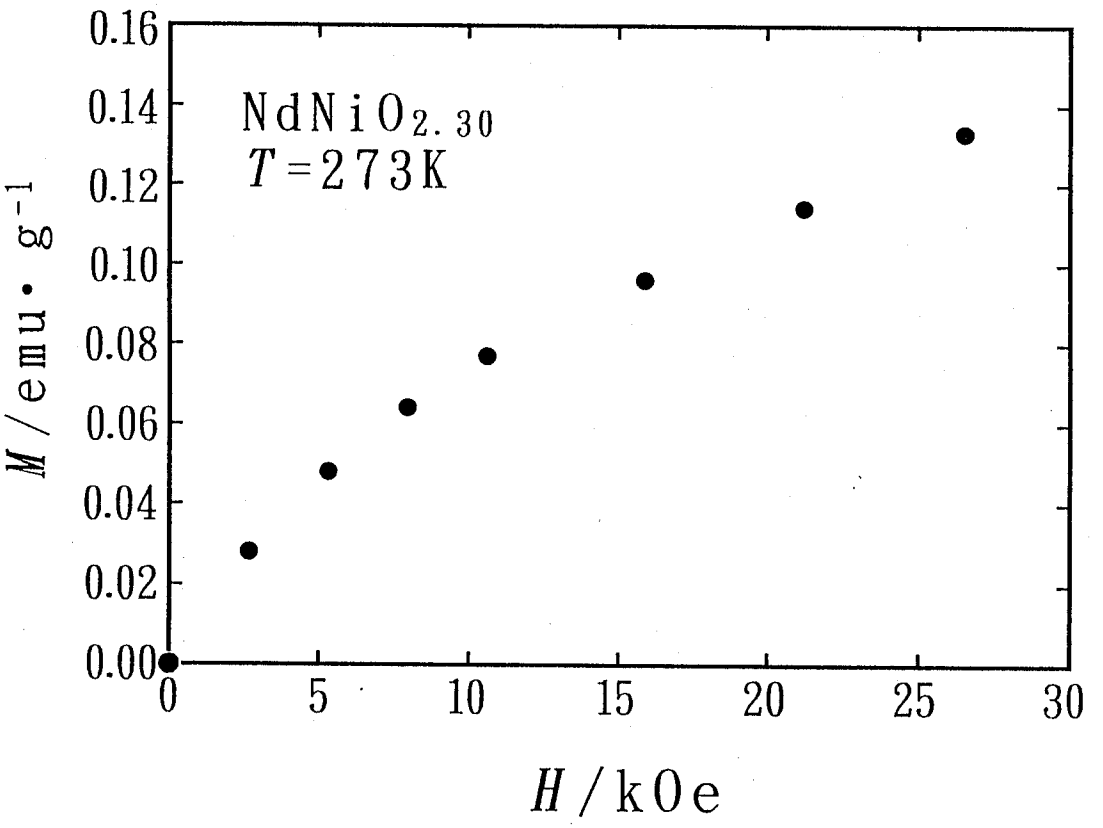

Fig. 4-5 Applied field dependence of magnetization of $NdNiO_{2.30}$.

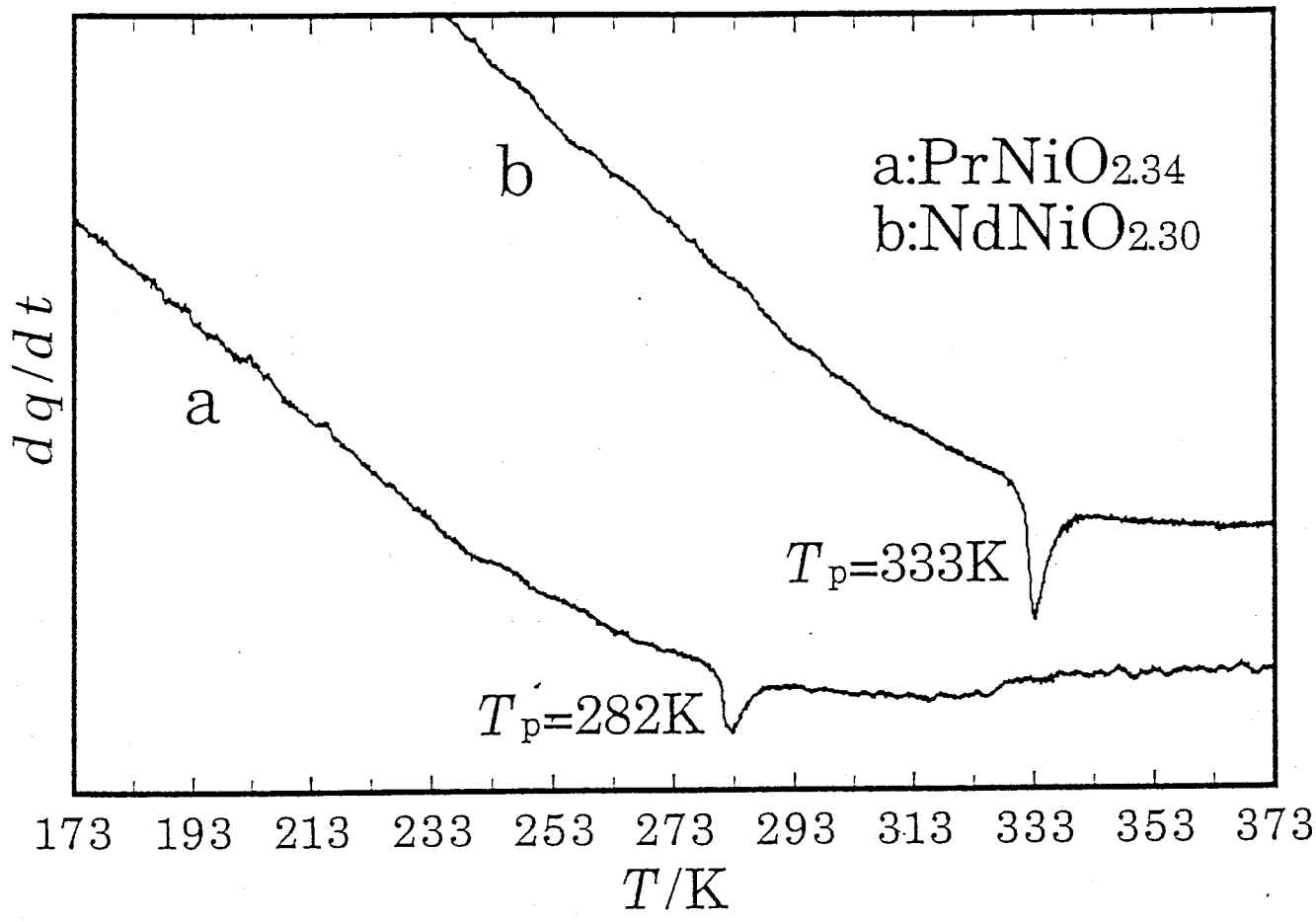

Fig. 4-6 The differential scanning calorimetric curve of a) $PrNiO_{2.34}$ and b) $NdNiO_{2.30}$.

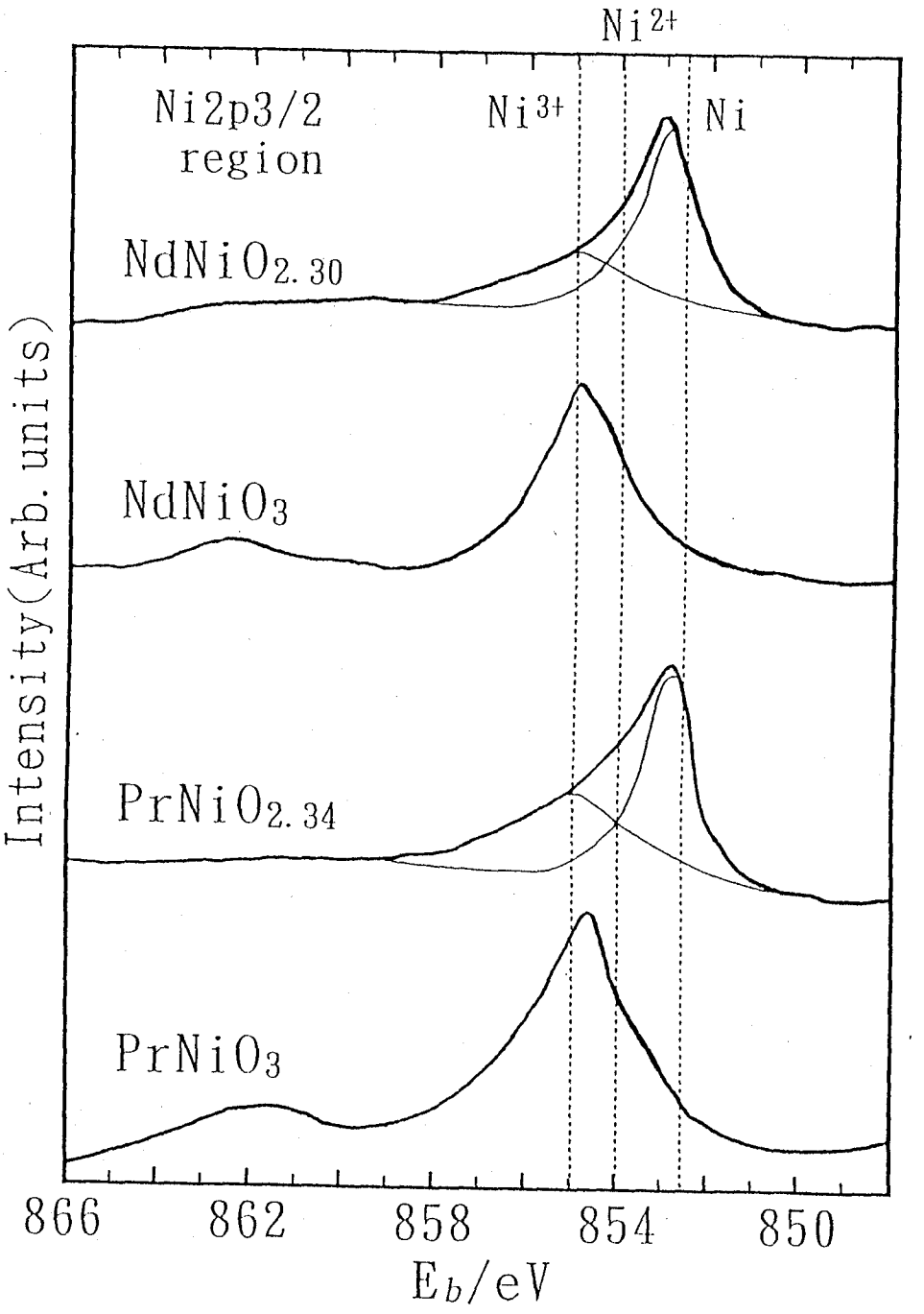

Fig. 4-7 Narrow scan XPS spectra in Ni2p3/2 region of $LnNiO_{3-x}$ (*Ln*=Pr and Nd). The results of curve-fitting analyses are also drawn with thin lines.

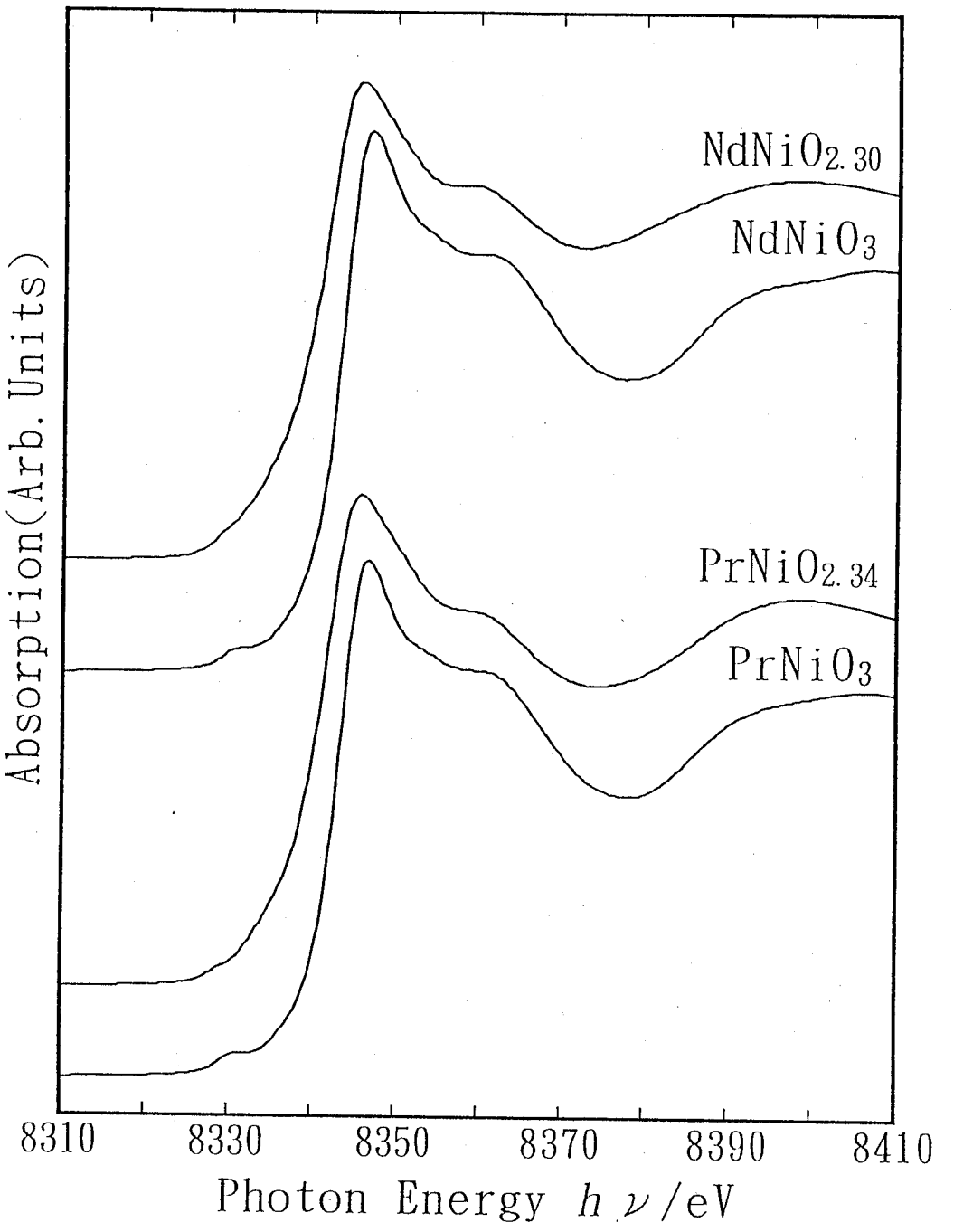

Fig. 4-8 The Ni K-edge XANES spectra of LnNiO$_{3-x}$ (Ln=Pr and Nd).

$PrNiO_3$ and $NdNiO_3$ showed an absorption peak in the pre-edge region observed at *ca.* 8332eV, which can be assigned to the 1s→3d electronic transition.[20] The transmission would be expected to appear as a relatively small peak for octahedral and square-planar coordinations and a fairly intense absorption for tetrahedral and pyramidal coordinations.[8,21] The spectra for both $PrNiO_{2.34}$ and $NdNiO_{2.30}$ have a very weak absorption at 8332eV compared to those for their respective parent $LnNiO_3$. This means that the reduced products with the composition around $Ln_3Ni_3O_7$ have neither tetrahedral nor pyramidal coordinations of nickel ions. It can be considered that nickel ions in the perovskite-related $LnNiO_{3-x}$ structures with oxygen-deficiency are favorable to have octahedral and square-planar coordinations. In view of the oxygen content, therefore, two-thirds of pairs of two apical oxygens in the NiO_6 octahedron in the fundamental perovskite-type cell are removed simultaneously so as to have no pyramidal coordinations of Ni ions. As $NdNiO_{2.30}$ was found to have the $3a_p$ x a_p x $3a_p$ supercell by X-ray diffractometry, three NiO_6 octahedra and six NiO_4 square-planes should be present in the superlattice if the composition of $Nd_3Ni_3O_7$ is assumed.

According to theses considerations mentioned above, the most likely structural model for $Nd_3Ni_3O_7$, as shown in Fig. 4-9 can be proposed, where the structure is shown as the (010) projection. The corner-shared NiO_6 octahedra are ordered in the [010] direction. Two sheets of NiO_4 square-planes with their corners shared connect the octahedra in the [100] and [010] directions. The octahedral chains would be formed toward the *b*-axis direction. A kind of an antiphase boundary[22] lies across the two neighboring NiO_4 square-planes, which is parallel to the (010) plane. In the region surrounding the planes, the same ordered arrangement as seen in $La_2Ni_2O_5$ is formed. Ni^{3+} ions generally adopt octahedral coordination while Ni^+ ions are thought to be stable by having square-planar coordination. Lacorre had also pointed out that Ni^+ ions prefer the square-planar coordination.[10] Then charge distributions in the compound can be expressed as $Nd_3[Ni^{3+}O_{6/2}][Ni^+O_{4/2}]_2$, where /2 means that the neighboring polyhedra are corner-shared with each other. Such charge distributions of Ni ions have also been observed in $La_2Ni_2O_5$ ($=La_2[Ni^{3+}O_{6/2}][Ni^+O_{4/2}]$). Schematic view of the structure of $Nd_3Ni_3O_7$ is depicted in Fig. 4-10.

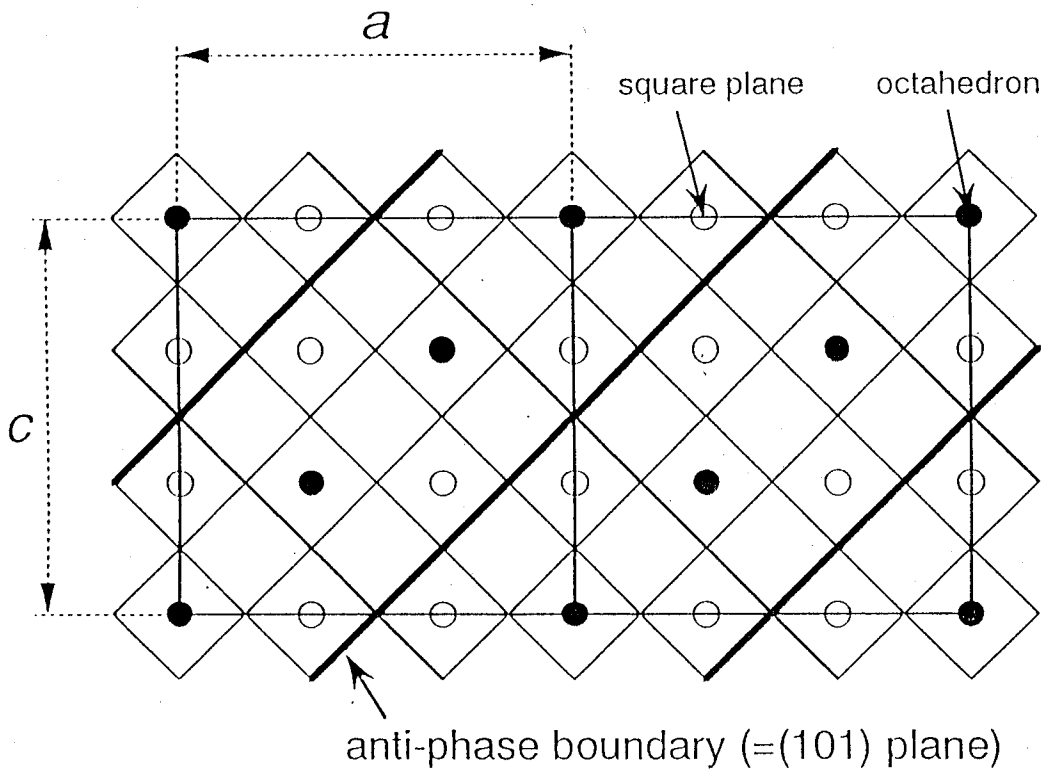

Fig. 4-9 The (010) projection of structural model for $Nd_3Ni_3O_7$. Nd ions are omitted for simplicity.

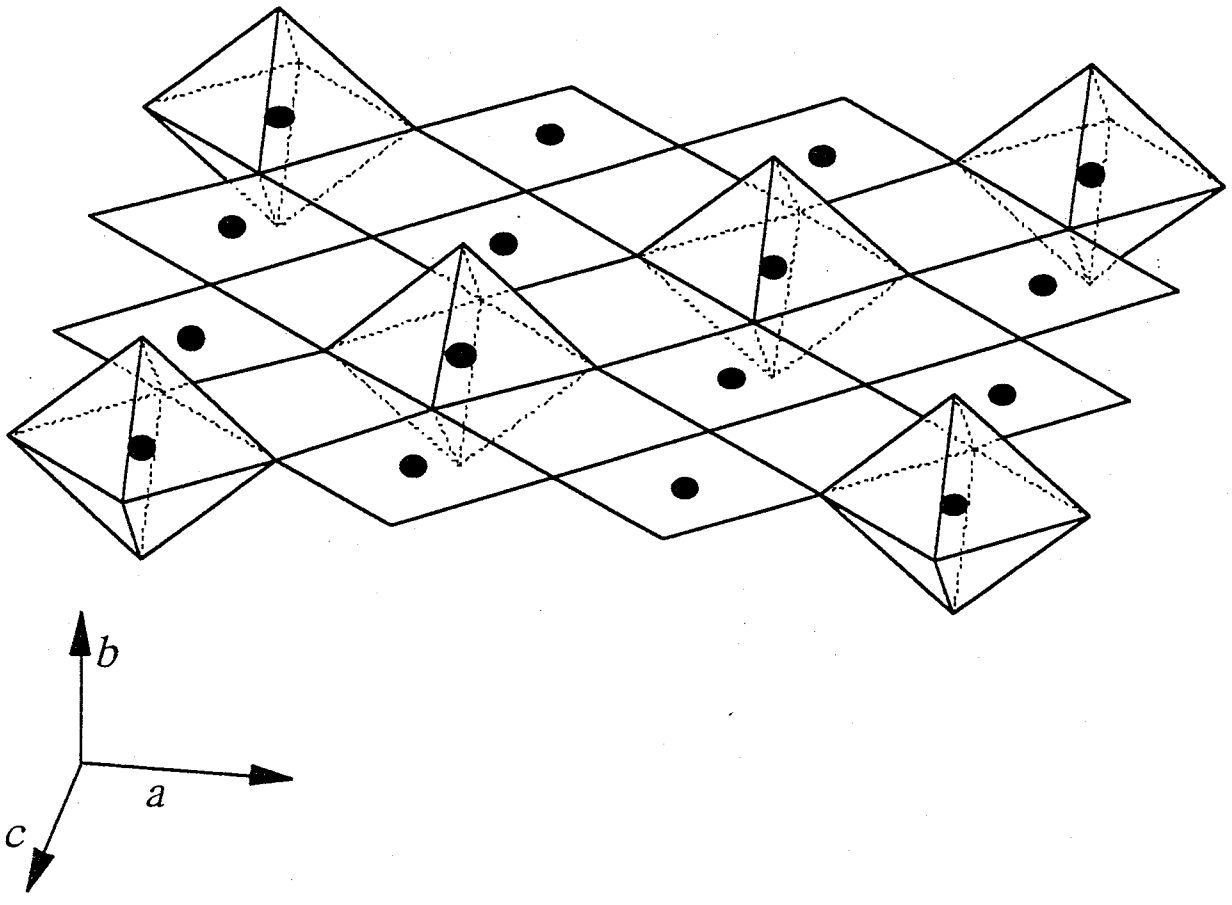

Fig. 4-10 Schematic view of the structure of $Nd_3Ni_3O_7$. Ni ions are represented by solid circles. Nd ions are not shown for simplicity.

Crystal Structure Refinement of $Nd_3Ni_3O_7$

Based on the structural model mentioned the last section, crystal structure refinement of $Nd_3Ni_3O_7$ was carried out. The cell determined for $Nd_3Ni_3O_7$ was the supercell of Z=3. Then, primitive lattice was chosen for simplicity. Figure 4-11 shows the relationship between the supercell and the primitive cell, whose length was calculated as follows: $a_p \simeq 8.5$Å, $b_p \simeq 3.7$Å, $c_p \simeq 5.3$Å and $\beta \simeq 75.7°$. A refinement of this primitive structure proceeded assuming a space group of P2 (unique axis *b*).[17] Initial coordinates were taken as follows: Nd(1), 1(b), (0, y, 1/2), y≃0.5; Nd(2), 2(e), (x,y,x), x≃0.333, y≃0.5, x≃0.833; Ni(1), 1(a), (0, y, 0), y=0 (fixed for determination of center in structure); Ni(2), 2(e), (x,y,z), x≃z≃0.333, y≃0; O(1), 2(e), (x,y,z), x≃z≃0.167, y≃0; O(2), 1(d), (1/2, y, 1/2), y≃0; O(3), 2(e), (x,y,z), x≃0.167, y≃0, z≃0.667; O(4), 1(c), (1/2, y, 0), y≃0; O(5), 1(a), (0, y, 0), y≃0.5. The refinement was carried out in stage by stage; the atomic coordinates were fixed in initial calculations, but were sussequently allowed to vary after the scale, background, half-wirth and unit cell parameters as as to be close to their optimum values; finally, the thermal parameter were refined. When the isotropic thermal parameters were refined, those for same elements had to be constrained to the same value.

Some of positional parameters for oxygens also had to be constrained. It may be attributable to that the sample had poor crystallinity for the Rietveld analysis due to low-temperature reduction. Then, the refinement was proceeded based on the assumptions as follows; (1) interatomic distance of Ni(2)-O(1) and that of Ni(2)-O(3), and interatomic distance of Ni(2)-O(2) and that of Ni(2)-O(4) take the same value, respectively. (2) the Ni(2) lies on the plane formed by the neighboring O(1), O(2), O(3) and O(4). The constraint conditions are illustrated in Fig. 4-12. The observed and calculated X-ray diffraction patterns, and their difference plots are shown in Fig. 4-13. The final parameters for the refinement are summarized in Table 4-2.

Figure 4-14 shows a schematic drawing of the Ni-O coordination. The bond of Ni(1)-O(5) directing to the *b*-axis is omitted for simplicity. The Ni(1)-O(5) distances calculated to be 1.88 and 1.89Å. The observed average interatomic Ni(1)-O distance in

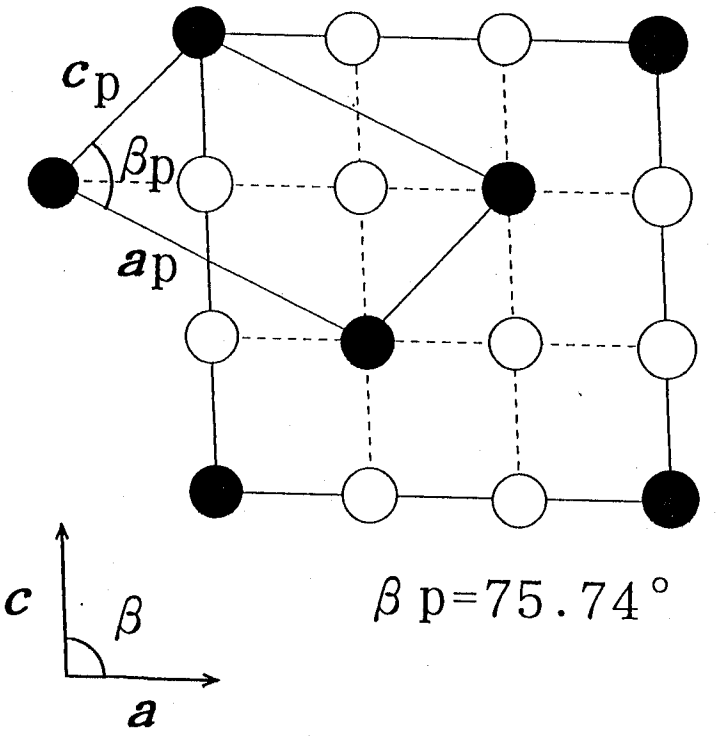

Fig. 4-11 The relation ship between the actual cell for $Nd_3Ni_3O_7$ (Z=3) and the primitive cell (Z=1).

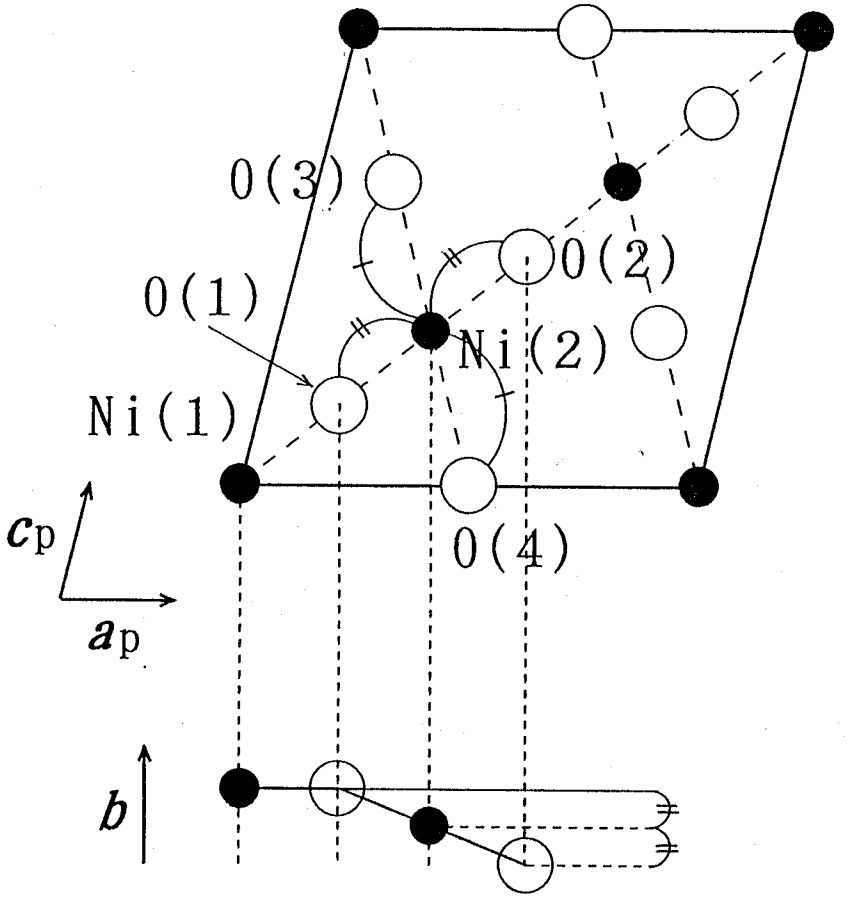

Fig. 4-12 Schematic drawings for the primitive cell for $Nd_3Ni_3O_7$. The constraint conditions for structural analysis are shown in the figures.

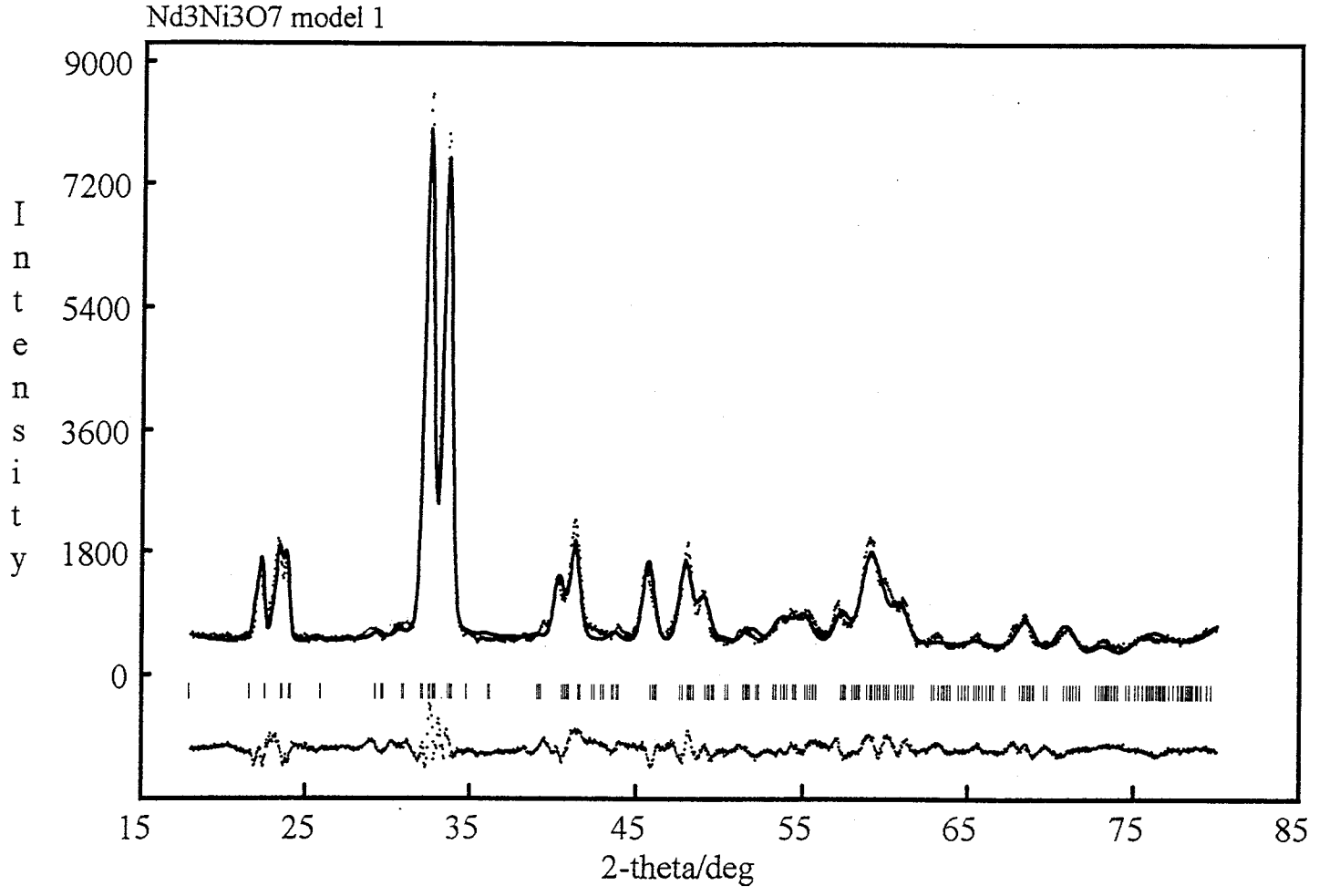

Fig. 4-13 Observed and calculated diffraction patterns, and their difference plots as a result of Rietveld analysis of $Nd_3Ni_3O_7$.

Table 4-2. Positional parameters refined for $Nd_3Ni_3O_7$. The cell constants are a=8.521(3)Å, b=3.783(2)Å, c=5.328(2)Å, β=75.52(2)° and Z=1 for P2. The reliability factors are R_{wp}=11.09% (S=R_{wp}/R_e=2.87), R_p=8.89%, R_I=3.27% and R_F=1.71%. *: constrained corresponding to the model.

Atom	site	g	x	y	z	B/Å^2
Nd(1)	1b	1.0	0.0	0.541(4)	0.5	1.1(6)
Nd(2)	2e	1.0	0.331(4)	0.534(4)	0.833(6)	1.1
Ni(1)	1a	1.0	0.0	0.0	0.0	1.9(9)
Ni(2)	2e	1.0	0.330(3)	-0.009(4)	0.335(4)	1.9
O(1)	2e	1.0	0.160*	0.0	0.170*	5.8(15)
O(2)	1d	1.0	0.5	-0.018*	0.5	5.8
O(3)	2e	1.0	0.160*	-0.009*	0.670*	5.8
O(4)	1c	1.0	0.5	-0.009*	0.0	5.8
O(5)	1a	1.0	0.0	0.498(10)	0.0	5.8

Conditions for constraint :
A(O1,x)=2×A(Ni2,x)-1/2, A(O1,z)= 2×A(Ni2,z)-1/2
A(O3,x)=2×A(Ni2,x)-1/2, A(O3,z)= 2×A(Ni2,z)
A(O2,y)=2×A(Ni2,y)-A(O1,y), A(O3,y)=A(O4,y)=A(Ni2,y).

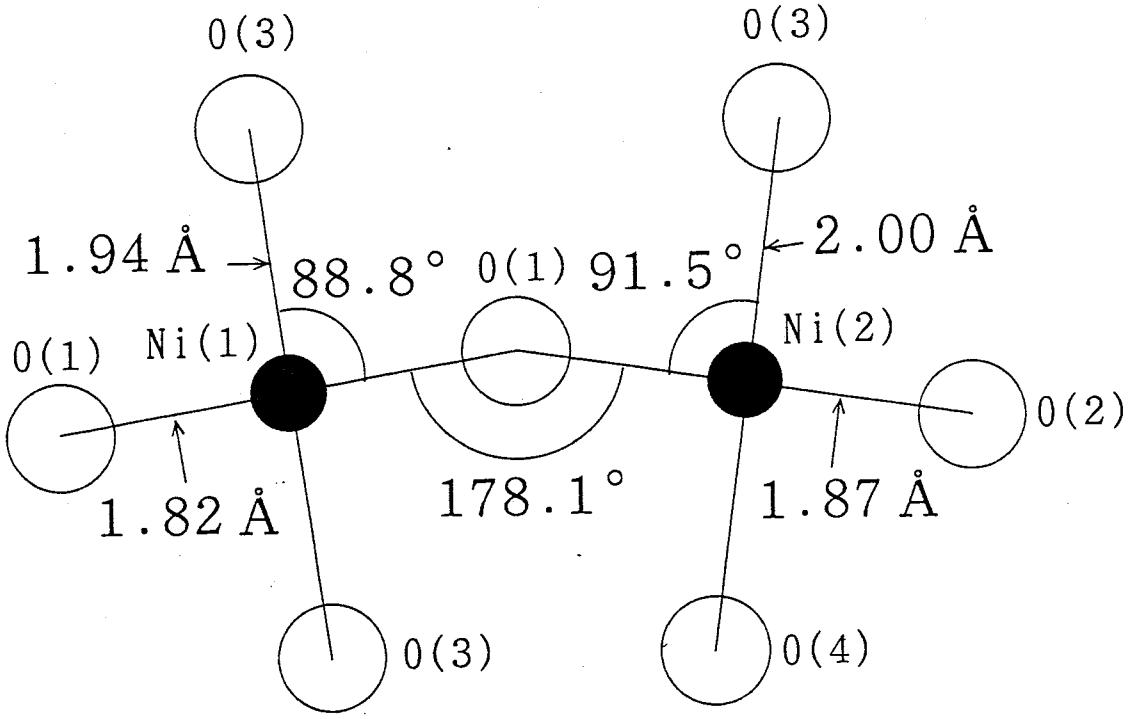

Fig. 4-14 Coordination polyhedra, $Ni(1)O_6$ and $Ni(2)O_4$, and Ni-O distances and angles in $Nd_3Ni_3O_7$.

the octahedron is 1.89 Å. This value agrees well with that of 1.91Å, which is the effective ionic radius sum between the 6-fold Ni^{3+} ion with a low-spin state and the 2-fold O^{2-} ion. The average Ni(2)-O distance in the square-plane is 1.93Å. The value also agrees well with that expected in the Ni^{+}(2)-O distance in the square-plane (1.94Å). It can be confirmed that the Ni(1) ion in the octahedron takes trivalent state and the Ni(2) ion in the square-plane takes monovalent state, as seen in $La_2Ni_2O_5$. The angle among O(1)-Ni(1)-O(3) is 88.8° and that among O(1)-Ni(2)-O(3) is 91.5°. That among Ni(1)-O(1)-Ni(2) is 178.1°. These facts mean that the diagonal angles in each polyhedron are almost normal to one onother. And the chains of O-Ni(1)-O-Ni(2)-O- on the [101] projection is almost linear.

The [101] section of primitive cell of $Nd_3Ni_3O_7$ is represented in the lower part of Fig. 4-15. The $Ni(2)O_{4/2}$ square-planes neighboring to each other are canted with the angle of about 2° from the $Ni(1)O_{6/3}$ basal planes. Superexchange interaction among d^9 metal ion-O^{2-}-d^9 metal ion has been reported to be antiferromagnetic.[23] In La_2NiO_4,[24,25] whose magnetic behavior is similar to $Nd_3Ni_3O_7$, the electron spin moment lies antiparallel directed to <110> of the fundamental perovskite-type structure, *i.e.*, to <001> of the primitive cell of $Nd_3Ni_3O_7$, which is also shown in the upper part of Fig. 4-13. If the spins are assumed to be directed to this direction, it would produce a net moment along the *c*-axis in the presence of an applied field. This may be the origin of the ferromagnetic behavior of $Nd_3Ni_3O_7$.

Neutron Diffraction for $Pr_3Ni_3O_7$

$Nd_3Ni_3O_7$ was found to take the monoclinic 3 x 1 x 3 supercell of the perovskite. But $Pr_3Ni_3O_7$ cannot be identified as a supercell. It could be indexed as the simple tetragonal cell. Then, a TOF neutron diffractometry for $Pr_3Ni_3O_7$ was carried out. Neutron diffraction enables the carrying out of investigations or determinations of the oxide ion sites in a compound containing heavy metals.[26] Fig. 4-16 shows the TOF neutron diffraction pattern for $PrNiO_{2.34}$. Ten-thousandth of TOF value nearly corresponds to the d-spacing. The TOF value around 38000 can be assigned to100

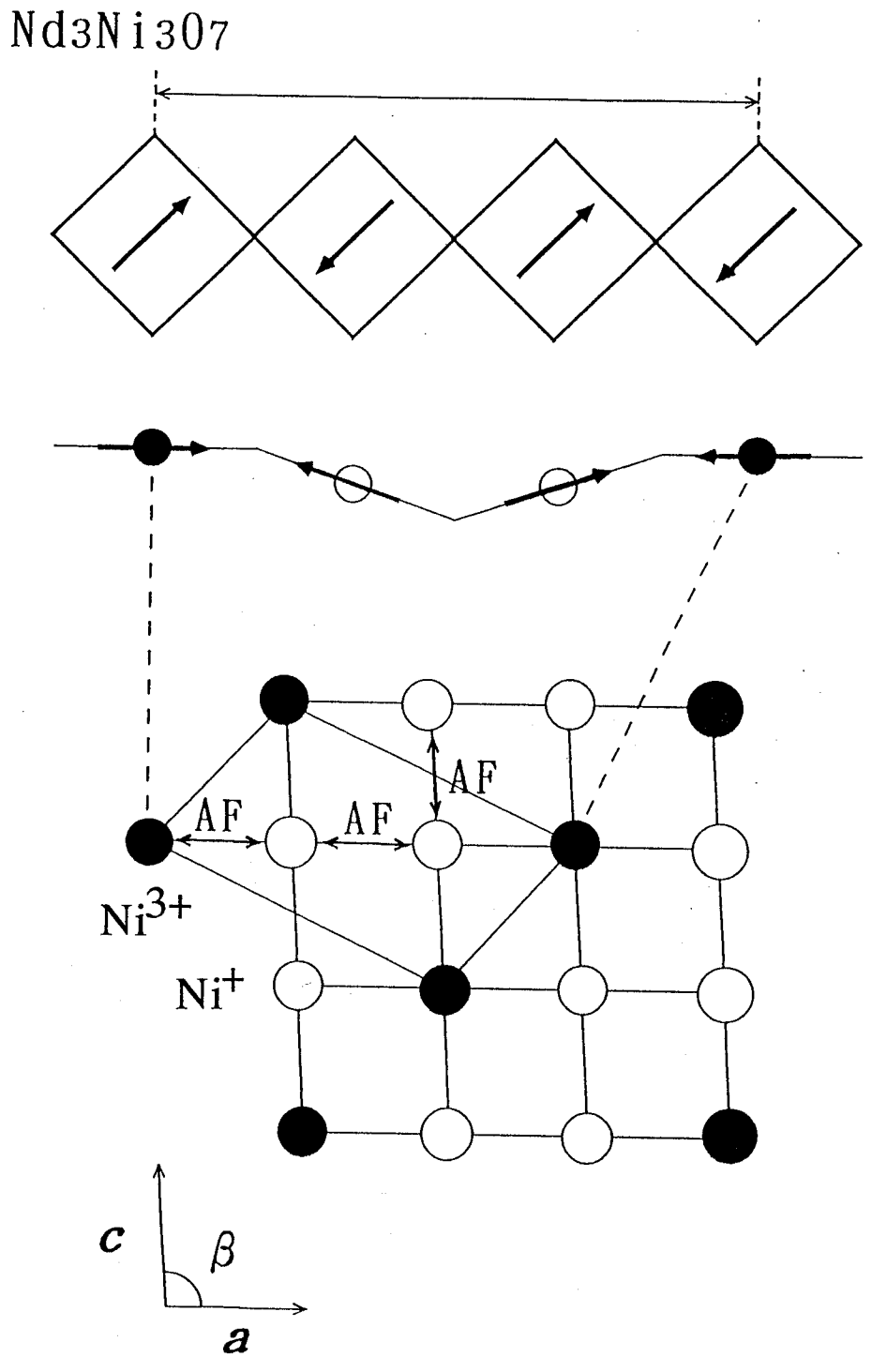

Fig. 4-15 Possible model for weak-ferromagnetic $Nd_3Ni_3O_7$.

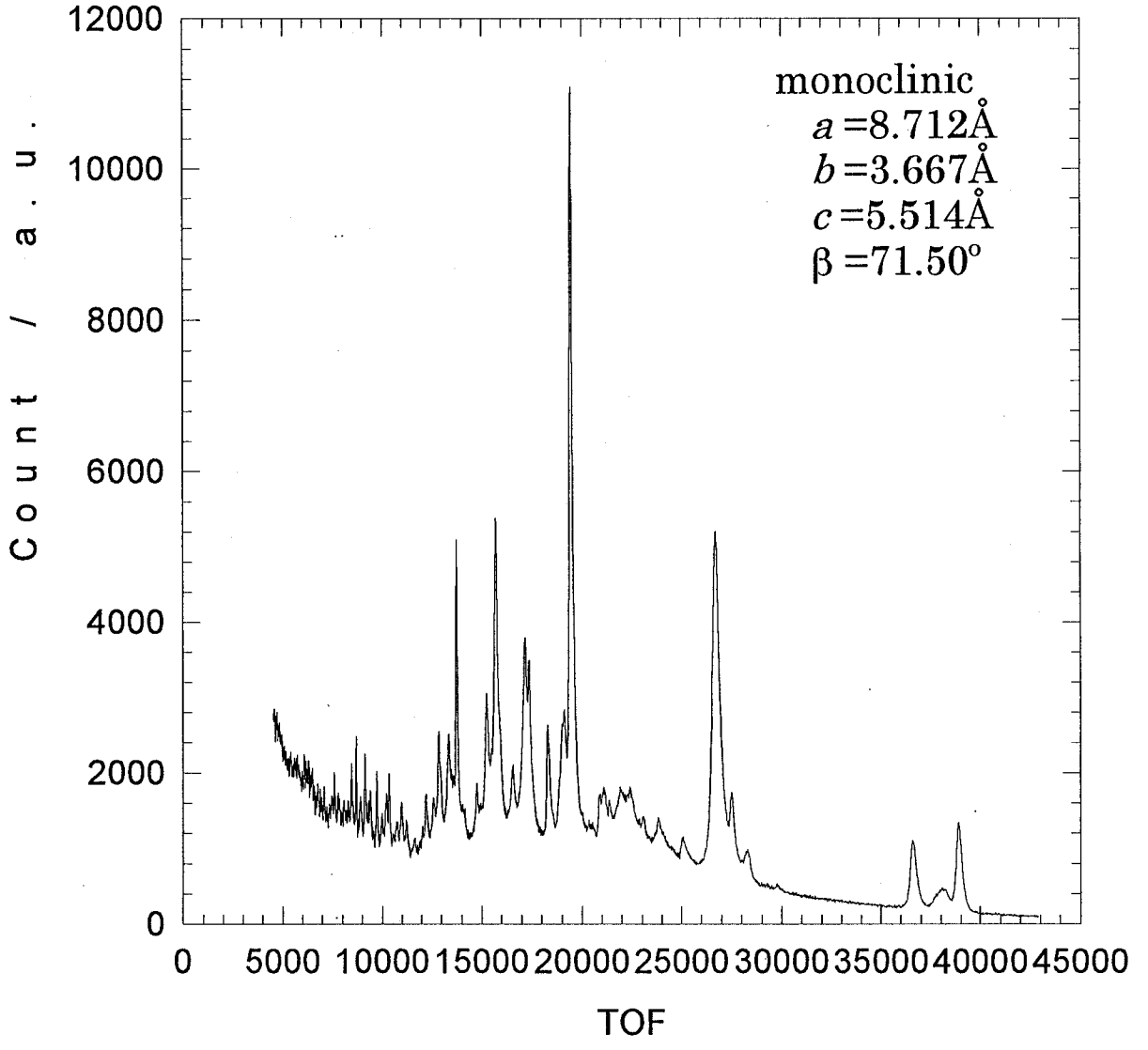

Fig. 4-16 TOF neutron diffraction patterns of $PrNiO_{2.34}$.

refrection of the fundamental perovskite. This reflection is splitted into at least three peaks. This penomenon cannot be explained by using the tetragonal cell of the fundamental perovskite..

The cell choice and initial parameter were determined by reference to the result of X-ray Rietveld analysis for $Nd_3Ni_3O_7$. The monoclinic $P2$ space group, and initial cell parameters of a=8.708Å, b=3.655Å, c=5.508Å, and β=71.57°, which can be calculated from the tetragonal cell, were applied. Up to now, only the cell parameters were refined. The final cell parameters were shown in Table 3-3. The peak positions are in a rather good agreement between observed and calculated ones. This indicates that $Pr_3Ni_3O_7$ also take 3 x 1 x 3 superstructure similar to $Nd_3Ni_3O_7$.

Giving a glance at Table 3-3, the refined cell parameters by neutron diffraction are almost identical with the initial ones calculated from the simple tetragonal cell by X-ray diffraction. Moreover, the initial and refined β values are same within the error. These facts mean that monoclinicity of $Pr_3Ni_3O_7$ is very small and nickel and neodymium ions must be sited just around the ideal positions, *i.e.*, (0, 0, 0) for octahedral Ni^{3+} ions, (1/3, 1/3, 1/3) for square-planar Ni^{+} ions, and (0, 1/2, 1/3) and (1/3, 1/2, 5/6) for Nd^{3+} ions, respectively (referred to Fig. 4-11). Neutron diffraction study shows that metal ions form pseudo-tetragonal cell. Symmetry reduction to the monoclinic system would be mainly induced by ordered array of oxide ions acommpanied with the disproportionation of nickel ions.

Table 4-3. Positional parameters refined for $Pr_3Ni_3O_7$. The cell constants are a=8.712(5)Å, b=3.667(1)Å, c=5.514(4)Å, β=71.50(7)° and Z=1 for P2. The reliability factors are R_{wp}=13.00% ($S=R_{wp}/R_e$=3.13), R_p=9.57%, R_I=15.96% and R_F=11.63%. *: constrained corresponding to the model.

Atom	site	g	x	y	z	B/Å^2
Nd(1)	1b	1.0	0.0	0.513(2)	0.5	1.0(6)
Nd(2)	2e	1.0	0.334(7)	0.495(2)	0.869(6)	1.1
Ni(1)	1a	1.0	0.0	0.0	0.0	0.6(2)
Ni(2)	2e	1.0	0.332(3)	-0.02(1)	0.331(5)	0.6
O(1)	2e	1.0	0.164*	0.0	0.162*	2.9(4)
O(2)	1d	1.0	0.5	-0.04*	0.5	2.9
O(3)	2e	1.0	0.164*	-0.02*	0.662*	2.9
O(4)	1c	1.0	0.5	-0.02*	0.0	2.9
O(5)	1a	1.0	0.0	0.498(10)	0.0	2.9

Conditions for constraint :
A(O1,x)=2×A(Ni2,x)-1/2, A(O1,z)= 2×A(Ni2,z)-1/2
A(O3,x)=2×A(Ni2,x)-1/2, A(O3,z)= 2×A(Ni2,z)
A(O2,y)=2×A(Ni2,y)-A(O1,y), A(O3,y)=A(O4,y)=A(Ni2,y).

References

[1] J.B.Goodenough and P.M.Raccah, *J. Appl. Phys.*, **36**, 1031 (1965).

[2] G.Demazeau, A.Marbeuf, M.Pouchard, and P.Hagenmuller, *J. Solid State Chem.*, **3**, 582 (1971).

[3] P.Laccorre, J.B.Torrance, J.Pannetier, A.I.Nazzal, P.W.Wang, and T.C.Huang, *J. Solid State Chem.*, **91**, 225 (1991).

[4] X.Obradors, L.M.Paulius, M.B.Maple, J.B.Torrance, A.I.Nazzal, J.Fontcuberta, and X.Granados, *Phys. Rev. B*, **47**, 12353 (1993).

[5] P.C.Canfield, D.Thompson, S-W. Cheong, and L.W.Rupp, *Phys. Rev. B*, **47**, 12357 (1993).

[6] J.K.Vassiliou, M.Hornbostel, R.Ziebarth, and F.J.Disalvo, *J. Solid State Chem.*, **81**, 208 (1989).

[7] J.Garcia, A.Gonzalez, M.J.Sanchis, M.D.Marcos, E.Martinez, F.Sapina, D.Beltran, and A.Beltran, *Solid State Ionics*, **63-65**, 52 (1993).

[8] T.Moriga, S.Kikkawa, M.Takahashi, F.Kanamaru, and I.Nakabayashi, *Jpn. J. Appl. Phys.*, **32** Suppl. 32-2, 764 (1993).

[9] T.Moriga, O.Usaka, T.Imamura, I.Nakabayashi, I.Matsubara, T.Kinouchi, S.Kikkawa, and F.Kanamaru, *Bull. Chem. Soc. Jpn.*, **67**, 687 (1994).

[10] P.H.Lacorre, *J.Solid State Chem.*, **97**, 495 (1992).

[11] Z.Zhang, M.Greenblatt, and J.B.Goodenough, *J. Solid State Chem.*, **108**, 402 (1994).

[12] M.Crespin, P.Levitz, and L.Gatineau, *J. Chem. Soc., Faraday Trans. 2*, **79**, 1181 (1983).

[13] P.Levitz, M.Crespin, and L.Gatineau, *J. Chem. Soc., Faraday Trans. 2*, **79**, 1195 (1983).

[14] F.Izumi, *J. Miner. Soc. Jpn.*, **17**, 37 (1985).

[15] N.Watanabe, H.Asano, H.Iwasa, S.Sato, H.Murata, K.Karahashi, S.Tomiyoshi, F.Izumi, and K.Inoue, *Jpn. J. Appl. Phys.*, **26**, 1164 (1987).

[16] Y.Maeno, H.Teraoka, and K.Matsukuma, *Kotai Butsuri (Solid State Physics)*, **26**, 235 (1991).

[17] "International Tables for X-ray Crystallography", Vol. IV, Kynoch Press, Birmingham, (1974).

[18] T.Yamaguchi, Master Thesis (ISIR, Osaka University, Japan, 1992).

[19] D.Briggs and M.P.Seah, " Practical Surface Analysis by Auger and X-ray Photoelectron Spectroscopy", 2nd Ed., Wiley, Chichester, 1990.

[20] M.Medarde, A.Fontaine, J.L.Garcia-Munoz, J.Rodriguez-Carvajal, M. de Dantis,

M.Sacchi, G.Rossi, and P.H.Lacorre, *Phys. Rev. B*, **46**, 14975 (1992).

[21] G.J.Colpas, M.J.Maroney, C.Bagyinka, M.Kumar, W.S.Willis, S.L.Suib, Nbaidya, and P.K.Mascharak, *Inorg. Chem.*, **30**, 920 (1991).

[22] T.Moriga, A.Yoshiasa, F.Kanamaru, K.Koto, M.Yoshimura, and S.Somiya, *Solid State Ionics*, **31**, 319 (1989).

[23] J.B.Goodenough, "Magnetism and Chemical Bond", Interscience, New York (1963).

[24] T.Freltoft, D.J.Buttrey, G.Aeppeli, D.Vaknin, and G.Shirane, *Phys. Rev. B*, **44**, 5046 (1991).

[25] P.Gopalan, M.W.McElfresh, Z.Kakol, J.Spalek, and J.M.Honig, *Phys. Rev. B*, **45**, 249 (1992).

[26] J.P.Eberhart, " Structural and Chemical Analysis of Materials", Wiley, Chichester, (1991).

Chapter 5.

General Discussion

Disproportionation of nickel ions in $LnNiO_{3-x}$ (Ln=La, Pr, Nd)

In the $La_2Ni_2O_5$ and $Nd_3Ni_3O_7$, nickel ions are found to take either trivalent or monovalent, not divalent. Especially $La_2Ni_2O_5$, though the average valence of nickel ions is +2, disproportionation of $2Ni^{2+}$ into Ni^{3+} and Ni^{+} occurs.

The energy required to break up a crystal into infinitely separated ions is called as the lattice energy U^1:

$$M_mX_x(s) \text{ ---> } mM^{Z_M}(g) + xX^{Z_X}(g).$$

If the bonding in the crystal were completely ionic, the lattice energy could be calculated from the ionic charges and the geometric arrangement of the ions in the lattice. It is convenient to express this theoretical electrostatic lattice energy U_e as a function of the stoichiometric numbers m and x, the ionic charges Z_M and Z_X, the closest interionic distance r, and a geometric factor called the reduced Madelung constant, M':

$$U_e = -M'\Sigma\{ Z_MZ_X(M+x)e^2 / 2r \} = -M \Sigma\{ Z_MZ_X e^2 / r \}$$

As the first approximation, the lattice energy can be determined by using the charge distribution and the interionic distance and the coordination number, *i.e.*, the lattice energy can be replaced for $-\Sigma Z_MZ_X/r$. The models for the calculation are (a) $La_2[Ni^{3+}O_{6/2}][Ni^{+}O_{4/2}]$ and (b) $La_2[Ni^{2+}O_{6/2}][Ni^{2+}O_{4/2}]$. The schematic arrays of these models are shown in Fig. 5-1. In the model (a), the Ni-O distances obtained in this study were used. In the model (b), reported Ni-O distances, which have been seen in La_2NiO_4, were used. The distances in the $Ni^{2+}O_6$ octahedron are 1.93Å (4-fold, in basal plane) and 2.24Å (2-fold, perpendicular to basal plane), respectively[2,3]. The distance in the $Ni^{2+}O_4$ square-plane is 1.84Å (4-fold), which is calculated from their effective radii. The Ni ion lying in the square-plane was chosen as the center for the calculation and the calculation was performed by considering contributions from all the species within the distance of about 6.2Å from the center. The contribution of the first- and second-neighbor lanthanum

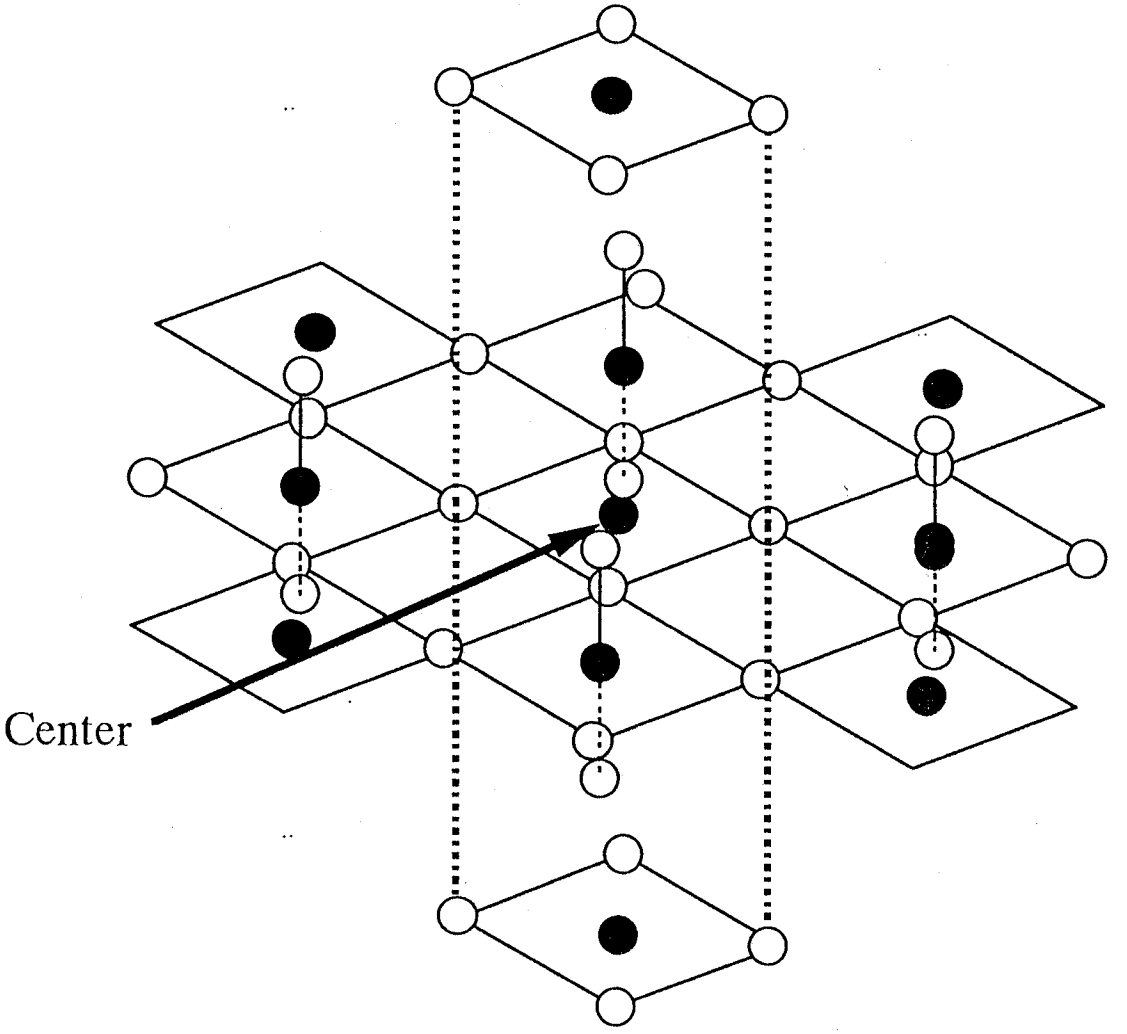

Fig. 5-1 Schematic arrays of ion species used for lattice energy calculation. Solid and open circles represent nickel and oxide ions, respectively. The first- and second-nearest lanthanum ions were included for calculation (not shown).

ions (8 + 12), which are not shown in Fig. 5-1, were also included in the calculation. The results are 12.424 for the model (a) and 11.135 for the model (b). It suggests that the model (a) is more stable than the model (b). These considerations support the disproportionation into Ni^{3+} and Ni^{+} in $La_2Ni_2O_5$ and would support that in $Ln_3Ni_3O_7$ (*Ln*=Pr, Nd).

The parent compound $LnNiO_3$ has Ni^{3+} ions. Topotactic elimination of apical oxide ions easily turns a half of octahedral $Ni^{3+}O_6$ into square-planar $Ni^{+}O_4$, with the other half of octahedral $Ni^{3+}O_6$ remaining unchanged. More energy would be needed, if a half of Ni^{3+} ions in the octahedral coordination turn into Ni^{2+} ions and the other half of Ni^{3+} ions turn into square-planarly coordinated Ni^{2+} ions.

Recently, Demourgues et al.[4,5] proposed that some disproportionation of divalent nickel may occur according to $2Ni^{2+} <---> Ni^{+} + Ni^{3+}$ in La_2NiO_{4+x} by EPR. Such disproportionations in lanthanide nickelates are not rare.

Local structure around Ni ions in $La_2Ni_2O_5$ and $Ln_3Ni_3O_7$ (Ln=Pr, Nd)

Structural analysis of $La_2Ni_2O_5$ and $Nd_3Ni_3O_7$ revealed that two kinds of Ni-O distance exist in the $[NiO_{4/2}]$ layer, or so-called the *ab*-plane. If two Ni-O bonds along the *a*-axis direction take a larger distance, the other two bonds along the *b*-axis direction take a shorter distance, or vice versa (this type is abbreviated as model 1). Generally, $Ni^{3+}O_6$ octahedron contains four short bonds in the $[NiO_{4/2}]$ layer and two slightly-long bonds normal to the $[NiO_{4/2}]$ layer (or along the *c*-axis). That is, in the $[NiO_{4/2}]$ layer, the Ni^{+}-O distance is longer than the Ni^{3+}-O distance. $Ni^{+}O_4$ square-plane is thought to contain four longer bonds than those in the $[NiO_{4/2}]$ layer in the octahedron (this type of coordinations is as model 2). Schematic representations of these arrays of ions are shown in Fig. 5-2, which are the case of $La_2Ni_2O_5$. A half of lattice parameters *a* and *b* was 3.908Å in average, which almost corresponds to Ni^{3+}-O-Ni^{+} distance on the $[NiO_{4/2}]$ layer. If Ni-O distance in the $Ni^{+}O_4$ square-plane in the model 2 take the ideal value of 1.94-1.99Å, that in the $Ni^{3+}O_6$ octahedron is calculated to be 1.968-1.918Å. This value seems to be rather large than that expected value of 1.84Å, which is the sum of effective ionic radii by Shannon.[6] This hypothesis in the model 2 is not acceptable.

$La_2Ni_2O_5$ is considered to be comprised of alternative laminates of the $[NiO_{4/2}]$ layer and $[LaO_{0.5}]$ layer. The Ln^{3+} ion takes 10-fold coordination. Compared to both models, no oxide ions exist in the direction denoted as the arrows in the model 2. Ions in ionic crystal would favor an isotropic coordination by the opposite-charged ion. The coordination of Ln^{3+} ion in model 1 is more isotropically coordinated by oxide ions than that in model 2. The structure like the model 1 would be more stable than that like the model 2. This consideration is applicable to $Ln_3Ni_3O_7$. The features of coordination around Ln^{3+} ion are the same one as the model 1 (10-fold Ln^{3+} ion) and the modified model 1 by all oxide ions removing from the $[LnO_{0.5}]$ layer (8-fold Ln^{3+} ion). Somewhat strange coordinations of Ni ion may be attributable to the favorable coordinations of Ln^{3+} ion.

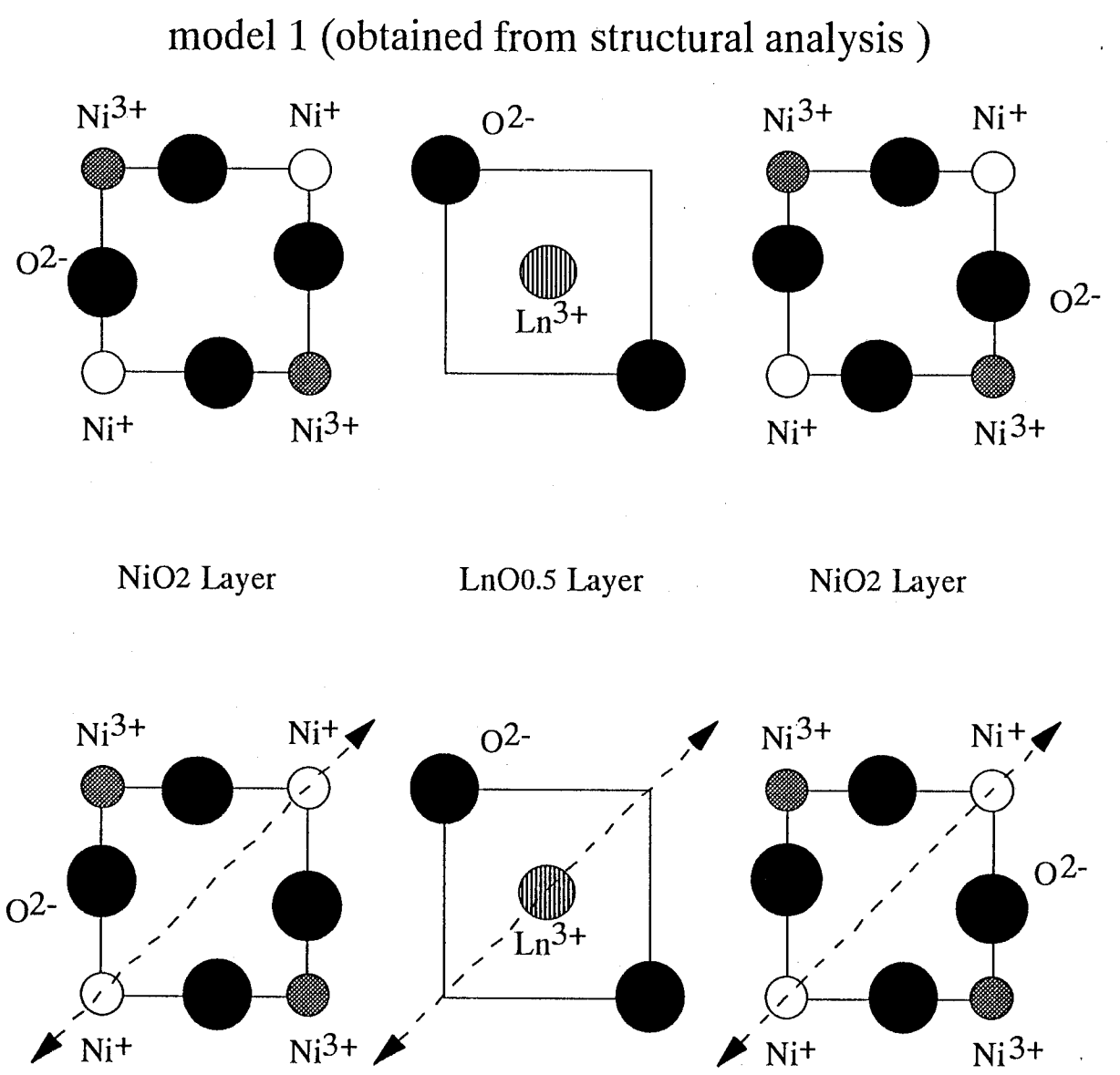

Fig. 5-2 Schematic drawings of array around Ln^{3+} ion in $La_2Ni_2O_5$.

Novel homologous series $Ln_{m+n}[Ni^{3+}O_{6/2}]_m[Ni^{+}O_{4/2}]_n$ (*Ln*=La, Pr, Nd)

Even though the chemical composition differs between $La_2Ni_2O_5$ and $Ln_3Ni_3O_7$ (*Ln*=Pr, Nd), these structures and electronic configuration of nickel ions are similar. As mentioned in Chapters 2 and 4, $La_2Ni_2O_5$ and $Nd_3Ni_3O_7$, as shown in Fig. 5-3, have the corner-shared octahedral NiO_6 chains along the [001] direction of the fundamental perovskite, and one or two sheets of NiO_4 square-planes with their corners shared connect the octahedra in the [100] and [010] directions. The Ni^{3+} ions occupy octahedral sites while Ni^{+} ions occupy square-planar sites. That is, charge distributions in the compound can be expressed as $La_2[Ni^{3+}O_{6/2}][Ni^{+}O_{4/2}]$ and $Nd_3[Ni^{3+}O_{6/2}][Ni^{+}O_{4/2}]_2$, respectively. Rao et al.[7] and Gonzalez-Calbet et al.[8] showed the existence of a homologous series of general formula $La_nNi_nO_{3n-1}$ where n-1 octahedra planes alternate with a NiO_4 square-plane along the [110] direction of the fundamental perovskite-type lattice. $La_2Ni_2O_5$ corresponds to the n=2 member of this family. In this study, the existence of a $Ln_{m+n}(Ni^{3+}O_3)_m(Ni^{+}O_2)_n$ homologous series could be proposed by careful examination of the valence states of nickel ions, where m octahedra layers alternate with n square-planar layers along the [110] direction of the fundamental perovskite-type lattice. This [110] direction corresponds to the [101] direction in the monoclinic cell of $Nd_3Ni_3O_7$. As for $Pr_3Ni_3O_7$, 3 x 1 x 3 supercell was found like $Nd_3Ni_3O_7$. The compounds $Nd_3Ni_3O_7$ and $Pr_3Ni_3O_7$ belong to the m=1, n=2 member, and $La_2Ni_2O_5$ does to the m=1, n=1 one, respectively. Though $La_3Ni_3O_8$ could not be indexed with the superstructure cell up to now, its XPS and XANES spectra show it is composed of $Ni^{3+}O_6$ octahedra and $Ni^{+}O_4$ square-planes. $La_3Ni_3O_8$ would be the m=2, n=1 member.

$Ln_{m+n}(Ni^{3+}O_3)_m(Ni^{+}O_2)_n$

$La_2Ni_2O_5$ (=$LaNiO_{2.5}$) m=1, n=1

$Nd_3Ni_3O_7$ m=1, n=2

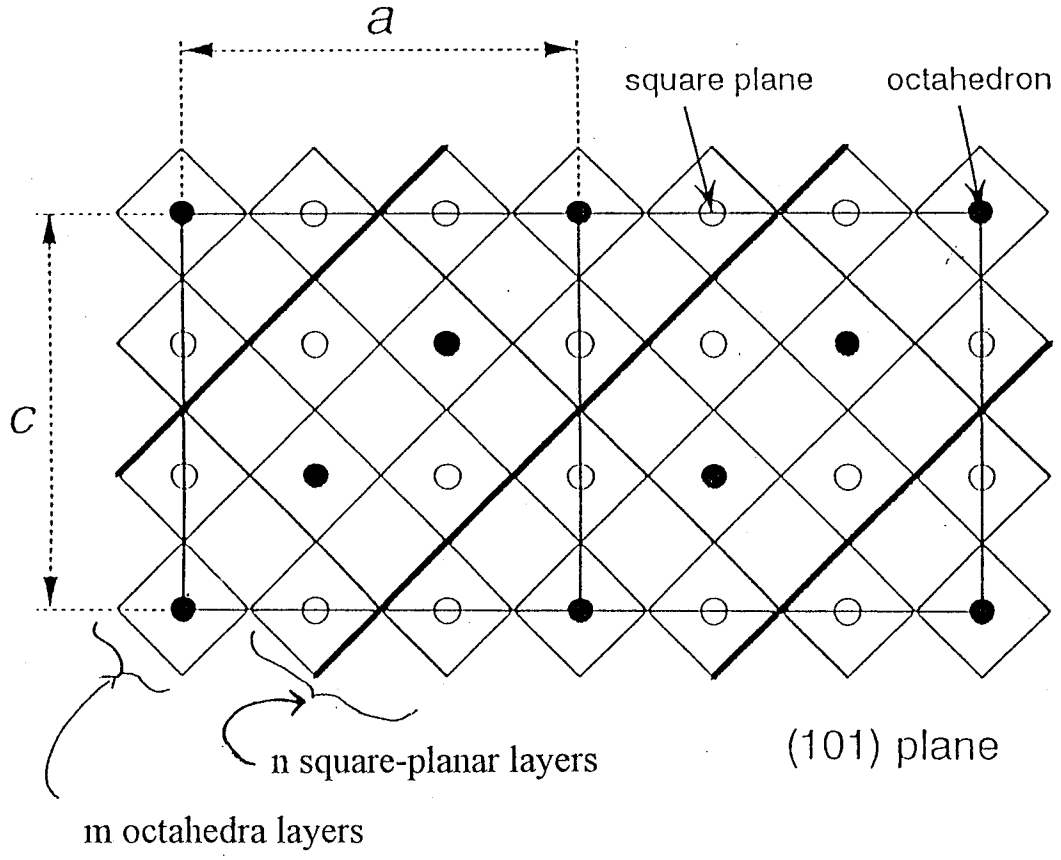

Fig. 5-3 Schematic representation of novel homologous series $Ln_{m+n}[Ni^{3+}O_{6/2}]_m[Ni^{+}O_{4/2}]_n$ (The m=1, n=2 member is shown).

References

[1] W.L.Jolly, " Modern Inorganic Chemistry, 3rd ed. ", McGraw-Hill Book Company, New York, (1989).

[2] J.Rodrigues-Carvajal, M.T.Fernandez-Diaz, and J.L.Martinez, *J. Phys.: Condens. Matter*, **3**, 3215 (1991).

[3] G.H.Lander, J.Spalek, and J.M.Honig, *Phys. Rev. B*, **40**, 4463 (1989).

[4] A.Demourgues, F.Weill, B.Darriet, A.Wattiauw, J.C.Grenier, P.Gravereau, and M.Pouchard, *J. Solid State Chem.*, **106**, 330 (1993).

[5] A.Demourgues, A.Wattiaux, J.C.Grenier, M.Pouchard, J.L.Soubeyroux, J.M.Dance, and P.Hagenmuller, *J. Solid State Chem.*, **105**, 458 (1993).

[6] R.D.Shannon, *Acta Crystallogr., Sect. A*, **32**, 751 (1976).

[7] C.N.R.Rao, J.Gopalakrishnan, K.Vidyasagar, A.K.Ganguli, A.Ramanan, and L.Ganapathi, J. Mater. Res., 1, 280 (1986).

[8] J.M.Gonzalez-Calbet, M.J.sayagues, and M.Vallet-Regi, *Solid State Ionics*, **32/33**, 721 (1989).

General Conclusion

The perovskite-related nickelates $La_2Ni_2O_5$ and $Ln_3Ni_3O_7$ (Ln=Pr, Nd) were prepared by a topotactic reduction of the parent perovskites $LnNiO_3$ (Ln=La, Pr, and Nd). Difference in chemical compositions between La and Pr or Nd is mainly due to size effect of lanthanide ions. The substitution of La to Pr or Nd enabled the Ni ions to be reduced until its formal valence is 1.67+.

$La_2Ni_2O_5$ was an antiferromagnet with T_N=140K. In the reduction process from $LaNiO_3$ to $La_2Ni_2O_5$, a ferromagnetic phase (Tc=230K) whose chemical composition was $LaNiO_{2.60}$ was found. This ferromagnetic phase could be considered to be $La_3Ni_3O_8$. Both $Pr_3Ni_3O_7$ and $Nd_3Ni_3O_7$ were ferromagnets with Tc=300K for Pr and Tc=350K for Nd, respectively.

$La_2Ni_2O_5$, $La_3Ni_3O_8$ and $Ln_3Ni_3O_7$ (Ln=Pr, Nd) were all comprised of $Ni^{3+}O_{6/2}$ octahedra and $Ni^{+}O_{4/2}$ square-planes, *i.e.*, disproportionation of Ni ions into monovalent and trivalent states occured. These compounds could be classified with the general formula $Ln_{m+n}[Ni^{3+}O_{6/2}]_m[Ni^{+}O_{4/2}]_n$, where m octahedra layers alternate with n square-planar layers along the [110] direction of the fundamental perovskite-type cell. Calculations of lattice energy of $La_2Ni_2O_5$ supported that $La_2[Ni^{3+}O_{6/2}][Ni^{+}O_{4/2}]$ is more stable than $La_2[Ni^{2+}O_{6/2}][Ni^{2+}O_{4/2}]$. Comparison of the obtained Ni-O distances showed that square-planarly coordinated Ni ion should not take the divalent state. In the $LnNiO_{3-x}$ systems, the disproportionation of Ni ions occurs when the $LnNiO_{3-x}$ takes the superstructure of the perovskite-type structure. That is, orderings of oxide ion vacancies produced by the reduction would induce the disproportionation, as shown in Fig. 6-1.

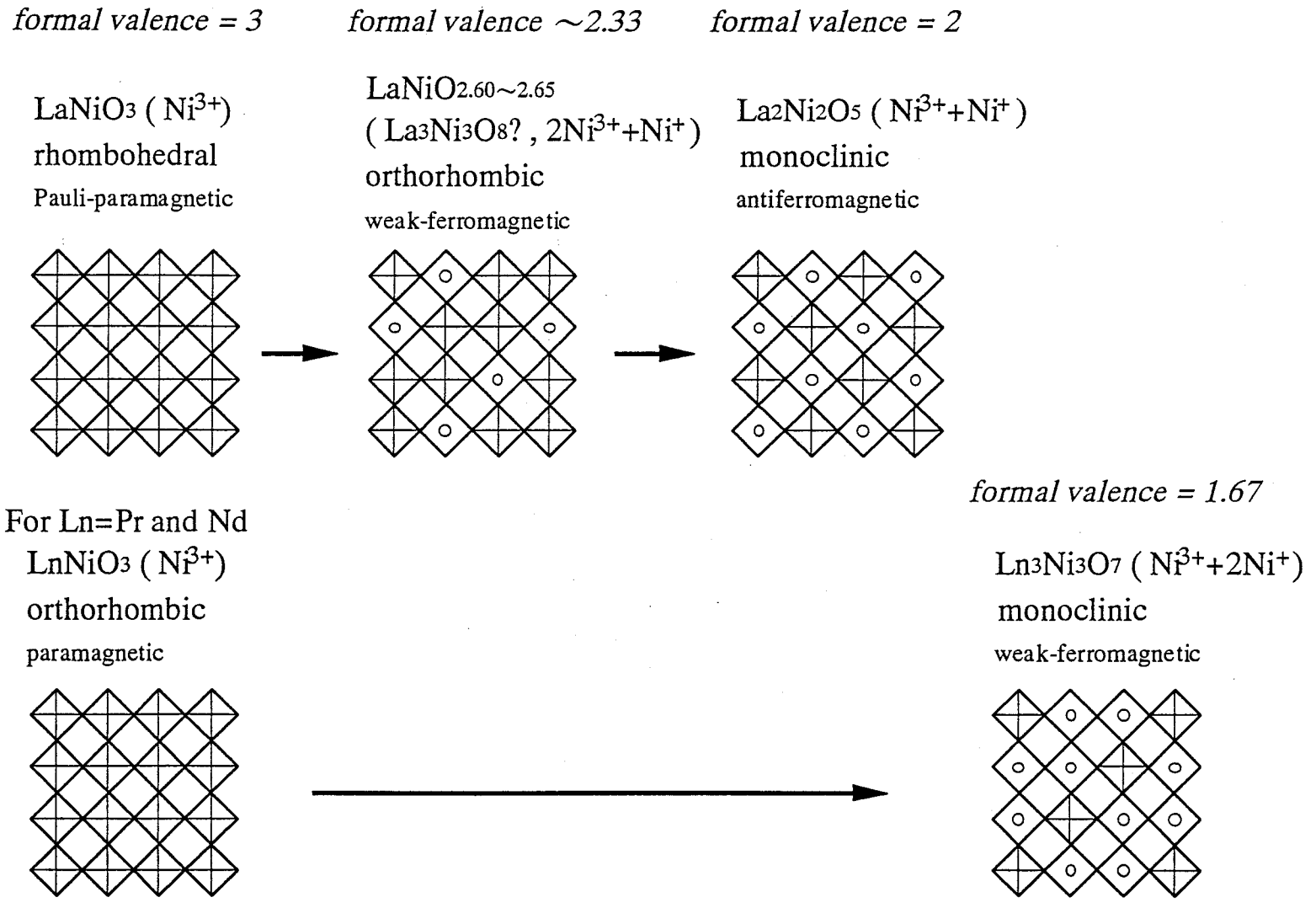

Fig. 6-1 Scheme of redution process for the perovskite-type *Ln*NiO_3 (*Ln*=La, Pr and Nd).

Acknowledgement

The author would like to express his greatest appreciation and gratitude to Professor F.Kanamaru and Dr. S.Kikkawa of Osaka University for their helpful discussion, continuing guidance and encouragement. He would also like to thank Profs. S.Kaizaki and H.Kushi of Osaka University for their kind advice and critical reading of this thesis. Thanks are also due to Prof. K.Koto and Dr. T.Kinouchi of Tokushima University, Drs. K.Nobugai, M.Takahashi, and A.Yoshiasa of Osaka University, Dr. R.Kanno of Kobe University, Dr. I.Matsubara of Government Industrial Research Institute of Osaka, Mr. Y.Hirashima of Tokushima Prefectural Industrial Research Center, and Dr. T.Kohno of Kochi Prefectural Industrial Research Center for their technical assistance and kind discussion.

The author is thankful to Mrs. O.Usaka, M.Hayashi and T.Sakamoto, and Miss T.Imamura in his laboratory for their help in experiments. He especially wish to thank Prof. I.Nakabayashi of Tokushima University for his kind advice, encouragement and financial support. A part of this work has been performed under the approval of the Photon Factory Program Advisory Committee (Proposal No. 91-017).